



UNIVERSITY OF LEEDS

This is a repository copy of *Metformin reduces liver glucose production by inhibition of fructose-1-6-bisphosphatase.*

White Rose Research Online URL for this paper:
<http://eprints.whiterose.ac.uk/135319/>

Version: Accepted Version

Article:

Hunter, RW, Hughey, CC, Lantier, L et al. (7 more authors) (2018) Metformin reduces liver glucose production by inhibition of fructose-1-6-bisphosphatase. *Nature Medicine*, 24. pp. 1395-1406. ISSN 1078-8956

<https://doi.org/10.1038/s41591-018-0159-7>

Reuse

Items deposited in White Rose Research Online are protected by copyright, with all rights reserved unless indicated otherwise. They may be downloaded and/or printed for private study, or other acts as permitted by national copyright laws. The publisher or other rights holders may allow further reproduction and re-use of the full text version. This is indicated by the licence information on the White Rose Research Online record for the item.

Takedown

If you consider content in White Rose Research Online to be in breach of UK law, please notify us by emailing eprints@whiterose.ac.uk including the URL of the record and the reason for the withdrawal request.



eprints@whiterose.ac.uk
<https://eprints.whiterose.ac.uk/>

1 **Metformin reduces liver glucose production by inhibition of fructose-1-6-bisphosphatase**

2 Roger W. Hunter^{1,7}, Curtis C. Hughey², Louise Lantier², Elias I. Sundelin³, Mark Pegg⁴, Elton
3 Zeqiraj^{5,8}, Frank Sicheri^{5,6}, Niels Jessen³, David H. Wasserman², Kei Sakamoto¹

4 ¹Nestlé Institute of Health Sciences SA, EPFL Innovation Park, bâtiment H, 1015 Lausanne,
5 Switzerland

6 ²Department of Molecular Physiology and Biophysics and the Vanderbilt Mouse Metabolic
7 Phenotyping Center, Vanderbilt University, Nashville, USA

8

9 ³Departments of Clinical Medicine and Biomedicine, Aarhus University, Aarhus, Denmark

10 ⁴MRC Protein Phosphorylation and Ubiquitylation Unit, College of Life Sciences, University of
11 Dundee, Dundee, UK

12 ⁵Lunenfeld-Tanenbaum Research Institute, Mount Sinai Hospital, Toronto, Canada

13 ⁶Departments of Biochemistry and Molecular Genetics, University of Toronto, Toronto, Canada

14 ⁷Present address: School of Physiology, Pharmacology & Neuroscience, University of Bristol, Bristol,
15 UK

16 ⁸Present address: Astbury Centre for Structural Molecular Biology, School of Molecular and Cellular
17 Biology, Faculty of Biological Sciences, University of Leeds, Leeds, UK

18 Correspondence should be addressed to K.S. (Kei.Sakamoto@rd.nestle.com)

19

20

21 **Abstract**

22 **Metformin is a first-line drug for the treatment of individuals with type 2 diabetes, yet its**
23 **precise mechanism of action remains unclear. Metformin exerts its anti-hyperglycemic**
24 **action primarily through lowering of hepatic glucose production (HGP). This suppression**
25 **is thought to be mediated through inhibition of mitochondrial respiratory complex I, and**
26 **thus elevation of 5'-adenosine monophosphate (AMP) levels and the activation of AMP-**
27 **activated protein kinase (AMPK), though this proposition has been challenged given**
28 **results in mice lacking hepatic AMPK. Here, we report that the AMP-inhibited enzyme**
29 **fructose-1,6-bisphosphatase-1 (FBP1, EC 3.1.3.11), a rate-controlling enzyme in**
30 **gluconeogenesis, functions as a major contributor to the therapeutic action of**
31 **metformin. We identified a point mutation in FBP1 that renders it insensitive to AMP**
32 **while sparing regulation by fructose-2,6-bisphosphate (F-2,6-P₂) and knockin (KI) of**
33 **this mutant into mice significantly reduces their response to metformin treatment. We**
34 **observe this during a metformin tolerance test and in a metformin-euglycemic clamp**
35 **that we have developed. The anti-hyperglycemic effect of metformin in high fat diet-fed**
36 **diabetic FBP1 KI mice was also significantly blunted compared to wild-type controls.**
37 **Collectively, we show a new mechanism of action of metformin, while providing further**
38 **evidence that molecular targeting of FBP1 can have anti-hyperglycemic effects.**

39 Diabetes is characterized by impaired glucose homeostasis partly due to abnormally elevated hepatic
40 glucose production (HGP). The biguanide drug metformin (N,N-dimethylbiguanide) works principally
41 through inhibition of HGP, although enhanced glucose disposal has also been reported in some
42 studies¹. It is widely accepted that metformin inhibits mitochondrial respiration through complex I²⁻⁴,
43 reducing hepatocellular energy charge. A previous study examined if metformin-mediated AMP-
44 activated protein kinase (AMPK) activation is responsible for its therapeutic effects and the reported
45 data supporting a mechanism involving AMPK-dependent inhibition of HGP and lipogenesis⁵ albeit
46 using an inhibitor of questionable selectivity⁶. Indeed a recent study has demonstrated that inhibitory
47 phosphorylation of acetyl-CoA carboxylase (ACC) by AMPK plays an important role in metformin-
48 induced improvements in insulin action by maintaining hepatic lipid homeostasis⁷. However, the
49 significance of AMPK in metformin action on HGP has been challenged in experiments using mice
50 lacking hepatic AMPK⁸. Recent studies report that metformin inhibits HGP through hepatic AMPK-
51 independent mechanisms, either by attenuating the ability of glucagon to increase 3',5'-cyclic
52 adenosine monophosphate (cAMP) levels and promote HGP⁹ or direct inhibition of mitochondrial
53 glycerol-3-phosphate dehydrogenase and subsequent increase in cytosolic free [NADH]:[NAD⁺]
54 leading to impaired utilization of lactate for gluconeogenesis¹⁰. These findings suggest that the
55 underlying mechanisms responsible for the HGP- and glucose-lowering effects of metformin in
56 diabetes may not be explained by any single target or pathway. Interestingly, a widely-used
57 pharmacological AMPK activator, 5-aminoimidazole-4-carboxamide-1-β-D-ribofuranoside (AICAR),
58 an AMP mimetic, profoundly suppressed glucose output in hepatocytes lacking AMPK^{8,11}, indicating
59 AMP *per se* but not AMPK plays a vital role in suppressing HGP. Similarly, a tight correlation
60 between the magnitude of increase in [AMP]:[ATP] and inhibition of glucose output in hepatocytes
61 has been noted⁸.

62 Given that the anabolic process of gluconeogenesis is energetically costly, hepatocytes must
63 balance this energy demand with production thereby maintaining energy homeostasis. Hepatocytes are
64 equipped with a mechanism to control the rate of hepatic gluconeogenesis in response to energy status
65 and fructose bisphosphatase 1 (FBP1) has long been recognized as a key component¹². FBP1 catalyzes
66 the irreversible hydrolysis of fructose-1,6-bisphosphate (F-1,6-P₂) to fructose-6-phosphate (F6P) and
67 inorganic phosphate (Pi) in the presence of divalent cations. FBP1 is a key rate-controlling enzyme in
68 the gluconeogenic pathway and individuals with FBP1 deficiency present with hypoglycemia and
69 metabolic acidosis due to impaired gluconeogenesis¹³. FBP1 activity is regulated synergistically by the

70 allosteric inhibitors AMP and F-2,6-P₂. AMP inhibits noncompetitively by binding to a unique
71 allosteric site whereas F-2,6-P₂ binds to the active site in competition with F-1,6-P₂. While levels of F-
72 2,6-P₂ are largely under hormonal control, AMP concentration is a function of the energy status of the
73 tissue and contributes to autoregulation of gluconeogenesis. We hypothesized that acute inhibition of
74 gluconeogenesis by metformin is due to inhibition of FBP1, secondary to increases in the AMP
75 concentration through reducing hepatocellular energy charge.

77 **Results**

79 **Identification of an AMP insensitive FBP1 mutant**

80 Demonstrating the importance of allosteric regulation of a rate-controlling enzyme in
81 metabolic flux control *in vivo* is difficult partly due to the lack of an established experimental strategy.
82 The only definitive approach is to generate a knockin (KI) animal model that specifically renders the
83 target enzyme insensitive to the ligand of interest, while leaving all other modes of regulation intact¹⁴.
84 Such a mutant cannot be designed from basic principles and can only be chosen on the basis of
85 available or predicted structure combined with detailed *in vitro* enzyme kinetic analysis. Before
86 designing such a point mutant of FBP1, we first established that metformin does not have a direct
87 inhibitory effect on FBP1 up to 10 mM (**Supplementary Fig. 1a**). Neither does it appear to inhibit the
88 reported target AMP deaminase 1 (AMPD1)¹⁵ (**Supplementary Fig. 1a**).

89 Next, to identify an AMP-resistant FBP1 mutant, we performed structure-guided mutagenesis
90 based on the reported structure of the human FBP1-AMP complex¹⁶ (PDBID 1FTA) (**Fig. 1a**) and
91 evolutionary conservation of key AMP-contacting residues (**Supplementary Fig. 1b**). Several point
92 mutants designed to disrupt AMP binding to mouse FBP1 were prepared using an *Fbp1*-null *E.coli*
93 strain. Native FBP1 from mouse liver was purified and used as a reference material to validate
94 recombinant mouse 6HIS-FBP1. We obtained high-purity recombinant and native FBP1 as judged by
95 Coomassie-stained SDS-PAGE gels (**Fig. 1b**). IC₅₀ values for AMP were comparable between
96 recombinant wild-type (WT) and native mouse liver FBP1 at ~14 and ~20 μM, respectively (**Fig. 1c**).
97 Among the mutants tested, we found that G27P and Y114F showed markedly higher IC₅₀ values for
98 AMP (4420 and 13300 μM, respectively) and were essentially unaffected by up to 1 mM AMP, a
99 concentration expected to greatly exceed *in vivo* limits (**Fig. 1c**). We subjected G27P and Y114F to
100 further analysis using untagged preparations and ultimately rejected further exploration of Y114F due
101 to an increased IC₅₀ for F-2,6-P₂ (data not shown), while we determined the detailed kinetic properties
102 of G27P (**Supplementary Table 1**). Core properties including specific activity and the apparent
103 affinity/Hill coefficient for ligands (F-1,6-P₂, Mg²⁺ and F-2,6-P₂) were essentially identical between
104 WT and G27P mutant. In contrast, IC₅₀ for G27P compared to WT protein was drastically higher for
105 AMP and related compounds, including the active form of AICAR, 5'-AICAR monophosphate
106 (ZMP), and two nucleotide-mimetic commercial FBPase inhibitors.

107 Interestingly, inhibition by 5-inosine monophosphate (IMP) was unaffected. While not a
108 physiologically relevant ligand for FBP1, this highlights that the substitution has not disrupted the
109 function of the allosteric pocket, but merely reduced the affinity for AMP beyond the physiological
110 range. Indeed, titration with the fluorescent AMP analogue, TNP-AMP demonstrated a significant
111 reduction in binding affinity (**Supplementary Table 1**), which was further confirmed by the inability
112 of G27P FBP1 to bind AMP immobilized on a solid support (**Supplementary Fig. 1c**). Finally, we
113 assessed thermal stability as an indicator of the stability of the folded state of the mutant
114 (**Supplementary Fig. 1d**). Melting temperature (T_m) was essentially unaffected by the G27P
115 substitution (69.2 ± 0.2 °C vs. 68.6 ± 0.2 °C). Interestingly, saturating AMP concentration did not shift
116 T_m for WT but substantially reduced resting fluorescence at ambient temperature revealing a clear

117 biphasic transition from the more closed tense (T) state upon heating. As expected, this was not
118 observed for G27P but the stabilizing effect of F-1,6-P₂ was conserved.

119

120 **Generation and characterization of an AMP insensitive FBP1 G27P KI mouse model**

121 To establish if AMP-mediated inhibition of FBP1 activity contributes to the anti-
122 hyperglycemic action of metformin *in vivo*, we generated an FBP1 KI mouse model in which the
123 codon for glycine 27 of *Fbp1* was modified to encode proline (**Fig. 1d**). FBP1 is predominantly
124 expressed in liver and kidney and to a much lesser extent in testes and small intestine (**Supplementary**
125 **Fig. 2a**). Although expression of FBP1 in islets has been reported¹⁷, it was undetectable in our hands
126 using a highly specific antibody (**Supplementary Fig. 2a**). We confirmed that expression and activity
127 of FBP1 were comparable between homozygous FBP1^{G27P/G27P} KI and control WT mice in liver and
128 kidney, although FBP1 expression in KI mice was modestly higher in small intestine and lower in
129 testes compared to WT (**Fig. 1e** and **Supplementary Fig. 2b,c**). Assayed in crude liver extracts, FBP1
130 G27P exhibited > 400-fold higher IC₅₀ for AMP compared to WT FBP1 (**Fig. 1e**), which is far beyond
131 the physiological range of cellular AMP concentrations¹⁸.

132 FBP1^{G27P/G27P} mice were born at the expected Mendelian frequency and displayed similar body
133 weight and growth curves (data not shown), food intake and respiratory exchange ratio, as well as
134 locomotor activity compared to WT mice (**Supplementary Fig. 3a-f**). Compared to WT, FBP1 KI
135 mice exhibited similar blood glucose, plasma insulin, glucagon and leptin levels, as well as hepatic
136 glycogen content under fasted and refeed (4 h *ad libitum* following overnight fast) conditions (**Fig. 2a-**
137 **e**). KI mice also displayed normal blood glucose tolerance (**Fig. 2f**) and gluconeogenic capacity
138 assessed by pyruvate tolerance test (**Fig. 2g**). Consistent with these observations, immunoblot analysis
139 revealed comparable expression of major metabolic proteins involved in hepatic glucose metabolism
140 (e.g. GLUT2, glucokinase (GCK) and its regulator protein GCKR, hexokinase 1 (HXK1),
141 phosphofructokinase (PFKL), 6-phosphofructo-2-kinase/fructose-2,6-bisphosphatase (PFKFB1),
142 FBP1 and glucose-6-phosphate dehydrogenase (G6PD)), glycogen metabolism (e.g. glycogen synthase
143 (GYS2) and glycogen phosphorylase (PYGL)) and gluconeogenesis (e.g. catalytic and transporter
144 subunit of glucose-6 phosphatase (G6PC/T), cytosolic/mitochondrial isoforms of
145 phosphoenolpyruvate carboxykinase (PEPCK-C/M), pyruvate carboxylase (PC), pyruvate kinase
146 (PKLR)) as well as the major metformin transporter organic cation transporter 1 (OCT1) between WT
147 and KI under fasted and refeed conditions (**Fig. 2h** and **Supplementary Fig. 4**). Moreover, the activity
148 of the major gluconeogenic/glycolytic enzymes were similar between WT and KI under both fasted
149 and refeed conditions (**Supplementary Fig. 5a-i**). At transcript level, mRNA expression of genes
150 involved in gluconeogenesis (*Pck1*, *Pparg1c*, *Foxo1a*) and lipogenesis (*Fasn*) were similar between
151 WT and KI mice (**Supplementary Fig. 5j-m**). Conversely, *G6pc* mRNA level was significantly lower
152 in KI mice under both fasted and refeed conditions (**Supplementary Fig. 5n**), although this did not
153 translate into a difference at protein level (**Fig. 2h** and **Supplementary Fig. 4b**) or activity
154 (**Supplementary Fig. 5b**). Similarly, *Gck* mRNA was higher in refeed KI mice (**Supplementary Fig.**
155 **5o**); however, again, protein levels and enzyme activity were unchanged (**Supplementary Fig. 4d** and
156 **Supplementary Fig. 5a**). Phosphorylation states of hormone- and/or nutrient-regulated proteins
157 showed the anticipated changes in response to refeeding such as increased phosphorylation of p70S6K
158 and S6, downstream components of mTOR, and decreased phosphorylation of GYS2 and PYGL, as
159 well as PFKFB1, the enzyme that synthesizes F-2,6-P₂ and a major substrate of cAMP-dependent
160 protein kinase (**Fig. 2h** and **Supplementary Fig. 4**). Hepatic lactate and pyruvate are the major three
161 carbon precursors for gluconeogenesis and their levels were unchanged between WT and KI mice
162 under both fasted and refeed conditions (**Supplementary Table 2**). Likewise, hepatic glucose and G6P
163 concentrations were similar between WT and KI. Furthermore, there was no difference in the levels of
164 F6P and F-1,6-P₂, the substrate and product of FBP1, respectively (**Supplementary Table 2**). The loss

165 of regulation by AMP of FBP1 does not have an apparent impact on gluconeogenic flux under normal
166 conditions. The mutant does remain sensitive to hormonal regulation by F-2,6-P₂, whose levels were
167 also unchanged between WT and KI. Hepatic adenine nucleotide levels and energy charge were
168 similar in fasted and refeed conditions and comparable between WT and KI mice (**Supplementary**
169 **Table 3**). Taken together, these results demonstrated that FBP1 KI mice possess normal hepatic
170 energy and metabolic homeostasis, as well as whole body glucose homeostasis.

171

172 **FBP1 G27P KI mice are resistant to the hypoglycemic action of AMP mimetic compounds**

173 Prior to testing the effect of metformin, we wanted to confirm if FBP1^{G27P/G27P} KI mice are
174 resistant to AMP-mediated blood glucose-lowering *in vivo*. For this purpose, we initially used the
175 AMP mimetic FBPase inhibitor MB06322 (ref. 19), the pro-drug of MB05032 (**Fig. 3a** and
176 **Supplementary Table 1**). We observed that recombinant mouse FBP1 was ~2-fold less sensitive to
177 MB05032 compared to rat FBP1 *in vitro*, while sensitivity to AMP was comparable between the two
178 species (**Fig. 3b**). As all available pre-clinical data was only performed in rats, we took this species
179 difference in drug response into account and 75 mg.kg⁻¹ of MB06322 was administered (*i.p.*) to WT
180 and KI mice. In WT animals MB06322 treatment resulted in a robust and sustained decrease (~40 % at
181 2-3 h post injection) in blood glucose levels (**Fig. 3c**), which was accompanied by an increase in blood
182 lactate levels (**Fig. 3d**). In contrast, even though plasma concentration of the drug was comparable
183 between genotypes (**Fig. 3e**), MB06322 had no significant effect on both blood glucose and lactate
184 concentration in KI mice (**Fig. 3f, g**). We next sought to determine if the well-documented
185 hypoglycemic effect of AICAR²⁰, which is converted intracellularly to the AMP-mimetic ZMP (**Fig.**
186 **4a**), is mediated through ZMP-dependent inhibition of FBP1 *in vivo*. Administration of AICAR (250
187 mg.kg⁻¹, *i.p.*) resulted in a profound (up to ~60 %) decrease in blood glucose levels in WT (**Fig. 4b**),
188 but not in KI (**Fig. 4c**) mice, while plasma concentration of AICAR was similar between the two
189 genotypes (**Fig. 4d**). Consistent with the results observed with MB06322, AICAR induced a marked
190 increase in blood lactate levels in WT (**Fig. 4e**), but only modestly in KI (**Fig. 4f**) mice. Plasma
191 glucagon levels were increased only in AICAR-treated WT (**Fig. 4g**), but not in KI (**Fig. 4h**) mice,
192 most likely to counteract the rapid induction of hypoglycemia (**Fig. 4b**). There was no significant
193 change in plasma insulin levels (**Fig. 4i,j**). As anticipated, AICAR robustly stimulated phosphorylation
194 of liver AMPK and its *bona fide* substrate ACC in both WT and KI mice (**Fig. 4k,l**). This was
195 accompanied by a profound increase in liver ZMP and ZTP concentrations in both genotypes
196 (**Supplementary Table 4**). As previously reported in both intact animals^{11,20} and isolated
197 hepatocytes^{12,21} AICAR administration in WT mice resulted in a substantial decrease in the total
198 adenine nucleotide pool (**Supplementary Table 4**). The conversion of AICAR to ZMP by adenosine
199 kinase consumes ATP and acts as a trap for phosphate, similar to the metabolic consequences of a
200 large fructose bolus. This effect is further enhanced by significant substrate cycling between AICAR
201 and ZMP due to dephosphorylation by 5'-nucleotidase²². This leads to depletion of Pi resulting in de-
202 inhibition of AMP deaminase and the loss of adenine nucleotides. However, this mechanism cannot be
203 fully responsible as AICAR had minimal effect on adenine nucleotides in KI mice despite similar
204 accumulation of ZMP (**Supplementary Table 4**). Furthermore, AICAR was previously observed to
205 have no significant effect on ATP levels in fed mice²⁰. The common factor here is likely the absence
206 of an acute glucose-lowering effect and inhibition of a high gluconeogenic flux which leads to the
207 accumulation of additional phosphorylated species (e.g. F-1,6-P₂ and the triose phosphates) as
208 additional sinks for Pi (data not shown). Interestingly, AICAR treatment lead to a similar increase in
209 hepatic NAD⁺ in both WT and KI mice (**Supplementary Table 4**), which is likely due to AMPK-
210 dependent inhibition of fatty acid synthesis and subsequent increase in β-oxidation.

211 In skeletal muscle, AICAR failed to increase AMPKα T172 phosphorylation and activity in
212 both genotypes (**Supplementary Fig. 6a-c**), although it enhanced phosphorylation of ACC and TBC1

213 domain family member 1 (TBC1D1) most likely via ZMP-dependent allosteric activation of AMPK
214 (**Supplementary Fig. 6d, e**). Notably, AICAR was unable to stimulate phosphorylation of RAPTOR
215 which is a marker of more robust AMPK activation²³ (**Supplementary Fig. 6f**). Indeed ZMP
216 concentration and [ZMP]:[ATP] ratio in skeletal muscle were > 50-fold and > 150-fold less,
217 respectively, compared to that detected in the liver following AICAR treatment, a consequence of the
218 significant first-pass metabolism of AICAR and low plasma concentration (**Supplementary Table 4**
219 **and Supplementary Fig. 6g**). Thus, it is presumed that the magnitude of AMPK activation following
220 AICAR treatment in skeletal muscle was below the threshold to cause blood glucose-lowering in KI
221 mice through promoting glucose uptake in this tissue. Collectively, using two AMP mimetic drugs we
222 have confirmed that the FBP1 KI model is suitable to investigate the effect of an AMP-elevating agent
223 (i.e. metformin) on blood glucose *in vivo*.

224

225 **FBP1 G27P KI mice are metformin intolerant**

226 To determine if FBP1 KI mice exhibited altered responses to an acute dose of metformin, we
227 performed a metformin tolerance test. Since metformin affects intestinal glucose absorption²⁴, we
228 intraperitoneally injected glucose (2 g.kg⁻¹) following an oral administration of 250 mg.kg⁻¹ metformin
229 (**Supplementary Fig. 7a**), a commonly used dose in rodents to elicit an acute glucose-lowering
230 effect^{7-9,25}. Prior administration of metformin promoted significantly faster disappearance of blood
231 glucose compared to vehicle-treated control in FBP1 WT mice (**Fig. 5a**). In contrast, metformin's
232 glucose-lowering effect was significantly lower in KI mice (**Fig. 5b**) even though plasma and liver
233 metformin levels (~125-150 μM and ~0.7 μmol.g⁻¹ respectively) were comparable between genotypes
234 (**Fig. 5c**). Metformin caused a comparable increase in hepatic [AMP]:[ATP] (~2-fold) and decreased
235 energy charge (~10 %) in both genotypes (**Supplementary Table 5**). This change in energy status was
236 associated with a robust increase in phosphorylation of liver AMPK and ACC (**Fig. 5d,e**).

237 To further investigate whether FBP1 KI mice were resistant to the glucose-lowering effect of
238 metformin *in vivo*, we developed and optimized a “metformin-euglycemic clamp” protocol in the
239 conscious, unrestrained mouse (**Supplementary Fig. 7b**). A similar technique has been used
240 previously to assess the effect of metformin on HGP in mice²⁶. Two different doses of metformin
241 (1.875 mg.kg⁻¹.min⁻¹ and 3.75 mg.kg⁻¹.min⁻¹) were tested. Metformin was infused intravenously at a
242 constant rate, while the glucose infusion rate (GIR) was adjusted to maintain euglycemia (**Fig. 5f**). We
243 observed that the lower dose (1.875 mg.kg⁻¹.min⁻¹) failed to increase GIR significantly from baseline
244 in WT (and also KI) mice under euglycemic condition (**Supplementary Fig. 7c,d**), even though
245 metformin had reached ~170 μM and ~0.8 μmol.g⁻¹ in plasma and liver, respectively (**Supplementary**
246 **Fig. 7e**). These concentrations were comparable to those observed following an acute oral
247 administration of 250 mg.kg⁻¹ (**Fig. 5c**). This is likely due to differences in the route of administration.
248 The first-pass of metformin from the gastrointestinal tract, via the portal vein and liver, into systemic
249 circulation is crucial for the glucose-lowering effect. Firstly, administration of metformin via the
250 portal-hepatic pathway produces more profound glucose-lowering than direct systemic infusion²⁷.
251 Secondly, it has been proposed that there is also a direct effect of metformin on the gut itself. For
252 example, it has been recently suggested that metformin reduces HGP through a gut-brain-liver
253 neuronal network via activation of AMPK in the duodenum resulting in release of GLP-1²⁸. Another
254 study has shown that metformin reshapes the gut microbiota through interacting with different
255 bacteria, possibly via metal homeostasis²⁹.

256 Infusion of a higher dose of metformin (3.75 mg.kg⁻¹.min⁻¹) resulted in a substantial increase
257 in GIR leading to steady state by the end of the 120 min clamp in WT mice (**Fig. 5g**). In contrast, KI
258 mice displayed only a modest increase in GIR (**Fig. 5g**), even though plasma and liver/muscle
259 metformin, as well as plasma insulin concentrations were similar between genotypes (**Fig. 5h** and
260 **Supplementary Fig. 7f,g**). Combining the metformin-euglycemic clamp with administration of ²H

261 stable isotope tracers enabled the quantification of endogenous glucose production (EndoRa) including
262 the relative contribution of glycogenolysis and gluconeogenesis. EndoRa was significantly suppressed
263 (~20 %) in WT during the clamp (**Fig. 5i**). This was due to reduction of both gluconeogenesis and
264 glycogenolysis (**Fig. 5j,k**). In contrast, metformin-induced suppression of EndoRa, gluconeogenesis
265 and glycogenolysis, was ablated in FBP1 KI mice (**Fig. 5i-k**). Overall, the clamp study revealed that
266 KI mice were largely insensitive to the glucose-lowering effect of metformin due to ablation of
267 metformin-induced suppression of HGP. However, it should be noted that due to the systemic route of
268 delivery (as mentioned above), much higher and supra-pharmacological doses were needed to elicit a
269 robust glucose-lowering effect resulting in artificially higher glucose disposal rate (~40-50 % increase
270 in both WT and KI) than is seen at therapeutic doses (**Fig. 5l**). It has been shown that metformin can
271 stimulate glucose uptake in isolated rat skeletal muscle at supra-pharmacological doses (but not at
272 clinical doses due to the absence of OCT1³⁰) by activating AMPK⁵, which could sensitize insulin
273 action and further promote glucose uptake in muscle³¹. In support of this premise, metformin
274 concentration in skeletal muscle was increased 2-fold when infused at the higher rate (3.75 mg.kg⁻¹.min⁻¹)
275 compared to the lower rate (1.875 mg.kg⁻¹.min⁻¹) (**Supplementary Fig. 7g**). The molecular
276 basis underlying reduced glycogenolysis in WT mice during the clamp is unknown, as we observed no
277 significant difference in the levels of phosphorylation/activity of glycogen synthase (GS) and glycogen
278 phosphorylase (GP_a), as well as hepatic glycogen content between genotypes at the end of the clamp
279 (**Supplementary Fig. 7h-m**). We monitored tissue distribution and pharmacokinetics of metformin
280 via systemic route and performed positron emission tomography (PET) analysis following an acute
281 intravenous infusion of [¹¹C]-metformin. We found that the kinetics and total metformin uptake in
282 liver was comparable between WT and KI mice (**Supplementary Fig. 8**) consistent with the snapshot
283 measurements of hepatic metformin concentration as shown in **Fig. 5c** and **Supplementary Fig. 7e**. In
284 addition, PET analysis highlighted a rapid and marked accumulation of metformin in the bladder,
285 corroborating the need for a much higher dose to achieve a glucose-lowering effect via systemic route
286 than gastrointestinal route.

287

288 **FBP1 G27P KI mice are resistant to the acute hypoglycemic action of metformin in an obesity-** 289 **induced model of diabetes**

290 We next assessed if FBP1 KI mice were resistant to the glucose-lowering effect of metformin
291 under hyperglycemic/diabetic condition. WT and KI mice were fed with high-fat diet (HFD) for 10
292 weeks and both genotypes had similar profiles of weight gain and food intake over the period of
293 dietary intervention (**Fig. 6a,b**). HFD-fed WT and KI mice showed hallmark features of type 2
294 diabetes, including glucose intolerance, hyperglycemia, hyperinsulinemia as well as
295 hypertriglyceridemia (**Fig. 6c-f**). At the end of HFD intervention, we orally treated WT and KI mice
296 with metformin (250 mg.kg⁻¹) or vehicle (water) and monitored blood glucose levels two hours post
297 treatment. We found that metformin, but not vehicle, produced a significant reduction of blood
298 glucose levels in WT (~30-40 %), but the effect was significantly blunted in KI mice ($P = 0.047$, **Fig.**
299 **6g,h**). We verified that hepatic metformin levels (**Fig. 6i**) and the magnitude of changes in
300 [AMP]:[ATP], energy charge (**Supplementary Table 6**), as well as associated increases in AMPK
301 phosphorylation (**Fig. 6j**) were comparable between genotypes. Inhibition of gluconeogenesis by
302 metformin in WT mice could also be supported by a modest fall in hepatic glucose and G6P levels,
303 which was blunted in KI animals. Similarly, inhibition of the step catalyzed by FBP1 was suggested
304 by a decrease in F6P ($P = 0.053$) and a concomitant increase in F-1,6-P₂, in livers from metformin-
305 treated mice ($P = 0.091$) that was lower in KI animals (**Supplementary Table 7**). However, given that
306 there was a modest (~10 %), but significant effect for metformin to decrease blood glucose in KI mice
307 (**Fig. 6h**), there must be additional mechanisms, independent of AMP-mediated FBP1 inhibition, to
308 lower blood glucose. This is unsurprising given that metformin has multiple proposed primary and

309 secondary targets¹, including mitochondrial complex I²⁻⁴ and glycerol-3-phosphate dehydrogenase¹⁰ in
310 the liver, as well as duodenal AMPK²⁸. While it has been proposed that one of the mechanisms of
311 action of metformin involves a reduction in hepatic cAMP⁹ (a key mediator of glucagon signaling),
312 there was no significant effect (**Fig. 6k**) and an actual increase in downstream phosphorylation of PKA
313 substrates (i.e., pS33 PFKFB1 and pS133 cAMP response element-binding protein (CREB))
314 (**Supplementary Fig. 9a,b**) under the conditions of our model system, (it has been reported that the
315 reduction in cAMP is only apparent at substantially higher dose [i.e. 400 mg.kg⁻¹]⁷), although we
316 cannot rule out the possibility that we have missed the time point where cAMP-PKA signaling was
317 suppressed following metformin treatment.

318

319 Discussion

320 Metformin has been in use for more than 50 years as an antihyperglycemic agent for the
321 treatment of diabetes. Despite the clinical success of metformin, there is no clear consensus as to its
322 mode of action and multiple, seemingly contradictory mechanisms, have been proposed. However, a
323 common narrative emerges when a clear distinction is drawn between acute vs. chronic effects of
324 metformin that can be mediated by either direct or indirect effects on HGP by metabolic or genic
325 means. We have focused specifically on the acute effect of metformin on HGP, where it is clear that
326 AMPK is dispensable. Hepatic AMPK-null mice do not exhibit a defect in either steady state
327 glycemia, glucose/pyruvate tolerance or the acute glucose-lowering effect of metformin⁸. Furthermore,
328 treatment of cultured hepatocytes⁸ or *i.v.* infusion of the specific AMPK activator A769662 has no
329 effect on glucose production¹⁰. While hepatic LKB1-null mice present with severe hyperglycemia and
330 hyperlipidemia due to upregulation of CREB/peroxisome proliferator-activated receptor-gamma
331 coactivator 1 α (PGC1 α) transcriptional targets (*Pck1* and *G6pc*)³², recent work suggests that this is due
332 to impaired activity of the AMPK-related kinase, salt-inducible kinase (SIK)³³, and not AMPK. Much
333 is often made of the short-term changes in *Pck1* and *G6pc* mRNA in response to pharmacological
334 activation of AMPK, but when protein levels are assessed they are invariably unaltered. Indeed, a poor
335 correlation has been noted between the expression of gluconeogenic genes and HGP³⁴. In short,
336 although biguanides can clearly activate AMPK, it is neither sufficient nor necessary for acute
337 inhibition of HGP.

338 Obesity-induced diabetes is a standard model in rodent studies and it is generally accepted that
339 the associated hyperglycemia is a consequence of hepatic insulin resistance in fatty livers. It is well
340 established that AMPK is a critical regulator of lipogenesis and chronic treatment of diabetic mice
341 with metformin significantly improves glucose tolerance by reducing hepatic steatosis and improving
342 insulin resistance. Of note, mice expressing non-phosphorylatable mutants of ACC1 and ACC2
343 (ACC1/2 knockin), were resistant to the lipid and glucose-lowering effect of chronic metformin
344 treatment. Significantly, the acute hypoglycemic effect of a single dose of metformin was unaffected⁷.
345 The same mechanism likely underpins the glucose-lowering effect of chronic A769662 treatment in
346 obese *ob/ob* mice where dramatic reductions in hepatic and plasma lipid were observed³⁵.
347 Consequently, AMPK plays a role in the chronic, indirect inhibition of HGP by alleviating hepatic
348 insulin resistance.

349 Plasma metformin concentration in humans is markedly variable, due in part to the complex
350 pharmacokinetics of the drug and profound inter-subject variations in absorption and elimination³⁶. It
351 is difficult to quote a meaningful elimination half-life ($t_{1/2}$) because the time course of plasma
352 concentrations of metformin follows a multiphasic pattern, but values in the range from 1.7 to 4.5
353 hours have been reported³⁶. Plasma metformin concentration in patients treated with a normally
354 prescribed dose of metformin (1 g, twice a day) has been reported within 0.4-32 μ M range (plasma
355 levels obtained 14 hours after last drug administration) in 159 type 2 well-regulated diabetic subjects
356 under controlled conditions³⁷. In contrast, plasma metformin levels between 0 and 113 mg/L (868 μ M)

357 have been measured in random blood samples from diabetic subjects³⁸. Both studies have provided
358 useful information, as the former³⁷ gives an estimate of nadir during multiple dosing, whereas the
359 latter³⁸ provides a valuable estimate of C_{max} of metformin during clinical use. However, overall it has
360 been to date a challenge to establish the therapeutic range of metformin concentrations in plasma.

361 The current debate on metformin has turned towards the issue of the validity of the
362 concentrations and doses used in rodent models. It has long been recognized that the effective
363 hypoglycemic dose exhibits a marked species dependence and researchers rightly use doses that
364 produce robust, reproducible effects. In this regard, it is difficult to compare studies that have not
365 measured plasma and/or liver accumulation as the drug formulation, route of administration and
366 degree of fasting will impact the pharmacokinetics. Species differences in OCT1 expression have also
367 been identified; while both rodent and human liver express OCT1, its expression in human intestines
368 appears much lower than in mice³⁹. As metformin is administered orally, differences in intestinal
369 OCT1 expression may affect portal vein levels of metformin and thereby hepatic uptake without
370 detectable effects on metformin levels in peripheral veins. In addition, hepatic exposure to the drug
371 depends not only on OCT1 but also multidrug and toxin extrusion (MATE) isoforms acting as influx
372 and efflux transporters, respectively. Differential hepatic expression of MATE1 between humans and
373 rodents has been reported⁴⁰, which may also affect metformin kinetics. It has been observed that a
374 glucose-lowering effect occurs in response to a single dose of 50 mg.kg⁻¹ in rats¹⁰. However, it should
375 be noted that metformin (50 mg.kg⁻¹) was given *intravenously*, which led to plasma metformin
376 concentration of ~74 μM 30 min after administration, while 100 mg.kg⁻¹ and 250 mg.kg⁻¹ doses
377 increased plasma metformin concentration of 345 μM and 1300 μM, respectively¹⁰. Further, the study
378 exploring the effect of metformin in ACC1/2 KI mice used a chronic dose of 50 mg.kg⁻¹ (*i.p.*) for 12
379 weeks, however, a dose of 200 mg.kg⁻¹ was needed (50 mg.kg⁻¹ had no effect) to observe a glucose-
380 lowering effect in single-dose experiments⁷. Taken together, the dose range 200-350 mg.kg⁻¹ has
381 consistently been used^{7-9,25} and indeed the dose used in our study is similar to the maximum daily
382 human dose (2 g) when allometric scaling is applied (dose for 25 g mouse = 2000×(0.025/65)^{0.75} = 5.5
383 mg = 220 mg.kg⁻¹).

384 With cultured hepatocytes it is typical to see claims of enhanced justification on the basis of
385 using lower doses but for greatly increased periods of time (often 16-24 h). Given that the uptake of
386 metformin in isolated hepatocytes is relatively slow² (in contrast to the rapid uptake in human and
387 rodent livers *in vivo*^{41,42}) and potentially antagonized by competing OCT substrates in complex
388 media⁴³, intracellular accumulation is both time and concentration dependent such that higher drug
389 concentrations will reach effective intracellular levels within more relevant time periods. The apparent
390 discrepancy in reported efficacy of metformin on isolated hepatocytes is likely due to the wide range
391 of culture conditions used with respect to media (complex vs. balanced salt solutions), carbon sources
392 and hormones. Indeed, under commonly used conditions for glucose production assays where the sole
393 carbon sources are typically lactate and pyruvate, metformin produces precipitous decreases in
394 intracellular ATP concentration (~85 % reduction at 1 mM) that closely follow apparent changes in
395 glucose production or gene expression⁸. Such extremes in adenylate energy charge are not observed in
396 any physiological setting *in vivo*. Consequently, the lack of standardization in hepatocyte protocols
397 and the ease with which extreme energy deprivation can be induced with metformin renders the many
398 reported results difficult to consolidate.

399 The final area of controversy concerns the role of changes in adenine nucleotides in metformin
400 action. Several early studies reported activation of AMPK in the apparent absence of increases in
401 AMP concentration⁴⁴, which has been used to argue that metformin does not alter cellular energetics.
402 However, experiments using AMP-resistant AMPKγ2 mutants have clarified that AMPK activation by
403 metformin and essentially all xenobiotic compounds is mediated by increases in AMP concentration⁴⁵.
404 Technical errors in many contemporary studies have resulted in misleading values reported for hepatic

405 adenine nucleotides ([ATP]:[AMP] <<10, often approaching 1). Hepatic AMP concentration is a very
406 sensitive indicator of stress and increases by ~10-fold within just 30 seconds of hypoxia¹⁸.
407 Consequently, tissues must be freeze-clamped *in-situ* to enable accurate measurements and reveal
408 subtle changes in energy status. Even then, AMPK can easily be activated by increases in free AMP
409 concentrations that are below the limit of quantification. Consequently, AMPK is a sensitive reporter
410 of subtle changes in [AMP]:[ATP] and AMPK α T172 phosphorylation is a more reliable indicator of
411 changes in the AMP concentration than technically demanding direct measurements. Hence, it can be
412 argued that a consensus emerges that metformin induces changes in hepatic energy status which is
413 sufficient to modify the activity of sensors such as AMPK and FBP1. Nonetheless, we observed here a
414 modest, but significant reduction in energy charge in response to metformin treatment in the liver,
415 which may have partly contributed to suppression of energy-demanding gluconeogenic flux⁸.

416 Understanding the mechanism by which metformin reduces HGP and normalizes blood
417 glucose levels in hyperglycemic type 2 diabetics is of considerable importance. Our results show that
418 metformin induces a mild energy stress in liver, leading to an increase in AMP concentration that
419 allosterically inhibits FBP1 to lower HGP. This is potentially a powerful mechanism as the subsequent
420 increase in F-1,6-P₂ will activate PK and increase glycolytic flux^{46,47}. Our study further supports the
421 advancement of FBP1 as a key target for the treatment of type 2 diabetes, either directly using targeted
422 inhibition⁴⁸ or indirectly, as a consequence of inducing energy stress. The later mechanism may
423 contribute significantly to the apparent glucose lowering effect of many biologically active secondary
424 metabolites and to novel antidiabetic drugs exploiting the emerging concept of mild mitochondrial
425 uncoupling⁴⁹.

426

427 **METHODS**

428 Methods and any associated references are available in the online version of the manuscript.

429 **ACKNOWLEDGMENTS**

430 We thank M. Deak for molecular biology assistance and S. Jakobsen and J. Frøkiær for support in
431 method development of the [¹⁴C]-metformin uptake study. We also thank E. Heikkilä for performing
432 islet isolation, S. Ducommun for performing pTBC1D1 blot, and S. Cotting for constructing
433 Wollenberger tongs. This study was supported by Vanderbilt Mouse Metabolic Phenotyping Center
434 Grant DK059637 (D.H.W.) and R37 DK050277 (D.H.W.), a Foundation Grant (FND 143277) from
435 the Canadian Institutes of Health Research (F.S.), the Danish Council for Independent Research DFF –
436 4183-00384 (N.J.) and the Novo Nordisk Foundation NNF13OC0003882 (N.J.). E.Z. was supported
437 by a Sir Henry Wellcome postdoctoral fellowship. C.C.H. was supported by a Canadian Diabetes
438 Association postdoctoral fellowship.

439 **AUTHOR CONTRIBUTIONS**

440 R.W.H. and K.S. designed the study. R.W.H. performed all the biochemical assays, and the majority
441 of *in vivo* experiments assisted by K.S. Analysis of FBP1 structure and design of the mutants were
442 performed by E.Z. and F.S. M.P. performed molecular cloning and mutagenesis of FBP1. N.J. and
443 E.I.S. performed [¹⁴C]-metformin uptake kinetics study and analyzed the data. C.C.H. and L.L.,
444 performed metformin-euglycemic clamp and analyzed the data. D.H.W. supervised C.C.H. and L.L.,
445 and contributed to data interpretation of the clamp study. R.W.H and K.S. wrote the manuscript. All
446 the authors reviewed, edited and approved the manuscript.

447 **COMPETING FINANCIAL INTERESTS STATEMENTS**

448 K.S. is a full-time employee of the Nestlé Institute of Health Sciences S.A., Switzerland.

450 REFERENCES

- 451 1. Rena, G., Pearson, E.R. & Sakamoto, K. Molecular mechanism of action of metformin: old or
452 new insights? *Diabetologia* **56**, 1898-1906 (2013).
- 453 2. Owen, M.R., Doran, E. & Halestrap, A.P. Evidence that metformin exerts its anti-diabetic
454 effects through inhibition of complex 1 of the mitochondrial respiratory chain. *Biochem J* **348**
455 **Pt 3**, 607-614 (2000).
- 456 3. El-Mir, M.Y., *et al.* Dimethylbiguanide inhibits cell respiration via an indirect effect targeted
457 on the respiratory chain complex I. *J Biol Chem* **275**, 223-228 (2000).
- 458 4. Bridges, H.R., Jones, A.J., Pollak, M.N. & Hirst, J. Effects of metformin and other biguanides
459 on oxidative phosphorylation in mitochondria. *Biochem J* **462**, 475-487 (2014).
- 460 5. Zhou, G., *et al.* Role of AMP-activated protein kinase in mechanism of metformin action. *J*
461 *Clin Invest* **108**, 1167-1174 (2001).
- 462 6. Vogt, J., Traynor, R. & Sapkota, G.P. The specificities of small molecule inhibitors of the
463 TGF β s and BMP pathways. *Cell Signal* **23**, 1831-1842 (2011).
- 464 7. Fullerton, M.D., *et al.* Single phosphorylation sites in Acc1 and Acc2 regulate lipid
465 homeostasis and the insulin-sensitizing effects of metformin. *Nat Med* **19**, 1649-1654 (2013).
- 466 8. Foretz, M., *et al.* Metformin inhibits hepatic gluconeogenesis in mice independently of the
467 LKB1/AMPK pathway via a decrease in hepatic energy state. *J Clin Invest* **120**, 2355-2369
468 (2010).
- 469 9. Miller, R.A., *et al.* Biguanides suppress hepatic glucagon signalling by decreasing production
470 of cyclic AMP. *Nature* **494**, 256-260 (2013).
- 471 10. Madiraju, A.K., *et al.* Metformin suppresses gluconeogenesis by inhibiting mitochondrial
472 glycerophosphate dehydrogenase. *Nature* **510**, 542-546 (2014).
- 473 11. Hasenour, C.M., *et al.* 5-Aminoimidazole-4-carboxamide-1-beta-D-ribofuranoside (AICAR)
474 effect on glucose production, but not energy metabolism, is independent of hepatic AMPK in
475 vivo. *J Biol Chem* **289**, 5950-5959 (2014).
- 476 12. Vincent, M.F., Marangos, P.J., Gruber, H.E. & Van den Berghe, G. Inhibition by AICA
477 riboside of gluconeogenesis in isolated rat hepatocytes. *Diabetes* **40**, 1259-1266 (1991).
- 478 13. Pagliara, A.S., Karl, I.E., Keating, J.P., Brown, B.I. & Kipnis, D.M. Hepatic fructose-1,6-
479 diphosphatase deficiency. A cause of lactic acidosis and hypoglycemia in infancy. *J Clin*
480 *Invest* **51**, 2115-2123 (1972).
- 481 14. Bouskila, M., *et al.* Allosteric regulation of glycogen synthase controls glycogen synthesis in
482 muscle. *Cell Metab* **12**, 456-466 (2010).
- 483 15. Ouyang, J., Parakhia, R.A. & Ochs, R.S. Metformin activates AMP kinase through inhibition
484 of AMP deaminase. *J Biol Chem* **286**, 1-11 (2011).
- 485 16. Gidh-Jain, M., *et al.* The allosteric site of human liver fructose-1,6-bisphosphatase. Analysis
486 of six AMP site mutants based on the crystal structure. *J Biol Chem* **269**, 27732-27738 (1994).
- 487 17. Zhang, Y., *et al.* Fructose-1,6-bisphosphatase regulates glucose-stimulated insulin secretion of
488 mouse pancreatic beta-cells. *Endocrinology* **151**, 4688-4695 (2010).
- 489 18. Faupel, R.P., Seitz, H.J., Tarnowski, W., Thiemann, V. & Weiss, C. The problem of tissue
490 sampling from experimental animals with respect to freezing technique, anoxia, stress and
491 narcosis. A new method for sampling rat liver tissue and the physiological values of glycolytic
492 intermediates and related compounds. *Arch Biochem Biophys* **148**, 509-522 (1972).
- 493 19. Erion, M.D., *et al.* MB06322 (CS-917): A potent and selective inhibitor of fructose 1,6-
494 bisphosphatase for controlling gluconeogenesis in type 2 diabetes. *Proc Natl Acad Sci U S A*
495 **102**, 7970-7975 (2005).
- 496 20. Vincent, M.F., Erion, M.D., Gruber, H.E. & Van den Berghe, G. Hypoglycaemic effect of
497 AICARiboside in mice. *Diabetologia* **39**, 1148-1155 (1996).
- 498 21. Guigas, B., *et al.* 5-Aminoimidazole-4-carboxamide-1-beta-D-ribofuranoside and metformin
499 inhibit hepatic glucose phosphorylation by an AMP-activated protein kinase-independent
500 effect on glucokinase translocation. *Diabetes* **55**, 865-874 (2006).

- 501 22. Vincent, M.F., Bontemps, F. & Van den Berghe, G. Substrate cycling between 5-amino-4-
502 imidazolecarboxamide riboside and its monophosphate in isolated rat hepatocytes. *Biochem*
503 *Pharmacol* **52**, 999-1006 (1996).
- 504 23. Hunter, R.W., *et al.* Mechanism of action of compound-13: an alpha-1-selective small
505 molecule activator of AMPK. *Chem Biol* **21**, 866-879 (2014).
- 506 24. Bailey, C.J., Wilcock, C. & Scarpello, J.H. Metformin and the intestine. *Diabetologia* **51**,
507 1552-1553 (2008).
- 508 25. Yoshida, T., *et al.* Metformin primarily decreases plasma glucose not by gluconeogenesis
509 suppression but by activating glucose utilization in a non-obese type 2 diabetes Goto-Kakizaki
510 rats. *Eur J Pharmacol* **623**, 141-147 (2009).
- 511 26. Takashima, M., *et al.* Role of KLF15 in regulation of hepatic gluconeogenesis and metformin
512 action. *Diabetes* **59**, 1608-1615 (2010).
- 513 27. Stepensky, D., Friedman, M., Raz, I. & Hoffman, A. Pharmacokinetic-pharmacodynamic
514 analysis of the glucose-lowering effect of metformin in diabetic rats reveals first-pass
515 pharmacodynamic effect. *Drug Metab Dispos* **30**, 861-868 (2002).
- 516 28. Duca, F.A., *et al.* Metformin activates a duodenal Ampk-dependent pathway to lower hepatic
517 glucose production in rats. *Nat Med* **21**, 506-511 (2015).
- 518 29. Wu, H., *et al.* Metformin alters the gut microbiome of individuals with treatment-naive type 2
519 diabetes, contributing to the therapeutic effects of the drug. *Nat Med* **23**, 850-858 (2017).
- 520 30. Grundemann, D., Gorboulev, V., Gambaryan, S., Veyhl, M. & Koepsell, H. Drug excretion
521 mediated by a new prototype of polyspecific transporter. *Nature* **372**, 549-552 (1994).
- 522 31. Kjobsted, R., *et al.* Prior AICAR stimulation increases insulin sensitivity in mouse skeletal
523 muscle in an AMPK-dependent manner. *Diabetes* **64**, 2042-2055 (2015).
- 524 32. Shaw, R.J., *et al.* The kinase LKB1 mediates glucose homeostasis in liver and therapeutic
525 effects of metformin. *Science* **310**, 1642-1646 (2005).
- 526 33. Patel, K., *et al.* The LKB1-salt-inducible kinase pathway functions as a key gluconeogenic
527 suppressor in the liver. *Nat Commun* **5**, 4535 (2014).
- 528 34. Samuel, V.T., *et al.* Fasting hyperglycemia is not associated with increased expression of
529 PEPCK or G6Pc in patients with Type 2 Diabetes. *Proc Natl Acad Sci U S A* **106**, 12121-
530 12126 (2009).
- 531 35. Cool, B., *et al.* Identification and characterization of a small molecule AMPK activator that
532 treats key components of type 2 diabetes and the metabolic syndrome. *Cell Metab* **3**, 403-416
533 (2006).
- 534 36. Graham, G.G., *et al.* Clinical pharmacokinetics of metformin. *Clin Pharmacokinet* **50**, 81-98
535 (2011).
- 536 37. Christensen, M.M., *et al.* The pharmacogenetics of metformin and its impact on plasma
537 metformin steady-state levels and glycosylated hemoglobin A1c. *Pharmacogenet Genomics*
538 **21**, 837-850 (2011).
- 539 38. Lalau, J.D., Lemaire-Hurtel, A.S. & Lacroix, C. Establishment of a database of metformin
540 plasma concentrations and erythrocyte levels in normal and emergency situations. *Clin Drug*
541 *Investig* **31**, 435-438 (2011).
- 542 39. Bleasby, K., *et al.* Expression profiles of 50 xenobiotic transporter genes in humans and pre-
543 clinical species: a resource for investigations into drug disposition. *Xenobiotica; the fate of*
544 *foreign compounds in biological systems* **36**, 963-988 (2006).
- 545 40. Terada, T., *et al.* Molecular cloning, functional characterization and tissue distribution of rat
546 H⁺/organic cation antiporter MATE1. *Pharm Res* **23**, 1696-1701 (2006).
- 547 41. Gormsen, L.C., *et al.* In Vivo Imaging of Human ¹¹C-Metformin in Peripheral Organs:
548 Dosimetry, Biodistribution, and Kinetic Analyses. *J Nucl Med* **57**, 1920-1926 (2016).
- 549 42. Jensen, J.B., *et al.* [¹¹C]-Labeled Metformin Distribution in the Liver and Small Intestine
550 Using Dynamic Positron Emission Tomography in Mice Demonstrates Tissue-Specific
551 Transporter Dependency. *Diabetes* **65**, 1724-1730 (2016).
- 552 43. Chen, L., *et al.* OCT1 is a high-capacity thiamine transporter that regulates hepatic steatosis
553 and is a target of metformin. *Proceedings of the National Academy of Sciences of the United*
554 *States of America* **111**, 9983-9988 (2014).

- 555 44. Hawley, S.A., Gadalla, A.E., Olsen, G.S. & Hardie, D.G. The antidiabetic drug metformin
556 activates the AMP-activated protein kinase cascade via an adenine nucleotide-independent
557 mechanism. *Diabetes* **51**, 2420-2425 (2002).
- 558 45. Hawley, S.A., *et al.* Use of cells expressing gamma subunit variants to identify diverse
559 mechanisms of AMPK activation. *Cell Metab* **11**, 554-565 (2010).
- 560 46. Argaud, D., Roth, H., Wiernsperger, N. & Leverve, X.M. Metformin decreases
561 gluconeogenesis by enhancing the pyruvate kinase flux in isolated rat hepatocytes. *European*
562 *journal of biochemistry / FEBS* **213**, 1341-1348 (1993).
- 563 47. McCarty, M.F. A proposal for the locus of metformin's clinical action: potentiation of the
564 activation of pyruvate kinase by fructose-1,6-diphosphate. *Med Hypotheses* **52**, 89-93 (1999).
- 565 48. van Poelje, P.D., Dang, Q. & Erion, M.D. Discovery of fructose-1,6-bisphosphatase inhibitors
566 for the treatment of type 2 diabetes. *Curr Opin Drug Discov Devel* **10**, 430-437 (2007).
- 567 49. Tao, H., Zhang, Y., Zeng, X., Shulman, G.I. & Jin, S. Niclosamide ethanolamine-induced
568 mild mitochondrial uncoupling improves diabetic symptoms in mice. *Nat Med* **20**, 1263-1269
569 (2014).
- 570
- 571

572 **FIGURE LEGENDS**

573 **Figure 1. Generation of an AMP-insensitive FBP1 knockin mouse model.** (a) Human FBP1
574 structure (PDBID 1FTA) represented as ribbons and AMP and interacting residues (numbered from
575 the initiator methionine) are shown as sticks. Dashed lines represent hydrogen bonding interactions,
576 whereas residues making hydrophobic contacts are illustrated as sticks and transparent surfaces. Red
577 and blue spheres represent backbone oxygen and nitrogen atoms respectively. (b) Coomassie-stained
578 SDS-PAGE of mouse liver FBPase and recombinant mouse 6HIS-FBP1 preparations with single point
579 mutations designed to disrupt AMP binding. (c) AMP inhibition curves of mouse 6HIS-FBP1 mutants.
580 FBPase activity is expressed as a ratio of the maximum activity in the absence of AMP (V/V_0). IC_{50}
581 values represent the mean \pm SD of three independent measurements on two enzyme preparations. The
582 line graph is representative of the results from a single preparation. (d) Schematic illustrating the
583 targeting strategy used to generate C57BL/6NTac FBP1^{G27P} knockin (KI) mice. Exons and FRT
584 recombination sites are represented by dark grey boxes and triangles respectively. The KI allele
585 containing the G27P mutation in exon 1 is shaded pale grey. Correct recombination was confirmed by
586 Southern blotting of PstI and KpnI digests of genomic DNA isolated from targeted embryonic stem
587 cells with the corresponding 5' and 3' probes (black boxes). Genotyping of the constitutive KI allele
588 was performed by PCR of genomic DNA using primers P1 and P2. (e) Liver biopsies from overnight
589 fasted (16 h) or refed (4 h) FBP1^{WT/WT} (WT) or FBP1^{G27P/G27P} (KI) mice were assayed for *Fbp1* mRNA
590 expression by qPCR (left chart) or FBPase activity (right chart) by spectrophotometric assay. The line
591 graph (below) represents AMP inhibition curves of FBPase activity in liver homogenates expressed as
592 a ratio of the activity in the absence of AMP (V/V_0). Results represent mean \pm SD, n = 5-7 per group.
593

594 **Figure 2. FBP1 G27P knockin mice display normal glucose homeostasis.** (a-e) FBP1^{WT/WT} (WT) or
595 FBP1^{G27P/G27P} (KI) mice were fasted overnight for 16 h (Fasted) or subsequently given free access to
596 standard chow for 4 h (Refed). Blood and liver biopsies were taken and the following parameters
597 determined: blood glucose (a), plasma insulin (b), plasma glucagon (c), plasma leptin (d) and liver
598 glycogen (e). n = 5-7 (WT) and 5-7 (KI) per group. (f) Glucose (2 g.kg⁻¹ *p.o.*) and (g) pyruvate (1 g.kg⁻¹
599 *i.p.*) tolerance was assessed on mice fasted for 16 h. Results represent mean \pm SE, n = 10 per group.
600 (h) Expression of the major enzymes and regulatory components of the gluconeogenic, glycogenic and
601 glycogenolytic pathways in liver samples from fasted or refed animals was determined by Western
602 blotting. Representative results from three mice per group are shown. * $P < 0.05$ (Fasted vs. refed).
603 Statistical significance was determined using unpaired, two-tailed Student's t-test and an alpha level of
604 0.05.
605

606 **Figure 3. FBP1 G27P KI mice are resistant to the hypoglycemic action of an AMP-mimetic**
607 **FBPase inhibitor.** (a) Diagram showing the structure of MB06322 and the active metabolite,
608 MB05032. (b) Mouse and rat FBP1 preparations were assayed for inhibition by AMP (closed
609 symbols) and MB05032 (open symbols). Results represent mean \pm SD, n = 3. * $P < 0.05$ (Mouse vs.
610 rat) (c-g) Vehicle (10:10:80 Solutol HS 15:PEG 400:water) or MB06322 (75 mg.kg⁻¹ *i.p.*) was
611 administered to fasted (16 h) WT (c) or KI (f) mice and blood glucose monitored at the indicated
612 intervals for 3 h. (d, g) Lactate was measured just prior to drug administration and at t = 120 min using
613 a lactate meter. (e) Plasma levels of MB05032 were assayed from blood samples drawn at the end of
614 the protocol (t = 180 min). Results represent mean \pm SE, n = 4-5 per treatment group. * $P < 0.05$
615 (Vehicle vs. MB06322). Statistical significance was determined using unpaired, two-tailed Student's t-
616 test and an alpha level of 0.05.
617

618 **Figure 4. FBP1 G27P KI mice are resistant to the hypoglycemic action of AICAR.** (a) Diagram
619 illustrating the structure of AMP and ZMP. (b-l) AICAR tolerance was determined by administering
620 vehicle (0.9 % saline) or AICAR (250 mg.kg⁻¹ *i.p.*) to fasted (16 h) WT (b, e, g, i) or KI (c, f, h, j)
621 mice. Blood glucose was measured at the indicated timepoints for a period of 3 h. (d) Plasma AICAR,
622 (e, f) blood lactate, (g, h) plasma glucagon and (i, j) plasma insulin were assayed from blood samples
623 drawn at t = 60 min. Results represent mean ± SE, n = 4-8 per treatment group. **P* < 0.05 (Vehicle vs.
624 AICAR). #*P* < 0.05 (WT vs. KI). (k, l) Vehicle (0.9 % saline) or AICAR (250 mg.kg⁻¹ *i.p.*) was
625 administered to fasted (16 h) mice and after 60 min exposure, liver biopsies were taken and assayed
626 for AMPK activation by Western blotting. The blot image depicts three representative mice from each
627 treatment group and a quantitative analysis of pT172 AMPKα phosphorylation from the entire sample
628 set is shown in (l). Results are expressed as pT172 AMPKα/AMPKα ratio normalized to the WT-
629 vehicle group. n = 4-5 per treatment group. **P* < 0.05 (Vehicle vs. AICAR). Statistical significance
630 was determined using unpaired, two-tailed Student's t-test and an alpha level of 0.05.

631
632 **Figure 5. FBP1 G27P KI mice exhibit resistance to the acute glucose-lowering effect of**
633 **metformin.** (a, b) Vehicle (water) or metformin (250 mg.kg⁻¹ *p.o.*) was administered to fasted (16 h)
634 mice and after 45 min, glucose tolerance (2 g.kg⁻¹ *i.p.*) was assessed by monitoring blood glucose over
635 a period of 2 h. Results represent mean ± SE, n = 18 (WT-vehicle), 17 (WT-metformin), 15 (KI-
636 vehicle) and 15 (KI-metformin). **P* < 0.05 (vehicle vs. metformin). (c-e) Mice were fasted for 16 h
637 and dosed with vehicle (water) or metformin (250 mg.kg⁻¹ *p.o.*). After 1 h exposure, blood and liver
638 biopsies were taken and assayed for metformin (c). (d) Western blotting of ACC and AMPKα
639 phosphorylation in livers from vehicle and metformin-treated mice. Representative results from three
640 mice per group are shown. (e) Quantitative analysis of pT172 AMPKα. Results are expressed as
641 pT172 AMPKα/AMPKα ratio normalized to the WT-vehicle group. n = 5. (f) Arterial blood glucose
642 and glucose infusion rate (GIR) (g) during metformin-euglycemic clamps in FBP1^{WT/WT} (WT) or
643 FBP1^{G27P/G27P} (KI) mice. Animals were fasted for 5 h and infused *i.v.* with metformin (3.75 mg.kg⁻¹
644 ¹.min⁻¹) and a variable infusion of 50 % glucose to maintain euglycemia at 120 mg.dl⁻¹ over a period of
645 120 min. **P* < 0.05 (WT vs. KI). (h) Plasma and liver metformin concentrations at the end of the
646 clamp period. (i-l) Rates of endogenous glucose production (EndoRa) (i), gluconeogenesis (GNG) (j),
647 glycogenolysis (GYG) (k) and glucose disappearance (Rd) (l) during the resting period (5 h fasted)
648 and steady state of the metformin clamp (average from 100-120 min). Results represent mean ± SE, n
649 = 8 (WT-resting), 8-9 (WT-clamp), 10 (KI-resting) and 9-11 (KI-clamp). **P* < 0.05. Statistical
650 significance was determined using unpaired, two-tailed Student's t-test and an alpha level of 0.05.

651
652 **Figure 6. FBP1 G27P KI mice are resistant to the glucose lowering effects of metformin in an**
653 **obesity-induced model of diabetes.** Body mass (a) and cumulative food intake (b) for FBP1^{WT/WT}
654 (WT) and FBP1^{G27P/G27P} (KI) fed a 60 % Kcal high fat diet *ad libitum* over a period of eight weeks. (c-
655 f) Glucose tolerance (1.5 g.kg⁻¹ *i.p.*) (Glycemia in c and corresponding AUC in d), plasma insulin (e)
656 and triglyceride (TG) (f) were assessed after eight weeks of dietary intervention. Results represent
657 mean ± SE (a-c), n = 10-12 per group. (g, h) After 10 weeks of dietary intervention mice were fasted
658 for 16 h, administered vehicle (water) or metformin (250 mg.kg⁻¹ *p.o.*) and blood glucose measured
659 after 2 h. n = 13 (WT-vehicle), 15 (WT-metformin), 8 (KI-vehicle) and 12 (KI-metformin). **P* < 0.05
660 (Vehicle vs. metformin). #*P* < 0.05 (Resting vs. 120 min) (i-k) After 12 weeks of dietary intervention
661 mice were fasted for 16 h, administered vehicle (water) or metformin (250 mg.kg⁻¹ *p.o.*) and liver
662 biopsies were taken after 2 h of drug treatment. Liver metformin (i), pT172 AMPKα phosphorylation
663 (expressed as pT172 AMPKα/AMPKα ratio normalized to the WT-vehicle group) (j), and cAMP (k)
664 are shown. n = 6-7 (WT-vehicle), 6 (WT-metformin), 6-7 (KI-vehicle) and 6 (KI-metformin). **P* <

665 0.05 (Vehicle vs. metformin). # $P < 0.05$ (WT vs KI). Statistical significance was determined using
666 unpaired, two-tailed Student's t-test and an alpha level of 0.05.
667

668 **Online Methods**

669

670 **Materials**

671

672 *E.coli* strain DF657 was sourced from the CGSC (Coli Genetic Stock Centre, Yale University) and
673 BL21-CodonPlus(DE3)-RIL were from Agilent. Casamino acids were from BD Biosciences. Talon®
674 cobalt IMAC resin was from Clontech. P11 and P81 phosphocellulose and BA-85 nitrocellulose were
675 from Whatman. Leupeptin, pepstatin A and isopropyl-β-D-thiogalactopyranoside (IPTG) were from
676 Serva. GST-HRV3C protease was from the Division of Signal Transduction Therapy (DSTT,
677 Dundee). Fructose-2,6-bisphosphate (F-2,6-P₂) (30 % purity) was from Toronto Research Chemicals.
678 Higher purity F-2,6-P₂ was kindly provided by Mark Rider (Université catholique de Louvain,
679 Belgium). FBPase-1 inhibitor was from Santa Cruz. MB06322 was synthesised by SpiroChem
680 (Zurich, Switzerland) as previously described¹. MB05032 was from MedChem Express. 1-methoxy-5-
681 methylphenazinium methyl sulfate was from Applichem. Sypro Orange and sterile 20 % (w/v) glucose
682 were from Life Technologies. 2',3'-O-trinitrophenyl-adenosine-5'-monophosphate (TNP-AMP),
683 2'/3'-O-(2-aminoethyl-carbamoyl)-adenosine-5'-monophosphate (2'/3'-EDA-AMP)-agarose and Z
684 (AICAR) nucleotide standards were from Jena Bioscience. KAPA2G Fast HotStart genotyping mix
685 was from Kapa Biosystems. Metformin-HCl, 5,5-diphenylhydantoin, Solutol (Kolliphor) HS 15, PEG
686 (Kollisolv) 400 and all HPLC-grade solvents and additives were from Sigma. Microcystin-LR was
687 from Enzo Life Sciences. NADH and AICAR (5-amino-1-(β-D-ribofuranosyl)-1H-imidazole-4-
688 carboxamide) were from Apollo Scientific Ltd. Acetyl-CoA, trilithium salt was from Roche Life
689 Science. Immobilon-P PVDF membrane was from Merck Millipore. Sephadex G-25, Blue Sepharose
690 6 FF, Superdex 10/300 GL and enhanced chemiluminescent reagent were from GE Healthcare. [γ -³²P]-
691 ATP, [U-¹⁴C]-uridine diphosphate glucose and [U-¹⁴C]-glucose-1-phosphate were from Perkin Elmer.
692 ²H₂O and [6,6-²H₂]-glucose were from Cambridge Isotope Laboratories (Tewksbury, MA). AMARA
693 substrate peptide (NH₂-AMARAASAAALARRR-COOH) was synthesized by GL Biochem
694 (Shanghai). Chicken muscle was sourced from a local supermarket and rabbit muscle was purchased
695 from Harlan UK Ltd. Unless otherwise stated, all other reagents were from Sigma.

696

697 **Antibodies**

698

699 PEPCK-M (#6924), pS641 GYS (#3891), GYS (#3886), pT389 p70S6K (#9234), p70S6K (#2708),
700 pS240/244 S6 (#2215), S6 (#2217), pS79/S212 ACC1/2 (#3661), ACC1/2 (#3676), pT172 AMPK α 1/2
701 (#2535), AMPK α 1/2 (#2532), AMPK α 1/2 mAb (#2793), pT792 RAPTOR (#2083), RAPTOR
702 (#2280), Fas (#3180), HXK1 (#2024), G6PD (#12263), TBC1D1 (#4629), pS133 CREB (#9198) and
703 streptavidin-HRP (#3999) were from Cell Signaling Technology. G6PT (sc-135479) and FBP1 (sc-
704 32435) were from Santa Cruz Biotechnology. PFKL (ab181064), PKLR (ab171744) and PEPCK-C
705 (ab28455) were from Abcam. GAPDH (G8795) and α -tubulin (T6074) were from Sigma.
706 SLC22A1/OCT1 (#ACT-011) antibody was from Alomone Labs. pS237 TBC1D1 was from Merck
707 Millipore (07-2268). PYGL (15851-1-AP) was from Proteintech. pS15 PYGL (S961A) was from
708 DSTT. AMPK α 1 and AMPK α 2 antibodies used for immunoprecipitation were raised in sheep against
709 C-³⁵⁵TSPPDSFLDDHHLTR³⁶⁹ and C-³⁵²MDDSAMHIPPGLKPH³⁶⁶ (human sequences) respectively.
710 GLUT2 antibody was provided by Bernard Thorens (University of Lausanne, Switzerland).
711 GCK/HXK4 antibody was provided by Mark Magnuson (Vanderbilt University, TN). GCKR antibody
712 was from Masakazu Shiota (Vanderbilt University, TN). G6PC antibody was provided by Giles
713 Mithieux (University of Lyon, France). pS33 PFKFB1 antibody was provided by Jianxin Xie (Cell
714 Signaling Technology). PFKFB1 antibody was provided by Simone Baltrusch (University of Rostock,
715 Germany). pS8 GYS2 antibody was provided by Joan Guinovart (University of Barcelona, Spain).
716 HRP-coupled and Alexa Fluor 680/Alexa Fluor 790-labelled secondary antibodies were from Jackson
717 Immunoresearch.

718

719

720 **Primers.** Oligonucleotides were synthesized by Life Technologies.

721

722 Genotyping primers for C57BL/6N^{G27P} mice:

723 for-TGACAGTTAAGATTCTGCTCTGC, rev-TTAGGGATGATACTGAATTAGAAGC

724

Target	Forward	Reverse
<i>Fasn</i>	AGCGGCCATTTCATTGCC	CCATGCCCAGAGGGTGGTTG
<i>Fbp1</i>	GTGTCAACTGCTTCATGCTG	GAGATACTCATTGATGGCAGGG
<i>Foxo1a</i>	CTACGAGTGGATGGTGAAGAGC	CCAGTTCCTTCATTCTGCACTCG
<i>G6pc</i>	ACTGTGGGCATCAATCTCCTC	CGGGACAGACAGACGTTTCAGC
<i>Gck</i>	GCATCTCTGACTTCCTGGACAAG	CTTGGTCCAGTTGAGCAGGATG
<i>Pck1</i>	CCATCACCTCCTGGAAGAACA	ACCCTCAATGGGTACTCCTTCTG
<i>Pparg1c</i>	ATACCGCAAAGAGCACGAGAAG	CTCAAGAGCAGCGAAAGCGTCACAG
<i>18S</i>	GTAACCCGTTGAACCCCAT	CCATCCAATCGGTAGTAGCG

725

726 **Cloning and mutagenesis.** Mouse *Fbp1* (NCBI reference AJ132693.1) was amplified from IMAGE
727 EST 5054854 using KOD Hot Start DNA Polymerase (Merck Millipore) and cloned into the *BamHI*
728 *NotI* sites to produce pET28a 6HIS-FBP1 and pET15 6HIS-HRV3C-FBP1. Mutations were created
729 following the QuikChange method (Agilent) but using KOD Hot Start DNA Polymerase. The
730 phosphatase domain of mouse 6-phosphofructo-2-kinase/fructose-2,6-biphosphatase 1 (NCBI
731 reference NM_008824.3) covering amino acids 251-440 was amplified from mouse liver RNA
732 (Agilent #736009-41) using GoTaq 1-step RT-qPCR kit (Promega). The resulting PCR product was
733 ligated into pGEX-6P-1 vector (GE Healthcare) as a *BamHI-NotI* fragment. Spinach chloroplast
734 fructose-1,6-bisphosphatase 58-415 was cloned from a synthetic fragment (GeneArt Strings, based on
735 Uniprot P22418) and ligated into a modified pET-15b plasmid as a *BamHI-NotI* fragment. The
736 sequence of all constructs was verified by in-house sequencing using the BigDye® Terminator 3.1 kit
737 on a 3500xL Genetic analyzer (ABI-Invitrogen).

738

739 **Preparation of rFBP1.** 6HIS-FBP1 was expressed in the *Fbp*-null *E.coli* strain, DF657(DE3) as
740 described by Giroux². DF657 was sourced from the CGSC (Yale University, CT) and the DE3 lysogen
741 prepared using the λDE3 lysogenization kit (Novagen #69734). Cells were transformed with pET28a
742 FBP1 and cultured in minimal media (M9 salts, 2 mM MgSO₄, 0.4 % (w/v) glycerol, 5 μg/ml
743 thiamine-HCl, 0.5 % (w/v) casamino acids and 50 μg/ml kanamycin) overnight at 37°C. Minimal
744 media (0.5 – 1 L containing 25 μg/ml kanamycin) was inoculated 1:40 with the starter culture and
745 induced with 0.4 mM IPTG at OD₆₀₀ ~ 0.4 for 16 h at 37°C. Cells were lysed in 5 ml/g 50 mM
746 phosphate pH 7, 150 mM NaCl, 0.5 mM TCEP, 0.2 mM PMSF and 5 μg/ml leupeptin by sonication (1
747 min, 40 % amplitude) and clarified at 20,000 g for 20 min at 4°C. 6HIS-FBP1 was batch bound to Co⁺-
748 charged IMAC resin (Talon®) for 30 min at 4°C, washed with 10 vol. lysis buffer, 10 vol. 5 mM
749 imidazole and eluted with 5 vol. 150 mM imidazole. Preparations were exchanged into 50 mM
750 imidazole pH 7.4, 0.3 M KCl, 0.2 mM EDTA and 0.5 mM TCEP over Sephadex G-25, concentrated
751 using 10 kD MWCO centrifugal devices (Sartorius Vivaspin) and stored at -20°C in 50 % (v/v)
752 glycerol. The presence of imidazole in concentrated solutions of 6HIS-FBP1 was essential to prevent
753 aggregation. Untagged FBP1 was prepared by on-column cleavage of 6HIS-LEVLQ*GPGS-FBP1
754 (constructed in pET15 and prepared as described above) with 50 μg HRV-3C protease per mg 6HIS-
755 FBP1 in 50 mM TES pH 7.4, 150 mM KCl, 0.5 mM TCEP. Preparations were polished over a
756 Superdex 200 10/300GL column equilibrated with 50 mM TES pH 7.4, 0.3 M KCl, 1 mM DTT and
757 stored at -20°C in 50 % (v/v) glycerol. Preparations were stable for at least 6 months. As a reference,
758 FBPase was purified from mouse liver essentially as described by Tashima³. Briefly, 20 g liver from
759 C57BL/6N mice was homogenized in four volumes of 20 mM phosphate pH 7, 150 mM KCl, 1 mM
760 EDTA, 1 mM DTT, 0.5 mM PMSF, 2 μg/ml leupeptin and clarified at 10,000 g for 20 min at 4°C. The
761 supernatant was subjected to heat denaturation at 60°C for 1 min and centrifuged at 20,000 g for 20

762 min at 4°C. The supernatant was subjected to a 55-75 % ammonium sulfate cut and the resulting pellet
 763 dissolved in 1 mM EDTA and dialyzed overnight against 10 mM sodium malonate pH 6.2, 1 mM
 764 EDTA (Buffer A). FBPase was batch bound to 30 g P11 phosphocellulose, washed with 300 ml Buffer
 765 A under suction and transferred to an XK26/20 column. The resin was washed with buffer A
 766 containing 50 mM NaCl until $A_{280} < 0.01$ and FBPase was eluted with 2 mM fructose-1,6-
 767 bisphosphate (F-1,6-P₂) and 20 μM 5'-adenosine monophosphate (AMP). Positive fractions were
 768 dialyzed against Buffer A, the pH adjusted to 5.8 with malonic acid and applied to a 1.6 × 10 cm
 769 column of Blue Sepharose FF (C16/20). The column was washed with 10 mM sodium malonate pH
 770 5.8, 1 mM EDTA and eluted with 1 mM F-1,6-P₂ and 1 mM AMP. The preparation was polished over
 771 a Superdex 200 10/300GL column equilibrated with 20 mM phosphate pH 7, 150 mM KCl, 1 mM
 772 EDTA and stored in 50 % (v/v) glycerol at -20°C.

773
 774 **FBPase assay.** Fructose-1,6-bisphosphatase (EC 3.1.3.11) activity was determined by monitoring the
 775 formation of fructose-6-phosphate (F6P) using a coupled spectrophotometric assay. The specific
 776 activity of rFBP1 was determined in 1 ml reactions containing 50 mM TES pH 7.4, 0.2 mM NADP⁺,
 777 0.1 M KCl, 0.05 mM EDTA, 2 mM (NH₄)₂SO₄, 2 mM MgCl₂, 0.05 % (w/v) BSA, 2 mM 2-
 778 mercaptoethanol, 0.8 U/ml phosphoglucose isomerase and 0.5 U/ml glucose-6-phosphate
 779 dehydrogenase. Reactions were started by the addition of 35 μM F-1,6-P₂ and A₃₄₀ recorded in a Cary
 780 100 spectrophotometer at 30°C. Reaction rates were calculated from the linear phase assuming
 781 $\epsilon(\text{NADPH}) = 6.22 \text{ mM}^{-1} \cdot \text{cm}^{-1}$. 1 U is defined as 1 μmol F6P formed per min at 30°C. Where
 782 appropriate, 1 U/ml AMP deaminase (purified from chicken muscle using P11 phosphocellulose
 783 essentially as described by Smiley⁴) was included to remove contaminating AMP from NADP⁺ as
 784 described by Han⁵. The activity ratio at pH 7.2/9.4 was determined under similar conditions in
 785 reactions buffered with 50 mM bis-tris propane at the appropriate pH. Other kinetic properties were
 786 determined in a 96 well format in non-binding black microplates (Greiner #655900), where the
 787 quantity of NADP⁺ was reduced to 0.15 mM and reactions were monitored by the increase in
 788 fluorescence ($\lambda_{\text{ex}} = 345 \text{ nm}$, $\lambda_{\text{em}} = 465 \text{ nm}$) calibrated by the addition of 5 nmol F6P. $K_m(\text{F-1,6-P}_2)$ was
 789 determined at 2 mM Mg²⁺ and fitted to equation 1:

791

$$V = \frac{V_m [S] \left(1 + \frac{b[S]}{K_s} \right)}{K_m + [S] \left(1 + \frac{[S]}{K_s} \right)} \quad (\text{Eq.1})$$

792
 793 Where: V = initial velocity, V_m = maximum velocity, [S] = F-1,6-P₂ conc., K_m = Michaelis constant for S, K_s =
 794 apparent substrate inhibition constant and b = factor determining maximum activity at high [S].

795
 796 K_m(Mg²⁺) was determined at 35 μM F-1,6-P₂ and fitted to equation 2:

797

$$V = \frac{V_m [S]^h}{K_m^h + S^h} \quad (\text{Eq.2})$$

798
 799 Where: V = initial velocity, V_m = maximum velocity, [S] = Mg²⁺ conc., K_m = Michaelis constant for S and h =
 800 hill coefficient.

801
 802 IC₅₀ for inhibitory compounds was determined at 2 mM Mg²⁺, 35 μM F-1,6-P₂ and fitted to equation 3:

803

$$\frac{V}{V_0} = \frac{V_m}{\left[1 + \left(\frac{I}{I_{0.5}} \right)^h \right]} \quad (\text{Eq.3})$$

804
 805
 806 Where: V = initial velocity, V₀ = maximum velocity in the absence of inhibitor, I = conc. inhibitor, I_{0.5} = conc. of
 807 inhibitor that gives 50 % inhibition and h = hill coefficient.

808 Stock solutions of F-1,6-P₂ were standardized by enzymatic assay in reactions containing 50 mM
 809 imidazole pH 7, 0.15 mM NADH, 0.02 U/ml aldolase, 1.2 U/ml triosephosphate isomerase and 0.16
 810 U/ml glycerol-3-phosphate dehydrogenase. Stock solutions of AMP, 5'-inosine monophosphate (IMP)
 811 and 5'-AICAR monophosphate (ZMP) were prepared in 20 mM TES pH 7.4, neutralized with NaOH
 812 and standardized by UV absorbance in 0.1 M phosphate pH 7 at A₂₅₉ (ε_{AMP} = 15.4 mM⁻¹.cm⁻¹), A₂₄₉
 813 (ε_{IMP} = 12 mM⁻¹.cm⁻¹) and A₂₆₅ (ε_{ZMP} = 12.5 mM⁻¹.cm⁻¹) respectively. F-2,6-P₂ is difficult to obtain
 814 commercially and the crude product available from Toronto Research Chemicals was solubilized in 10
 815 mM NaOH and standardized in reactions containing 50 mM HEPES pH 7.1, 5 mM MgCl₂, 0.1 mM
 816 EDTA, 0.15 mM NADP⁺ by sequential addition of 0.1 U/ml glucose-6-phosphate dehydrogenase, 0.2
 817 U/ml phosphoglucose isomerase and 0.25 U/ml GST-FBPase-2 P251-N440 while recording the
 818 increase in A₃₄₀.

819
 820 **Thermal Stability Assays.** TSA was performed on untagged FBP1 preparations using a Roche
 821 LightCycler 480 II. FBP1 was diluted to 0.2 mg/ml in 20 mM HEPES pH 7.4, 100 mM KCl, 1 mM
 822 MgCl₂ and the indicated ligands and 5× Sypro Orange added sequentially. Solutions (20 μl) were
 823 dispensed in quadruplicate into 384-well white plates, sealed with optical tape and centrifuged at 200 g
 824 for 1 min. Fluorescence (λ_{ex} = 465 nm, λ_{em} = 580 nm, Melt factor = 1, Quant factor = 10) was
 825 monitored while the block temperature was ramped from 20°C to 95°C at ~1°C/min (24 acquisitions/°C
 826 in continuous mode). The melting temperature (T_m) was determined from the maximum of the first
 827 derivative of the raw data using Roche Protein Melting software.

828
 829 **TNP-AMP fluorescence spectroscopy.** Titration of 2',3'-O-trinitrophenyl-adenosine-5'-
 830 monophosphate (TNP-AMP) was determined as described by Nelson⁶ using 1 μM FBP1 in 50 mM
 831 tris-acetate pH 7.4, 5 mM F6P, 5 mM P_i and 2 mM MgCl₂ at 25°C. Raw fluorescence (λ_{ex} = 410 nm,
 832 λ_{em} = 535 nm) was corrected for dilution and inner filter effects using equation 4:

$$834 \quad F_{corr} = (F_{obs} - F_{blank}) \cdot \left(\frac{V}{V_0} \right) \cdot 10^{\frac{(A_{410} + A_{535})}{2}} \quad (\text{Eq.4})$$

835
 836 Where F_{corr} is the corrected fluorescence, V is the volume at a specific titration point and V₀ is the initial volume.

837
 838 Data were analyzed by non-linear regression to equation 5:

$$840 \quad \frac{\Delta F}{\Delta F_0} = \frac{(\Delta F_{max} / F_0) \cdot L^h}{K_d + L^h} \quad (\text{Eq.5})$$

841
 842 Where ΔF is the change in fluorescence caused by the addition of ligand (L), F₀ is the initial fluorescence in the
 843 absence of ligand, K_d is the dissociation constant of L and h is the hill coefficient.

844
 845 **Immobilized ligand affinity binding.** FBP1 (2 μg) in 20 mM TES pH 7.4, 100 mM KCl, 1 mM
 846 MgCl₂, 0.1 mM F-1,6-P₂ and 0.01 % (w/v) BRIJ-35 was mixed with 5 μl 2'/3'-O-(2-aminoethyl-
 847 carbamoyl)-adenosine-5'-monophosphate (2'/3'-EDA-AMP)-agarose or unconjugated agarose for 30
 848 min at 4°C. Excess free ligand (0.5 mM AMP) was included as a negative control. Resin was pelleted
 849 at full-speed for 5 s, washed 3× 0.5 ml binding buffer and eluted with 20 μl Laemmli sample buffer.
 850 Samples were denatured at 95°C for 2 min, fractionated by SDS-PAGE and stained with colloidal
 851 Coomassie G-250.

852
 853

854 **Animals.** Animal studies were approved by the local ethics committee and all protocols were
855 approved by the Service Vétérinaire Cantonal (Lausanne, Switzerland) under license VD2841.
856 C57BL/6NTac FBP1^{G27P} mice were generated by Taconic Biosciences GmbH as described in **Fig. 1d**.
857 Animals were kept in a standard temperature and humidity controlled environment on a 12/12 h
858 light/dark cycle and had free access to water and standard chow or 60 kcal% fat diet (Research Diets
859 Inc. D12492) as described. [¹¹C]-metformin positron emission tomography (PET) was performed in
860 accordance with the Danish Animal Experimentation Act and the European convention for the
861 protection of vertebrate animals used for experimental and other purposes and was approved by the
862 Animal Experiments Inspectorate, Denmark. Metformin-euglycemic clamps were completed with the
863 approval of the Vanderbilt Animal Care and Use Committee. Animals were housed on a 12/12 h
864 light/dark cycle in a temperature (23°C) and humidity-stable environment. Mice were maintained on a
865 standard chow diet (5L0D LabDiet, St. Louis, MO). Male mice between the ages of 14-22 weeks were
866 used for all procedures. Basic phenotyping was performed by PhenoPro (Illkirch, France) in a licensed
867 animal facility (agreement #A67-218-40). All experiments were approved by the local ethical
868 committee (Com⁷Eth, accreditations #2014-011), and were supervised by B.P.D. or M.F.C. who are
869 qualified in compliance with the European Community guidelines for laboratory animal care and use
870 (2010/63/UE). For glucose tolerance test, pyruvate tolerance test, metformin tolerance test, AICAR
871 injection and MB06322 injection, the appropriate sample size was estimated to be 8-10 based on a
872 power calculation assuming $\alpha = 0.05$, power = 0.8 and variance from previous studies. However,
873 based on pilot experiments, responses to some of the compounds were much larger than anticipated
874 and less animals were required as indicated in figure legends. Animals were arbitrarily but not
875 randomly assigned to experimental groups and investigators were unblinded.

876
877 **Tissue homogenization.** Liver biopsies were powdered in a liquid nitrogen cooled mortar and pestle
878 and homogenized in 10 volumes of extraction buffer using a rotor-stator homogenizer (Polytron,
879 Kinematica AG). For Western blotting and assay of G6PC, PK and FBP1, tissues were homogenized
880 in 50 mM tris-HCl pH 7.5, 0.27 M sucrose, 1 mM EDTA, 1 % (w/v) Triton X-100, 20 mM glycerol-2-
881 phosphate, 50 mM NaF, 5 mM Na₄P₂O₇, 0.5 mM PMSF, 1 µg/ml leupeptin, 1 µg/ml pepstatin A, 1
882 µg/ml aprotinin, 1 µM microcystin-LR, 1 mM DTT and clarified at 3500 g for 5 min at 4°C. Glycerol-
883 2-phosphate was omitted for extracts used for assay of GS and GP. DTT was omitted for extracts
884 prepared for the assay of CS and PC. For GCK, PFK and PEPCK-C assays, tissues were gently
885 homogenized in 50 mM HEPES-KOH pH 7.4, 100 mM KF, 15 mM EGTA, 5 % (w/v) glycerol, 1
886 µg/ml leupeptin, 1 µg/ml pepstatin A, 1 µg/ml aprotinin and 5 mM DTT and centrifuged at 100,000 g
887 for 30 min to prepare a cytosolic fraction free of mitochondrial and microsomal fragments. Skeletal
888 muscle biopsies were powdered in a liquid nitrogen cooled Bessman pulverizer and homogenized in
889 10 volumes of Triton X-100 extraction buffer supplemented with 50 mM KCl to prevent gelling.

890
891 **Western blotting.** Tissue extracts were denatured in Laemmli buffer at 95°C for 2 min, fractionated
892 by tris-glycine SDS-PAGE and transferred to PVDF membrane at 100 V for 1 h in Towbin buffer (25
893 mM tris, 192 mM glycine, 10 % (v/v) methanol). Membranes were blocked with 5 % (w/v) skimmed
894 milk in TBS-T (20 mM tris-HCl pH 7.5, 137 mM NaCl, 0.1 % (v/v) Tween-20) for 1 h at room
895 temperature and incubated in primary antibodies prepared in TBS-T containing 5 % (w/v) BSA
896 overnight at 4°C. Membranes were developed using HRP-conjugated secondary antibodies and ECL
897 reagent. For integral membrane proteins (GLUT2, G6PC and G6PT) samples were not boiled, but
898 heated at 37°C for 30 min. Pyruvate carboxylase was detected using HRP-conjugated streptavidin.
899 OCT1 (SLC22A1) was detected by immunoprecipitation from 200 µg detergent extracts with 2 µg
900 anti-OCT1 (Alomone ACT-011) and 5 µl protein G-Sepharose for 2 h at 4°C. Immune complexes
901 were washed 3× 1 ml lysis buffer and eluted with 20 µl Urea-SDS sample buffer (62.5 mM tris-HCl
902 pH 6.8, 2 % (w/v) SDS, 0.5 mM EDTA, 6 M urea, 0.01 % (w/v) bromophenol blue and 10 % (w/v)
903 glycerol) for 1 h at RT. Specificity of detection was confirmed using liver extracts from OCT1 KO
904 mice (provided by Niels Jessen, Aarhus University Hospital, Denmark). Quantitative blotting was
905 performed using detection with either infrared fluorescent secondary antibodies (AF680 and AF790)
906 on nitrocellulose membranes using an Odyssey CLx infrared imaging system (Li-COR) or developed
907 films following ECL detection were scanned and quantitated by densitometry using ImageJ.

908 **Metabolic phenotyping.** Mice were weighed and food consumption monitored on the same day. Mice
909 were starved for 16 h, starting at 17:00 on the previous day so that all procedures commenced at 09:00
910 the following morning. Blood glucose was monitored using a glucometer (AlphaTRAK 2, Abbott
911 Logistics B.V.) on venous blood drawn from the tail. Blood lactate was assayed using a meter (Lactate
912 Pro 2, Arkray Inc.). The genotype of experimental animals was confirmed by PCR on 1 μ l blood lysed
913 in 20 μ l 20 mM NaOH, 60 % (w/v) PEG-200⁷ using KAPA2G polymerase. Glucose tolerance was
914 determined by administration of 2 g.kg⁻¹ D-glucose *p.o.* or *i.p.* from a 20 % (w/v) glucose solution
915 after 16 h fast. Pyruvate tolerance was determined by administration of 1 g.kg⁻¹ pyruvate (free acid)
916 *i.p.* from a 12.7 % (w/v) sodium pyruvate solution (pH 6) after a 16 h fast. The pyruvate stock solution
917 was standardized by assay in 50 mM phosphate pH 7, 0.15 mM NADH and 0.1 U/ml lactate
918 dehydrogenase. AICAR tolerance was determined by administration of 250 mg.kg⁻¹ *i.p.* from a 12.5
919 mg.ml⁻¹ solution in 0.9 % (w/v) saline after a 16 h fast. The acute glucose lowering effect of MB06322
920 was assessed by administration of 75 mg.kg⁻¹ *i.p.* from a 7.5 mg.ml⁻¹ solution in a vehicle composed of
921 10:10:80 Solutol HS 15:PEG 400:water (Compound was dissolved in PEG 400 by gentle
922 heating/sonication, combined with warm liquid Solutol HS 15 and dispersed in water). Energy
923 expenditure, food intake and spontaneous activity (beam-break) was determined by indirect
924 calorimetry (Labmaster, TSE Systems GmbH, Germany). Following a 3 h acclimatization period, mice
925 were monitored for a 21 h period from 14:00 on day 1 to 23:00 on day 2 (12/12 h light/dark cycle at
926 21 \pm 2°C).

928 **Plasma metabolites.** Blood was drawn by tail bleeding into lithium heparin coated capillaries
929 (Sarstedt Microvette CB-200) and plasma prepared by centrifugation at 3,000 g for 5 min at 4°C.
930 Plasma was stored at -80°C prior to analysis. Insulin and glucagon were determined by sandwich
931 ELISA using kits from Mercodia (#10-1249-01 and #10-1281-01). Leptin was measured using an
932 ELISA from Merck Millipore (#EZML-82K). Triglyceride was determined using an enzymatic assay
933 from Sigma (TR0100).

935 **Metformin tolerance test.** Animals were starved for 16 h and 250 mg.kg⁻¹ metformin-HCl
936 administered *p.o.* by gavage. After 45 min, resting blood glucose (t = 0) was recorded and 2 g.kg⁻¹
937 glucose was administered *i.p.* Blood glucose was monitored at t = 20, 40, 60 and 120 min. At the end
938 of the procedure ~30 μ l of blood was drawn into heparinized capillaries for determining plasma
939 metformin concentration.

941 **Metformin assay.** Metformin was assayed in plasma and tissues by ion-pair reverse phase
942 chromatography on a Dionex Ultimate-3000 RS HPLC essentially as described by Zarghi⁸. Plasma
943 was deproteinized with three volumes 80 % (v/v) acetonitrile containing 5 μ g/ml 5,5-
944 diphenylhydantoin as internal standard. Protein was pelleted at 10,000 g for 5 min and the supernatant
945 used directly. Standards were prepared by spiking metformin (1 mg/ml standard prepared in methanol
946 and stored at 4°C) into drug-free heparinized plasma (Innovative Research Inc. #IMS-C57BL6-N) so
947 that the final concentration after solvent extraction ranged from 0.3 to 5 μ g/ml. Tissue samples were
948 powdered in a liquid nitrogen cooled mortar and pestle and homogenized with 10 volumes 10 mM
949 NaOH using a bead mill (Qiagen TissueLyser II, 2 \times 2 min at 30 Hz) and 100 μ l was extracted with 1
950 ml 1:1 acetonitrile:methanol containing 5 μ g/ml 5,5-diphenylhydantoin. Samples were centrifuged at
951 16,000 g for 10 min and 0.3 ml supernatant was evaporated in a Speedvac at 45°C. The residue was
952 dissolved in 100 - 200 μ l 40 % (v/v) acetonitrile and particulate material removed by centrifugation
953 before analysis. Standards were prepared by spiking metformin into alkaline tissue extracts from drug-
954 free animals so that the final concentration ranged from 0.3 to 5 μ g/ml. Samples and standards (20 μ l)
955 were injected onto a Synchronis 150 \times 4.6 mm, 5 μ m C18 column (Thermo 97105-154630) with a
956 10 \times 4.0 mm guard column (Thermo 97105-014001) equilibrated with mobile phase containing 10 mM
957 NaH₂PO₄, 10 mM SDS pH 5.1 and 40 % (v/v) acetonitrile at 1.3 ml/min at 26°C. Metformin and 5,5-
958 diphenylhydantoin were resolved isocratically with retention times of 4.0 and 4.4 min and monitored
959 by UV absorbance (235 nm). Chromatograms were acquired and integrated using Chromeleon v7.1.
960 Results for tissue metformin are uncorrected for blood contamination. For correction of apparent drug
961 tissue concentrations for residual blood volume, tissues were homogenized in 10 volumes ice-cold 40
962 mM potassium phosphate pH 8.1 and blood content determined by assaying the pseudoperoxidase

963 activity of haemoglobin⁹ in reactions containing 85 mM NaCl, 5.8 M acetic acid, 0.83 mM EDTA, 33
964 mM chlorpromazine and 0.6 % H₂O₂ assuming an average haematocrit of 46.6 %. Reactions were
965 monitored at A₅₂₅ and a standard curve prepared using a reference sample of whole mouse blood
966 collected in 4 mM EDTA. Metformin was extracted from homogenates in phosphate buffer and
967 assayed as described above.

968
969 **AICAR assay.** Blood was drawn into EDTA capillaries and immediately supplemented with 25 µM
970 dipyridamole and 25 nM A13457 to prevent further uptake and metabolism of AICAR by
971 erythrocytes¹⁰. Plasma was deproteinized with three volumes 0.4 N PCA and pelleted at 16,000 g for 5
972 min at 4°C. Supernatant was neutralized with 0.16 volumes 2 N KHCO₃ and solid KClO₄ removed at
973 16,000 g for 5 min. Standards were prepared by spiking AICAR into drug-free plasma in the range 0 –
974 100 µM. Samples/standards (20 µl) were injected onto a Synchronis 150×4.6 mm, 5 µm C18 column
975 with a 10×4.0 mm guard column equilibrated with mobile phase containing 95:5 10 mM phosphate pH
976 8.2:acetonitrile at 1 ml.min⁻¹ at 26°C. AICAR was resolved isocratically with a retention time of 3.2
977 min and monitored at A₂₆₀. Chromatograms were acquired and integrated using Chromeleon v7.1
978

979 **MB05032 assay.** Plasma was deproteinized with two volumes methanol and pelleted at 16,000 g for
980 10 min at 4°C. Standards were prepared by spiking MB06322 and MB05032 (1 mM solutions in
981 methanol) into the methanol precipitant so that the effective plasma concentration ranged from 0 to 80
982 µM. Samples and standards (20 µl) were injected onto a Synchronis 150×4.6 mm, 5 µm C18 column
983 with a 10×4.0 mm guard column equilibrated with mobile phase (A – 20 mM phosphate pH 6.2, 10 %
984 acetonitrile) at 1.5 ml.min⁻¹ at 40°C. The column was resolved with an acetonitrile gradient (B – 80 %
985 acetonitrile): 0 min – 0 % B, 1 min – 0 % B, 13 min – 100 % B, 15 min – 0 % B and re-equilibrated
986 with A for 8 min. Peaks were detected at A₃₀₀. Water used for mobile phase preparation was filtered
987 through Empore SBD-XC cartridge filters to remove impurities and improve baseline stability.
988 Chromatograms were acquired and integrated using Chromeleon v7.1.

989
990
991 **Metformin-euglycemic clamp.** Prior to the onset of the study an estimation of the required sample
992 size was determined according to:

993
994
$$n = (z_{\alpha/2} + z_{1-\beta})^2 (s \cdot \delta^{-1})^2$$

995

996 where the level of significance was $\alpha = 0.05$ and desired power was $1-\beta = 0.8$. The quantities $z_{\alpha/2}$ and
997 $z_{1-\beta}$ are critical values from the normal distribution being 1.96 and 0.8416, respectively. The sampled
998 standard deviation, s , has a value of 2 mg.kg⁻¹.min⁻¹. This quantity was used as initial studies in our
999 laboratory using stable isotopes to quantify *in vivo* EndoRa in the fasted mouse provided a standard
1000 deviation of 2 mg.kg⁻¹.min⁻¹. δ (2 mg.kg⁻¹.min⁻¹) represents the difference we aimed to identify for
1001 EndoRa. As such, the resulting sample size rounded off at $n = 8$. Experimenters were blinded to the
1002 genotype until the conclusion of the study. Values were excluded from means reported based on the
1003 following pre-determined exclusion criteria:

- 1004
- 1005 1. Following completion of metformin clamps for all mice designated for study the glucose infusion
1006 rates (GIR) were assessed. Any mouse that displayed GIR outliers during the steady state sampling
1007 period (100-120 minutes) was removed from any further analysis. Outliers were designated as those
1008 with values ± 1.5 standard deviations from the group mean of a specific time point.
1009
 - 1010 2. Estimated glucose fluxes (EndoRa, Rd, gluconeogenesis and glycogenolysis) were excluded from
1011 reported means if the value was ± 2 standard deviations from the group mean.
1012

1013 Mice were chronically catheterized approximately seven days prior to study, as described previously¹¹.
1014 Briefly, catheters were implanted in the carotid artery and jugular vein for sampling and infusing,
1015 respectively. Animals were housed individually post-surgery and monitored for distress. Prior to
1016 study, mice were within 10 % of pre-surgery weight. On the day of study, mice were placed in bedded
1017 containers without food or water at 07:00 (t = -300 min), five hours prior to initiation of the clamp. An

1018 arterial blood sample (80 μ l) was drawn for evaluating the unlabeled, natural isotopic abundance of
1019 glucose after three hours of fasting ($t = -120$ min). Subsequently, a bolus of $^2\text{H}_2\text{O}$ (99.9 %) was
1020 delivered over 25 minutes to enrich total body water to 4.5 %. A $[6,6\text{-}^2\text{H}_2]\text{glucose}$ prime (80 $\text{mg}\cdot\text{kg}^{-1}$)
1021 was dissolved in the bolus. Following the prime, $[6,6\text{-}^2\text{H}_2]\text{glucose}$ was continuously infused (0.8
1022 $\text{mg}\cdot\text{kg}^{-1}\cdot\text{min}^{-1}$) for the remainder of the fasting period. An arterial blood sample (110 μ l) was taken to
1023 determine basal glucose kinetics, arterial glucose and insulin ($t = -5$ min). Metformin was delivered as
1024 a continuous infusion (1.875 or 3.75 $\text{mg}\cdot\text{kg}^{-1}\cdot\text{min}^{-1}$) followed by a variable infusion of 50 % dextrose
1025 (8 % $[6,6\text{-}^2\text{H}_2]\text{glucose}$) to clamp blood glucose levels at 120 $\text{mg}\cdot\text{dl}^{-1}$. All infused solutions were
1026 prepared in a 4.5 % $^2\text{H}_2\text{O}$ -saline solution. Blood glucose was monitored (AccuCheck; Roche
1027 Diagnostics, Indianapolis, IN) every 10 minutes and donor erythrocytes were infused to maintain
1028 hematocrit levels during the study. Three arterial blood samples (~ 100 μ l each) were obtained during
1029 the clamp steady-state period, 90 min after metformin infusion was initiated for determination of
1030 glucose fluxes as well as arterial glucose, insulin and/or metformin levels. Plasma was stored at -20°C
1031 until analysis. Mice were rapidly euthanized through cervical dislocation immediately after the final
1032 steady-state sample. Tissues were rapidly dissected (within 30 s), freeze-clamped in liquid nitrogen
1033 and stored at -80°C until further analysis.

1034
1035 **Preparation of glucose derivatives for GC-MS analysis.** Plasma samples were separated into three
1036 aliquots. Each aliquot was derivatized separately to obtain di-*O*-isopropylidene propionate, aldonitrile
1037 pentapropionate, and methyloxime pentapropionate derivatives of glucose as previously described^{12,13}.

1038
1039 **GC-MS analysis.** GC-MS analysis employed an Agilent 7890A gas chromatography system with an
1040 HP-5ms capillary column (Agilent J&W Scientific) interfaced with an Agilent 5975C mass
1041 spectrometer and was executed as previously described¹² with minor modifications. Injection volumes
1042 were 1 μ l with purge flow times between 20 and 120 s. A custom MATLAB function was used to
1043 integrate each derivative peak in order to obtain mass isotopomer distributions (MIDs) for the
1044 following ion ranges: aldonitrile, m/z 173–178, 259–264, 284–289, and 370–375; methyloxime, m/z
1045 145–149; di-*O*-isopropylidene, m/z 301–308. MIDs of each fragment were averages of two injections
1046 per sample. Root mean square error was determined to provide uncertainty and was calculated by
1047 comparing the MIDs of unlabeled glucose samples to the theoretical MIDs obtained from the known
1048 abundances of naturally occurring isotopes.

1049
1050 **Glucose positional deuterium enrichment analysis.** The positional deuterium enrichment at each
1051 carbon of glucose was determined by least-squares regression as previously described¹³ using the six
1052 glucose fragments, all glucose isotopomers up to $M+2$, and INCA software¹⁴ (available at
1053 <http://mfa.vueinnovations.com/mfa>). Goodness of fit was assessed by a chi-square test and confidence
1054 intervals of 95 % were determined as previously described^{12,15}. Fits were accepted according to a chi-
1055 square test ($P = 0.05$) with nine degrees of freedom.

1056
1057 **Glucose Kinetics.** The infusion rate of $[6,6\text{-}^2\text{H}_2]\text{glucose}$ and model-derived, plasma $[6,6\text{-}^2\text{H}_2]\text{glucose}$
1058 enrichment were used to determine glucose turnover (R_t). Assuming steady state conditions, glucose
1059 disappearance (R_d ; $\text{mg}\cdot\text{kg}^{-1}\cdot\text{min}^{-1}$) is equivalent to R_t . Endogenous glucose production (EndoRa;
1060 $\text{mg}\cdot\text{kg}^{-1}\cdot\text{min}^{-1}$) was calculated by subtracting the glucose infusion rate (GIR) from total R_t . The
1061 model-derived positional deuterium enrichment at carbon 5 (D5) and carbon 2 (D2) of plasma glucose
1062 allowed the fractional contribution of gluconeogenesis and glycogenolysis to be determined as
1063 previously outlined^{16,17}. Briefly, fractional contribution of gluconeogenesis (GNG) was obtained by the
1064 ratio between D5 and D2 ($\text{GNG}=\text{D5}/\text{D2}$). Fractional contribution of glycogenolysis (GYG) to EndoRa
1065 was determined from the equation, $\text{GYG} = 1-\text{GNG}$. Multiplying by EndoRa allowed for absolute rates
1066 of glycogenolysis and gluconeogenesis to be calculated. Glucose flux rates for the three clamp steady-
1067 state samples were averaged to obtain representative values for each mouse.

1068
1069 **$[^{11}\text{C}]\text{-Metformin MicroPET.}$** $[^{11}\text{C}]\text{-Metformin}$ was synthesized by methylation of 1-methylbiguanide
1070 with $[^{11}\text{C}]\text{methyl triflate}$ ¹⁸ and prepared as a solution (0.1-0.5 $\mu\text{g}/\text{ml}$) in 100 mM $(\text{NH}_4)_2\text{HPO}_4$, pH 5.
1071 Animals were anesthetized in a chamber filled with 5 % isoflurane in a mixture of O_2 (0.4 $\text{L}\cdot\text{min}^{-1}$) and
1072 air (1.5 $\text{L}\cdot\text{min}^{-1}$). After induction of anesthesia, the head of the animal was placed in an acrylic glass

1073 holder and anesthesia maintained with isoflurane (1.8–2.0 %) in O₂ (0.4 L.min⁻¹) and air (1.5 L.min⁻¹).
1074 A single bolus of [¹¹C]-metformin (4.6 ± 0.3 MBq/mouse) was injected via a catheter inserted into the
1075 tail vein, followed by 60 min dynamic PET- and 15 min MR-imaging in a Mediso nanoScan PET/MR
1076 (Mediso Ltd, Hungary). Respiratory frequency was monitored and body temperature maintained at 36–
1077 37°C. Animals were euthanized at the end of the procedure by cervical dislocation. Data obtained from
1078 the dynamic PET was reconstructed with a 3D OSEM algorithm (Tera-Tomo 3D, full detector model
1079 and normal regularization; Mediso Ltd, Hungary) with four iterations and six subsets, voxel size
1080 0.4×0.4×0.4 mm³. Corrections were made for randoms, dead-time and decay using a delayed
1081 coincidence window. Attenuation and scatter was not corrected. The 60 min dynamic PET-scans were
1082 reconstructed as 30 frames increasing in duration from 5 s to 10 min. Multiple regions of interest
1083 (ROIs) were placed on coronal slices in the organ of interest using PMOD version 3.6 (PMOD
1084 Technologies Ltd, Zurich, Switzerland) creating a volume of interest (VOI). An image-derived input
1085 function was generated by averaging images from the first 20 s and placing a circle with a diameter of
1086 15 pixels on the six slices with the highest activity in the heart (68 µl), representing primarily the
1087 blood-pool in left ventricle. Hepatic VOIs were drawn in the anterior part of the liver on PET-images
1088 averaged from 0–60 min in which it can be easily identified. Positioning of all VOIs was controlled in
1089 each time frame. MR-images were used for defining size and demarcation of liver and left ventricle.
1090 Time-activity curves were generated from the VOIs. Results are expressed as tissue-to-blood ratio by
1091 dividing the tissue concentration of [¹¹C]-metformin by the blood concentration at each time point for
1092 each animal. Area under the curve (AUC) of the tissue-to-blood ratio is a reflection of the tissue
1093 extraction ratio and represents the distributional relationship between uptake and elimination from the
1094 tissue of interest.

1095
1096 **RT-PCR.** RNA was extracted from powdered livers using Trizol reagent and silica columns
1097 (ThermoFisher #12183-555) using the standard protocol with the exception that Trizol homogenates
1098 were centrifuged at 12,000 g for 10 min at 4°C prior to phase separation and the RNA fraction was
1099 loaded onto silica columns in 25 % (v/v) ethanol to prevent co-precipitation of RNA with glycogen.
1100 RNA integrity was monitored by electrophoresis. Samples were denatured in
1101 formamide/formaldehyde loading buffer (Sigma R1386) containing 0.1 % (v/v) SYBR® Safe and
1102 separated on 1 % (w/v) agarose gels in TAE. cDNA was synthesized using random hexamers and
1103 oligo(dT) primers using iScript cDNA synthesis kit (Bio-Rad #1725038). RT-PCR was performed
1104 using SYBR green detection on a Roche LightCycler 480 II. Reactions contained 50 ng template, 0.5
1105 µM primers and 1×LightCycler 1536 DNA Green master reagent (Roche #05573092001) and
1106 amplification was performed using a hot-start, touchdown protocol: 95°C, 7 min followed by 35 cycles
1107 of 95°C for 10s, 63°C > 58°C (0.5°C/cycle) for 10s and 72°C for 10s. Specificity was determined by
1108 melting curves and agarose gel electrophoresis of reaction products. Relative quantification of target
1109 genes and propagation of error was determined using 18S as a reference gene and the ΔΔCt method of
1110 Livak¹⁹. Statistical significance of relative expression ratios was tested using REST© 2009
1111 (<http://www.gene-quantification.com/rest-2009.html>).

1112
1113 **Tissue Metabolites.** To avoid even transient hypoxia which results in severe disturbances in tissue
1114 metabolites²⁰, mice were anaesthetized using isoflurane, the abdomen was exposed and the left lobe of
1115 the liver was freeze-clamped *in-situ* using liquid nitrogen cooled Wollenberger tongs. Prior to
1116 analysis, powdered livers were stored in cryovials in vapour phase liquid nitrogen. Glycogen was
1117 assayed by a modification of the method of Keppler and Decker²¹. Briefly, samples were digested with
1118 10 volumes 1 M KOH at 80°C for 20 min, adjusted to pH 4.8 with 0.5 volumes 4 N acetic acid and
1119 incubated with 5 U/ml amyloglucosidase for 2 h at 40°C. Samples were clarified at 16,000 g for 10
1120 min and free glucose assayed in reactions containing 50 mM tris-HCl pH 8.1, 1 mM MgCl₂, 0.1 %
1121 (w/v) BSA, 0.5 mM ATP, 0.5 mM NADP⁺, 0.5 mM iodonitrotetrazolium chloride (INT), 10 µM 1-
1122 methoxy-5-methylphenazinium methyl sulfate, 0.5 U/ml hexokinase and 0.1 U/ml glucose-6-
1123 phosphate dehydrogenase by following the increase in A₄₉₅. Glucose in perchloric acid extracts was
1124 assayed as described above but omitting coupling to INT, which forms an insoluble perchlorate
1125 precipitate. Adenine and Z nucleotides were assayed by ion-pair, reverse phase chromatography on an
1126 Ultimate 3000-RS HPLC essentially as described by Ryll²². Powdered liver was homogenized in 6
1127 volumes ice-cold 0.6 N perchloric acid, 0.5 mM EGTA and centrifuged at 16,000 g for 3 min at 4°C.

1128 Protein pellets were dissolved in 10 volumes 0.5 M NaOH and [protein] determined using Bradford
1129 reagent. Perchloric acid was extracted from the supernatant by shaking with two volumes 1:3
1130 trioctylamine:chloroform (~0.6 N trioctylamine) and centrifugation at 2000 g for 1 min at 4°C to
1131 induce phase separation. The upper aqueous phase was recovered and neutralized by the addition of 5
1132 mM phosphate pH 7. Samples were analyzed immediately by injection (20 µl) on a Supelcosil LC-18
1133 T 150×4.6 mm, 3 µm C18 column equilibrated with mobile phase (A - 100 mM potassium phosphate
1134 pH 5.5, 8 mM tetrabutylammonium hydrogen sulfate) at 26°C. The column was resolved with a
1135 methanol gradient (B = A:methanol 70:30, pH 6): 0 min – 0 % B, 2 min – 0 % B, 16 min – 40 % B, 17
1136 min – 100 % B, 23 min – 100 % B, and re-equilibrated with A for 8 min. Peaks were detected at A₂₅₄.
1137 Skeletal muscle was powdered in a liquid nitrogen-cooled Bessman pulverizer and homogenized with
1138 10 volumes 0.6 N PCA, 0.5 mM EGTA using a rotor-stator homogenizer. Samples were clarified at
1139 16,000 g for 5 min at 4°C, the supernatant neutralized with two volumes 1:3 trioctylamine:chloroform
1140 as described above and 10 nM P₁,P₅-di(adenosine 5') pentaphosphate (A₅pA) added to inhibit any
1141 residual myokinase activity. Samples were analyzed immediately by injection (10 µl) on an Accucore
1142 100×3.0 mm, 2.6 µm C18 column (Thermo 17126-103030) with a 10×3.0 mm guard column (Thermo
1143 17126-013005) equilibrated with mobile phase (A - 100 mM potassium phosphate pH 5.5, 5 mM
1144 tetrabutylammonium hydrogen sulfate) at 0.6 ml.min⁻¹ at 26°C. The column was resolved with an
1145 acetonitrile gradient (B = A:acetonitrile 75:25, pH 6): 0 min – 0 % B, 1.5 min – 0 % B, 5 min – 10 %
1146 B, 9 min – 50 % B, 10 min – 100 % B, 13 min – 100 % B and re-equilibrated with A for 6 min. Peaks
1147 were detected at A₂₅₄. Water used for mobile phase preparation was filtered through Empore SBD-XC
1148 cartridge filters to remove impurities and improve baseline stability. Chromatograms were acquired
1149 and integrated using Chromeleon v7.1 and calibrated using standards prepared in water and
1150 standardized at A₂₅₉ (ε = 15.4 mM⁻¹ in 0.1 M phosphate pH 7). Remaining metabolites were assayed in
1151 0.6 N perchloric acid, 1 mM EDTA extracts neutralized with 0.25 volumes 2 M KOH, 0.4 M KCl, 0.4
1152 M imidazole. To prevent excessive loss of pyruvate it was necessary to add 500 U/ml catalase
1153 immediately upon neutralization to remove H₂O₂, which forms spontaneously in neutralized perchloric
1154 acid extracts of blood rich tissues and decarboxylates pyruvate to acetate. Lactate was assayed using a
1155 modification of the method of Noll²³ in reactions containing 0.1 M 2-amino-2-methyl-1-propanol pH
1156 9.2, 20 mM glutamate, 1.5 mM NAD⁺, 10 µM 1-methoxy-5-methylphenazinium methyl sulfate, 0.5
1157 mM WST-1, 20 U/ml lactate dehydrogenase and 5 U/ml glutamate-pyruvate transaminase. A₄₄₀ was
1158 recorded and [lactate] determined by interpolation of a standard curve prepared using lithium lactate.
1159 Pyruvate was assayed as described by Passonneau and Lowry²⁴ in reactions containing 50 mM
1160 phosphate pH 7, 20 µM NADH and 0.04 U/ml lactate dehydrogenase. The decrease in fluorescence
1161 (λ_{ex} = 345 nm, λ_{em} = 465 nm) was recorded and calibrated using known quantities of sodium pyruvate.
1162 G6P, F6P and F-1,6-P₂ were assayed using a modification of the method of Racker²⁵ in reactions
1163 containing 50 mM tris-HCl pH 8.5, 5 mM MgCl₂, 0.1 mM EDTA, 100 µM NADP⁺, 0.2 U/ml
1164 diaphorase and 20 µM resazurin. Glucose-6-phosphate dehydrogenase (0.1 U/ml), phosphoglucose
1165 isomerase (0.2 U/ml) and recombinant spinach chloroplast fructose-1,6-bisphosphatase (1 U/ml,
1166 prepared in *E.coli*) were added sequentially and the increase in resorufin fluorescence (λ_{ex} = 540 nm,
1167 λ_{em} = 590 nm) recorded and calibrated by addition of known quantities of NADH. Fructose-2,6-
1168 bisphosphate was assayed using PP_i-dependent fructose-6-phosphate 1-phosphotransferase from potato
1169 exactly as described by Van Schaftingen²⁶. 3',5'-cAMP was assayed in trichloroacetic acid (TCA)
1170 extracts using a commercial enzyme immunoassay from Sigma (CA-201). Briefly, powdered tissue
1171 was homogenized in 10 volumes ice-cold 5 % (w/v) TCA and centrifuged at 16,000 g for 10 min at
1172 4°C. The supernatant was extracted 4× 3 volumes water-saturated diethyl ether, frozen and lyophilized
1173 in a Speedvac. Samples were reconstituted in the supplied assay buffer and analyzed according to the
1174 manufacturer's instructions.

1175
1176 **Enzyme assays.** GCK (EC 2.7.1.2) activity was assayed in cytosolic fractions (which substantially
1177 improves the assay by removing G6PC) prepared using the recommendations of Davidson²⁷ in
1178 reactions containing 50 mM HEPES pH 7.4, 0.1 M KCl, 0.1 mM EDTA, 7.5 mM ATP, 0.5/100 mM
1179 glucose, 0.5 mM NAD⁺, 2.5 mM DTT, 1 % (w/v) BSA, 2 U/ml glucose-6-phosphate dehydrogenase
1180 and 10 µM rotenone at 30°C. Activity at 0.5 mM glucose was subtracted from that at 100 mM glucose
1181 to correct for hexokinase-1 activity. Blanks were performed in the absence of glucose and/or ATP. 6-
1182 phosphofructo-1-kinase (EC 2.7.1.11) activity was determined by the method of Castano²⁸. Extracts

1183 (40 µg) were incubated in 50 mM HEPES pH 7.1, 0.1 M KCl, 6.5 mM MgCl₂, 1.5 mM ATP, 0.25 mM
1184 fructose-6-phosphate, 0.75 mM glucose-6-phosphate, 0.1 mM AMP, 5 mM P_i, 1 mM NH₄Cl, 0.2 mM
1185 NADH, 0.05 % (w/v) BSA, 2 mM 2-mercaptoethanol, 10 µM rotenone, 1 U/ml aldolase, 10 U/ml
1186 triosephosphate isomerase, 2 U/ml glycerol-3-phosphate dehydrogenase and 1 U/ml phosphoglucose
1187 isomerase at 30°C. Coupling enzymes were buffer exchanged over Sephadex G-25 equilibrated with
1188 10 mM tris-HCl pH 7.1 to remove sulfate. Total PK (EC 2.7.1.40) activity and ratio at 1.3/6.6 mM
1189 phosphoenolpyruvate at 66 mM KCl was determined as described by Blair²⁹. Lysates (10 µg) were
1190 incubated in reactions containing 100 mM tris-HCl pH 7.5, 66 mM KCl, 10 mM MgSO₄, 2.5 mM
1191 ADP, 0.2 mM NADH, 10 µM rotenone, 1 µM microcystin-LR, 0.05 % (w/v) BSA, 3.2 U/ml lactate
1192 dehydrogenase and 1.3 or 6.6 mM phosphoenolpyruvate. PEPCK-C (EC 4.1.1.32) was assayed using
1193 the method of Petrescu³⁰. Cytosolic extracts (100 µg) were incubated in reactions containing 50 mM
1194 tris-HCl pH 7.4, 1 mM MnCl₂, 0.1 mM EGTA, 0.05 % (w/v) BSA, 0.5 mM PEP, 0.2 mM NADH, 10
1195 µM rotenone, 0.2 mM 2-deoxy-GDP, 2 U/ml malate dehydrogenase and either 20 mM NaCl or 20 mM
1196 NaHCO₃ (saturated with CO₂) at 30°C. FBP1 (EC 3.1.3.11) activity was assayed as described above.
1197 AMPD1 (EC 3.5.4.6) was assayed in reactions containing 50 mM MOPS pH 7.2, 100 mM KCl, 1 mM
1198 DTT, 0.05 % (w/v) BSA, 1 mM ATP, 0.2 mM AMP, 7.5 mM 2-oxoglutarate, 0.15 mM NADH and 5
1199 U/ml glutamate dehydrogenase. All assays were performed in a final volume of 200 µl and monitored
1200 by changes in A₃₄₀. Initial rates were determined from the linear phase and activity calculated
1201 assuming εNAD(P)H = 6.22 mM⁻¹.cm⁻¹. G6PC (EC 3.1.3.9) activity was determined by monitoring the
1202 release of P_i using the compleximetric method of Saheki³¹. Extracts (20 µg) were incubated in 20 mM
1203 MOPS pH 7.2, 100 mM NaCl, 2 mM 2-mercaptoethanol containing 10 mM glucose-6-phosphate or
1204 glycerol-2-phosphate (to correct for background due to non-specific phosphatases) for 20 min at 30°C.
1205 Reactions were quenched by the addition of 1 % (w/v) SDS and an aliquot (25 µl) was removed for
1206 determination of released phosphate by sequential addition of 180 µl 15 mM zinc acetate, 100 mM
1207 ammonium molybdate and 45 µl 10 % (w/v) ascorbic acid (adjusted to pH 5 with 10 N NaOH).
1208 Reactions were left to develop for 15 min at 30°C and A₈₅₀ recorded. P_i was calculated by interpolation
1209 of a standard curve prepared using desiccated KH₂PO₄. CS (EC 2.3.3.1) was assayed using the method
1210 of Sreer³². Lysates (10 µg) were incubated in reactions containing 50 mM tris-HCl pH 8.1, 0.1 mM
1211 EDTA, 0.1 mM 5'-dithiobis(2-nitrobenzoic acid) (DTNB), 0.3 mM acetyl-CoA and 0.5 mM
1212 oxaloacetate at 30°C. Blanks were performed in the absence of oxaloacetate. A₄₁₂ was monitored and
1213 activity calculated from the linear phase assuming εTNB²⁻ = 14.15 mM⁻¹.cm⁻¹. PC (EC 6.4.1.1) was
1214 assayed by coupling the formation of oxaloacetate to the reduction of DTNB using CS. Lysates (20
1215 µg) were incubated in reactions containing 50 mM tris-HCl, 50 mM NaHCO₃, 5 mM MgCl₂, 2.5 mM
1216 ATP, 0.1 mM acetyl-CoA, 0.2 mM DTNB, 5 mM pyruvate and 5 U/ml citrate synthase at 30°C.
1217 Blanks were performed in the absence of pyruvate and A₄₁₂ was monitored as described for CS. GS
1218 (EC 2.4.1.11) was assayed by the method of Thomas³³. Lysates (50 µg) were incubated in reactions
1219 containing 25 mM tris-HCl pH 7.8, 50 mM NaF, 1 mM EDTA, 0.9 % (w/v) glycogen, 1 mM DTT, 20
1220 µM 1-deoxynojirimycin, 4.4 mM [U-¹⁴C] UDP-glucose (0.1-0.2 mCi.mmol⁻¹) in the absence and
1221 presence of 10 mM G6P for 20 min at 30°C. Reactions were stopped by spotting on squares of 3MM
1222 filter paper and immersion in ice-cold 66 % (v/v) ethanol. Filters were washed 3×20 min with 66 %
1223 (v/v) ethanol, rinsed with acetone and [¹⁴C] incorporation into glycogen determined by scintillation
1224 counting in Emulsifier Safe (Perkin Elmer). GPa (EC 2.4.1.1) was assayed in the reverse direction
1225 using the method of Gilboe³⁴ following the recommendations of Stalmans³⁵. Lysates (50 µg) were
1226 incubated in reactions containing 50 mM MES pH 6.5, 50 mM [U-¹⁴C] glucose-1-phosphate (0.02
1227 mCi.mmol⁻¹), 150 mM NaF, 5 mM EDTA, 1 % (w/v) glycogen, 20 µM 1-deoxynojirimycin, 15 mM 2-
1228 mercaptoethanol and 0.5 mM caffeine at 30°C for 20 min. Reactions were spotted on filters and
1229 processed as described for GS with the exception that room temperature 66 % (v/v) ethanol was used
1230 for quenching to prevent high blanks caused by the co-precipitation of glucose-1-phosphate. AMPK
1231 phosphotransferase activity (EC 2.7.11.1) was assayed using immunoprecipitates. Briefly, lysates (50
1232 µg) were incubated with 2 µg anti-AMPKα1 or anti-AMPKα2 and 5 µl protein G Sepharose for 2 h at
1233 4°C. Immune complexes were pelleted at 500 g for 1 min and washed 3× 1 ml lysis buffer and 2× 1 ml
1234 50 mM tris-HCl pH 8, 0.1 mM EGTA. Phosphotransferase activity was determined in reactions
1235 containing 50 mM HEPES pH 7.5, 10 mM MgCl₂, 0.1 mM EGTA, 0.1 mM [γ-³²P] ATP (250
1236 CPM.pmol⁻¹), 0.1 mM AMARA (NH₂-AMARAASAAALARRR-COOH). Reactions were quenched
1237 by spotting onto P81 filters and immersion in 75 mM phosphoric. Filters were washed 3× 10 min with

1238 75 mM phosphoric acid, rinsed with acetone and [³²P] incorporation determined by Cherenkov
1239 counting. With the exception of AMPK, 1 U = 1 μmol product formed per min at 30°C. For AMPK, 1
1240 U = 1 nmol phosphate incorporated per min at 30°C.

1241

1242 **Data Analysis.** Fitting to models was performed by least squares non-linear regression using
1243 Levenberg-Marquardt minimization using Graphpad Prism v5.0. Area under the curve was calculated
1244 using the trapezoidal rule with subtraction of the area below baseline (t = 0). Statistical significance
1245 was determined using unpaired, two-tailed Student's t-test and an alpha level of 0.05. All data were
1246 normally distributed based on D'Agostino-Pearson omnibus tests and sample variance was similar
1247 between groups being compared.

1248

1249 **Reporting summary.** Further information on experimental design is available in the Nature Research
1250 Reporting Summary linked to this article.

1251

1252 **Data availability.** Uncropped Western blot images are available in Supplementary section. A Life
1253 Sciences Reporting Summary is available (linked to this article).

1254

1255 References

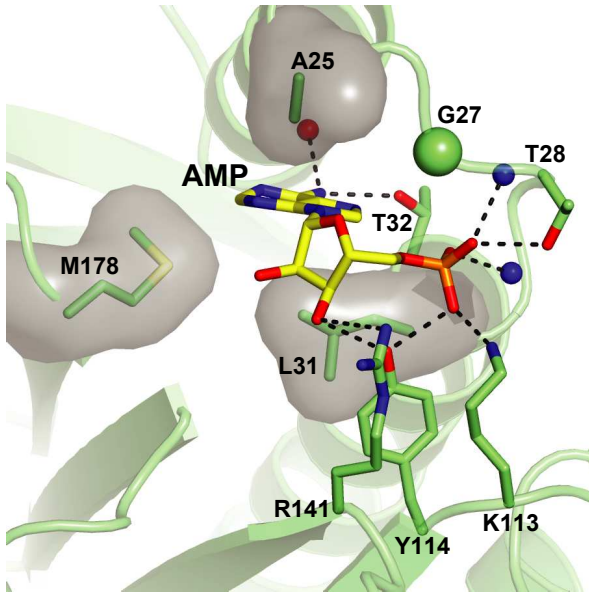
1256

- 1257 1. Dang, Q., *et al.* Discovery of potent and specific fructose-1,6-bisphosphatase inhibitors and a
1258 series of orally-bioavailable phosphoramidase-sensitive prodrugs for the treatment of type 2
1259 diabetes. *J Am Chem Soc* **129**, 15491-15502 (2007).
- 1260 2. Giroux, E., Williams, M.K. & Kantrowitz, E.R. Shared active sites of fructose-1,6-
1261 bisphosphatase. Arginine 243 mediates substrate binding and fructose 2,6-bisphosphate
1262 inhibition. *J Biol Chem* **269**, 31404-31409 (1994).
- 1263 3. Tashima, Y., Mizunuma, H. & Hasegawa, M. Purification and properties of mouse liver
1264 fructose 1,6-bisphosphatase. *J Biochem* **86**, 1089-1099 (1979).
- 1265 4. Smiley, K.L., Jr., Berry, A.J. & Suelter, C.H. An improved purification, crystallization, and
1266 some properties of rabbit muscle 5'-adenylic acid deaminase. *J Biol Chem* **242**, 2502-2506
1267 (1967).
- 1268 5. Han, P., Han, G., McBay, H. & Johnson, J. Adenosine 5'-monophosphate-removing system in
1269 fructose-1,6-bisphosphatase assay mixture: a new approach. *Anal Biochem* **122**, 269-273
1270 (1982).
- 1271 6. Nelson, S.W., Choe, J.Y., Honzatko, R.B. & Fromm, H.J. Mutations in the hinge of a dynamic
1272 loop broadly influence functional properties of fructose-1,6-bisphosphatase. *J Biol Chem* **275**,
1273 29986-29992 (2000).
- 1274 7. Chomczynski, P. & Rymaszewski, M. Alkaline polyethylene glycol-based method for direct
1275 PCR from bacteria, eukaryotic tissue samples, and whole blood. *Biotechniques* **40**, 454, 456,
1276 458 (2006).
- 1277 8. Zarghi, A., Foroutan, S.M., Shafaati, A. & Khoddam, A. Rapid determination of metformin in
1278 human plasma using ion-pair HPLC. *J Pharm Biomed Anal* **31**, 197-200 (2003).
- 1279 9. Nakamura, K., Maeda, H. & Kawaguchi, H. Enzymatic assay of hemoglobin in tissue
1280 homogenates with chlorpromazine. *Anal Biochem* **165**, 28-32 (1987).
- 1281 10. Bosselaar, M., Smits, P., van Loon, L.J. & Tack, C.J. Intravenous AICAR during
1282 hyperinsulinemia induces systemic hemodynamic changes but has no local metabolic effect. *J*
1283 *Clin Pharmacol* **51**, 1449-1458 (2011).
- 1284 11. Ayala, J.E., *et al.* Hyperinsulinemic-euglycemic clamps in conscious, unrestrained mice. *J Vis*
1285 *Exp* (2011).
- 1286 12. Hasenour, C.M., *et al.* Mass spectrometry-based microassay of (2)H and (13)C plasma glucose
1287 labeling to quantify liver metabolic fluxes in vivo. *Am J Physiol Endocrinol Metab* **309**, E191-
1288 203 (2015).
- 1289 13. Antoniewicz, M.R., Kelleher, J.K. & Stephanopoulos, G. Measuring deuterium enrichment of
1290 glucose hydrogen atoms by gas chromatography/mass spectrometry. *Anal Chem* **83**, 3211-
1291 3216 (2011).

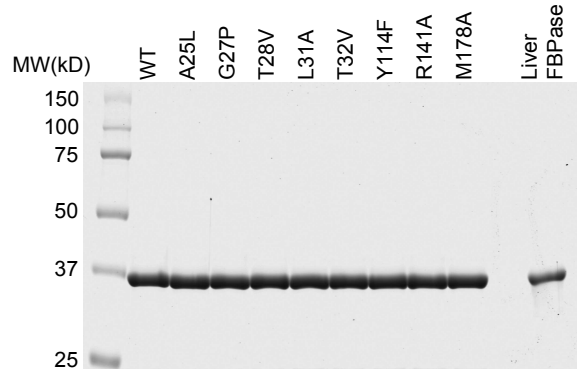
- 1292 14. Young, J.D. INCA: a computational platform for isotopically non-stationary metabolic flux
1293 analysis. *Bioinformatics* **30**, 1333-1335 (2014).
- 1294 15. Antoniewicz, M.R., Kelleher, J.K. & Stephanopoulos, G. Determination of confidence
1295 intervals of metabolic fluxes estimated from stable isotope measurements. *Metab Eng* **8**, 324-
1296 337 (2006).
- 1297 16. Landau, B.R., *et al.* Contributions of gluconeogenesis to glucose production in the fasted state.
1298 *J Clin Invest* **98**, 378-385 (1996).
- 1299 17. Satapati, S., *et al.* Elevated TCA cycle function in the pathology of diet-induced hepatic
1300 insulin resistance and fatty liver. *J Lipid Res* **53**, 1080-1092 (2012).
- 1301 18. Jakobsen, S., *et al.* A PET Tracer For Renal Organic Cation Transporters, 11C-metformin:
1302 Radiosynthesis and Preclinical Proof-of-Concept Studies. *Journal of nuclear medicine :
1303 official publication, Society of Nuclear Medicine* (2016).
- 1304 19. Livak, K.J. & Schmittgen, T.D. Analysis of relative gene expression data using real-time
1305 quantitative PCR and the 2(-Delta Delta C(T)) Method. *Methods* **25**, 402-408 (2001).
- 1306 20. Faupel, R.P., Seitz, H.J., Tarnowski, W., Thiemann, V. & Weiss, C. The problem of tissue
1307 sampling from experimental animals with respect to freezing technique, anoxia, stress and
1308 narcosis. A new method for sampling rat liver tissue and the physiological values of glycolytic
1309 intermediates and related compounds. *Arch Biochem Biophys* **148**, 509-522 (1972).
- 1310 21. Keppler, D. & Decker, K. Glycogen determination with amyloglucosidase. in *Methods of
1311 Enzymatic Analysis*, Vol. 3 (ed. Bergmeyer, H.U.) 1127-1131 (1974).
- 1312 22. Ryll, T. & Wagner, R. Improved ion-pair high-performance liquid chromatographic method
1313 for the quantification of a wide variety of nucleotides and sugar-nucleotides in animal cells. *J
1314 Chromatogr* **570**, 77-88 (1991).
- 1315 23. Noll, F. *Methods of Enzymatic Analysis*, (1984).
- 1316 24. Passonneau, J.V. & Lowry, O.H. *Enzymatic analysis. A practical guide*, (1993).
- 1317 25. Racker, E. *Methods of Enzymatic Analysis*. (ed. Bergmeyer, H.U.) 160-163 (1965).
- 1318 26. Van Schaftingen, E., Lederer, B., Bartrons, R. & Hers, H.G. A kinetic study of pyrophosphate:
1319 fructose-6-phosphate phosphotransferase from potato tubers. Application to a microassay of
1320 fructose 2,6-bisphosphate. *Eur J Biochem* **129**, 191-195 (1982).
- 1321 27. Davidson, A.L. & Arion, W.J. Factors underlying significant underestimations of glucokinase
1322 activity in crude liver extracts: physiological implications of higher cellular activity. *Arch
1323 Biochem Biophys* **253**, 156-167 (1987).
- 1324 28. Castano, J.G., Nieto, A. & Feliu, J.E. Inactivation of phosphofruktokinase by glucagon in rat
1325 hepatocytes. *J Biol Chem* **254**, 5576-5579 (1979).
- 1326 29. Blair, J.B., Cimbala, M.A., Foster, J.L. & Morgan, R.A. Hepatic pyruvate kinase. Regulation
1327 by glucagon, cyclic adenosine 3'-5'-monophosphate, and insulin in the perfused rat liver. *J
1328 Biol Chem* **251**, 3756-3762 (1976).
- 1329 30. Petrescu, I., *et al.* Determination of phosphoenolpyruvate carboxykinase activity with
1330 deoxyguanosine 5'-diphosphate as nucleotide substrate. *Anal Biochem* **96**, 279-281 (1979).
- 1331 31. Saheki, S., Takeda, A. & Shimazu, T. Assay of inorganic phosphate in the mild pH range,
1332 suitable for measurement of glycogen phosphorylase activity. *Anal Biochem* **148**, 277-281
1333 (1985).
- 1334 32. Srere, P.A. Citrate synthase. *Methods in Enzymology* **13**, 3-11 (1969).
- 1335 33. Thomas, J.A., Schlender, K.K. & Larner, J. A rapid filter paper assay for UDPglucose-
1336 glycogen glucosyltransferase, including an improved biosynthesis of UDP-14C-glucose. *Anal
1337 Biochem* **25**, 486-499 (1968).
- 1338 34. Gilboe, D.P., Larson, K.L. & Nuttall, F.Q. Radioactive method for the assay of glycogen
1339 phosphorylases. *Anal Biochem* **47**, 20-27 (1972).
- 1340 35. Stalmans, W. & Hers, H.G. The stimulation of liver phosphorylase b by AMP, fluoride and
1341 sulfate. A technical note on the specific determination of the a and b forms of liver glycogen
1342 phosphorylase. *Eur J Biochem* **54**, 341-350 (1975).
- 1343
- 1344

Figure 1

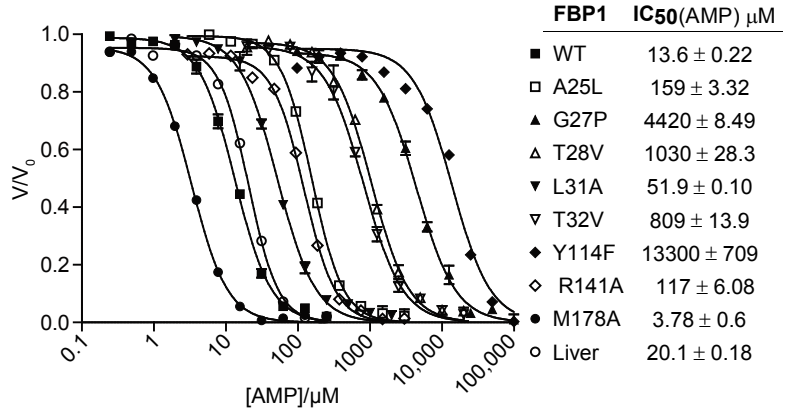
a



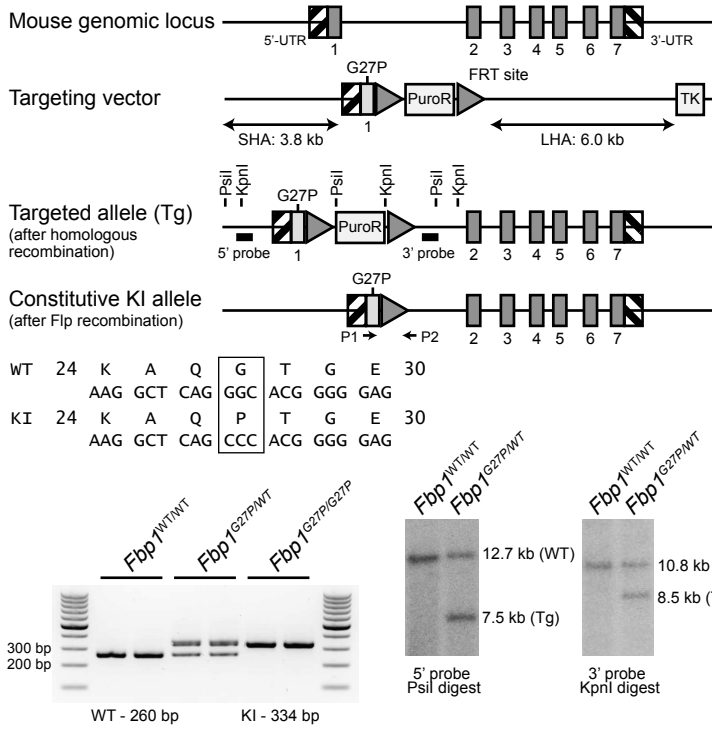
b



c



d



e

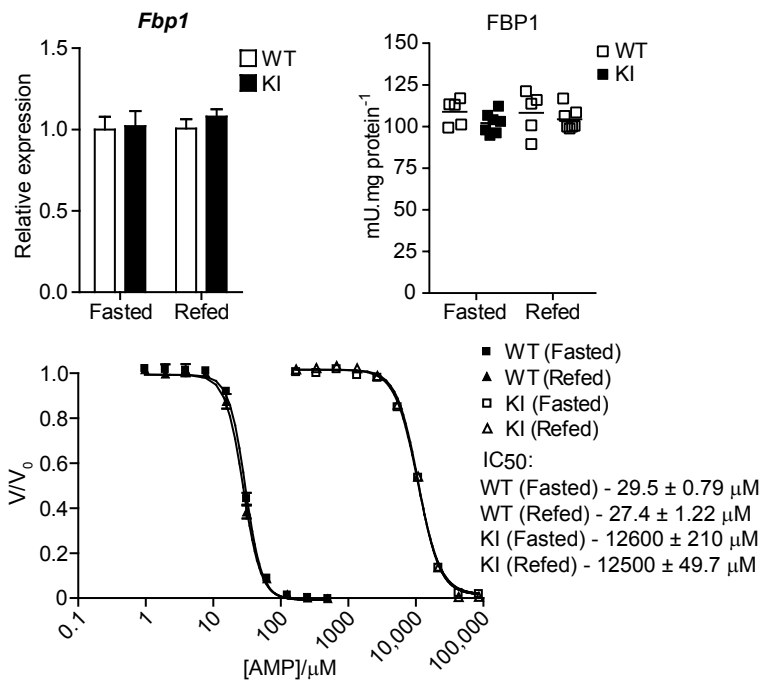


Figure 2

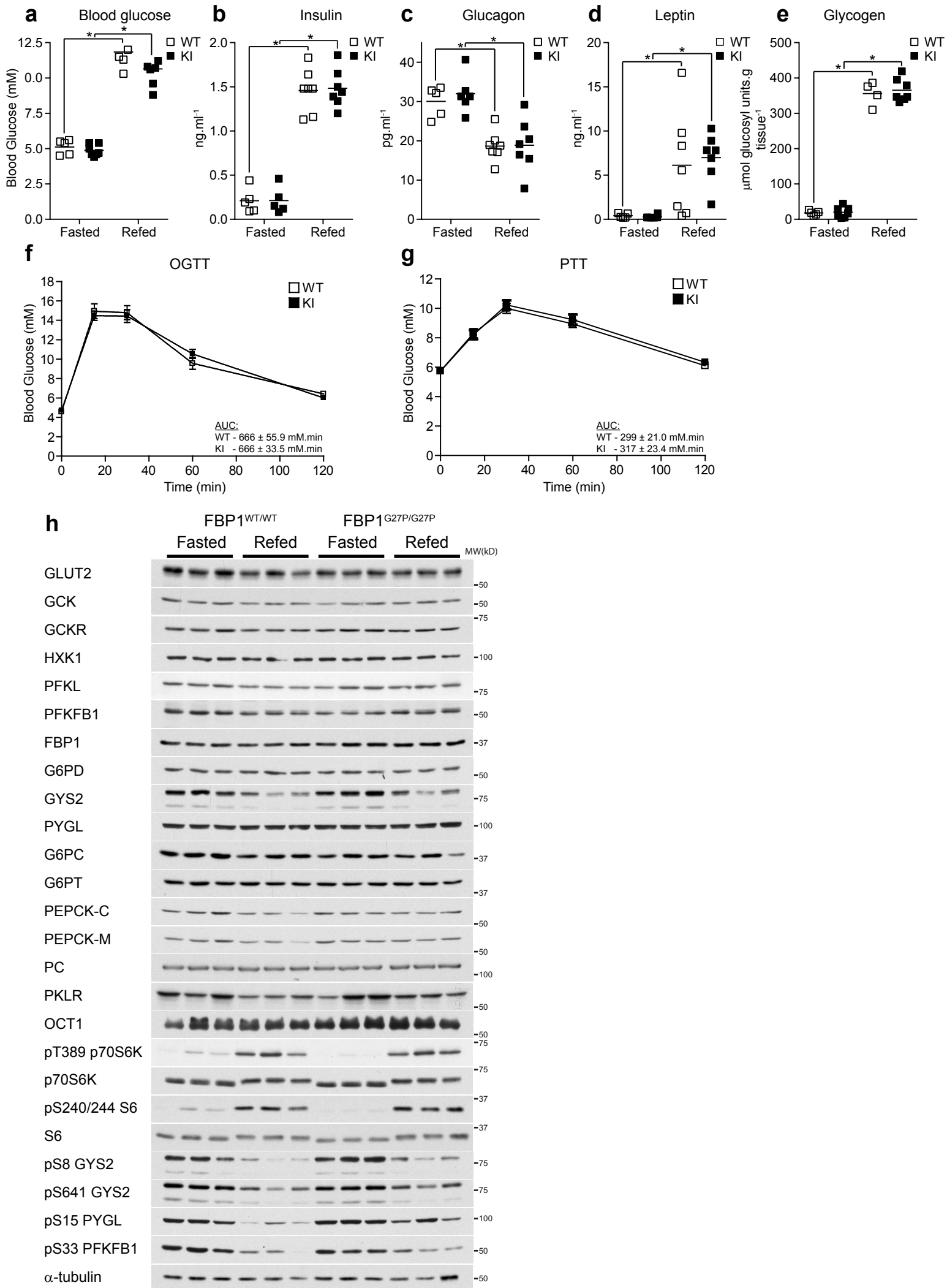


Figure 3

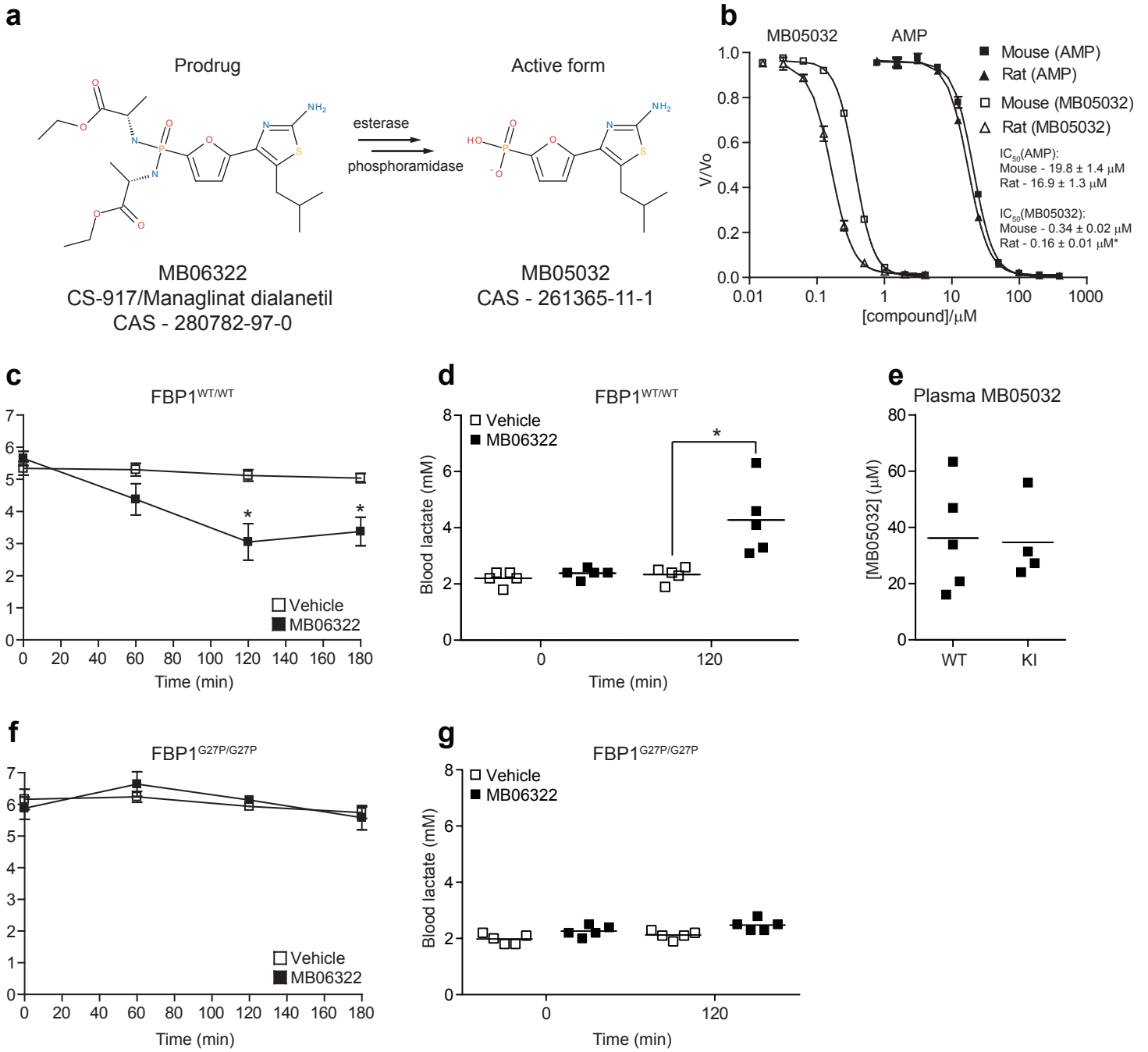
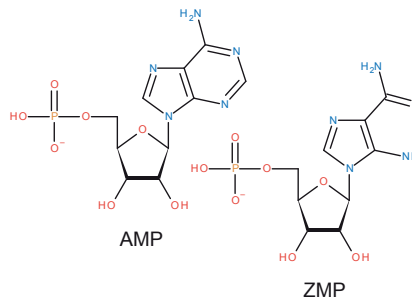
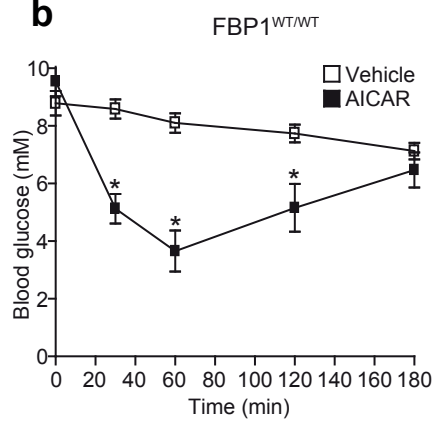


Figure 4

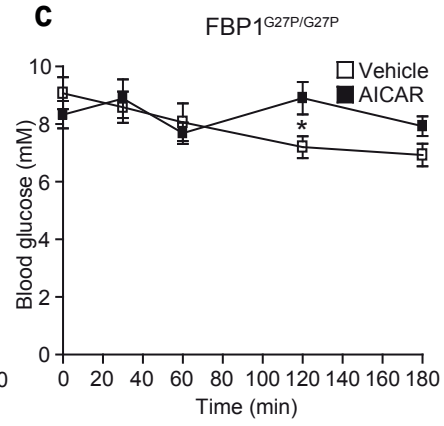
a



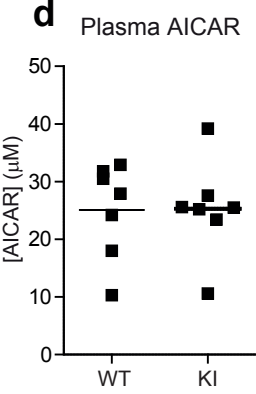
b



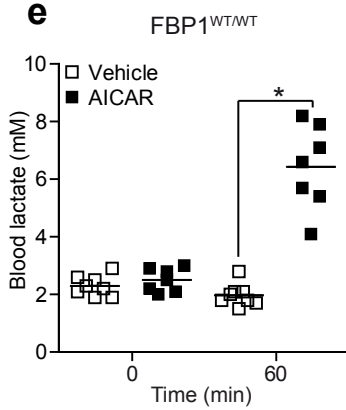
c



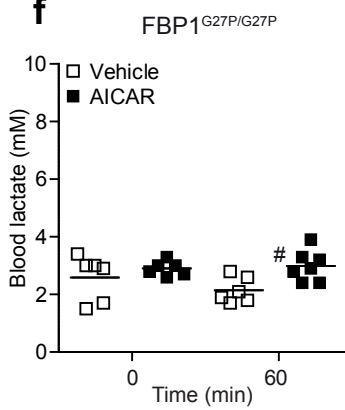
d



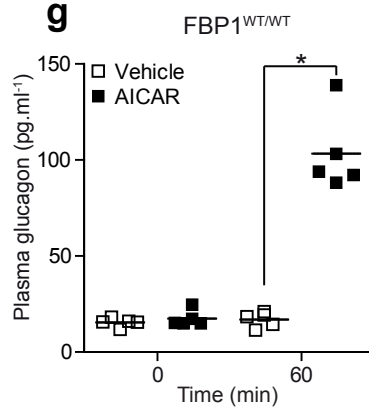
e



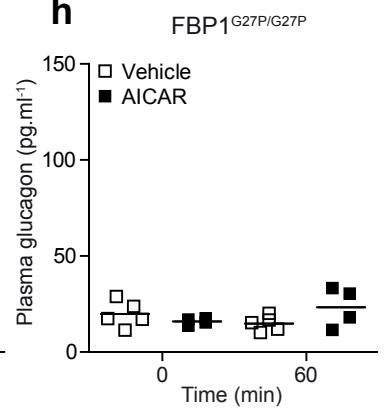
f



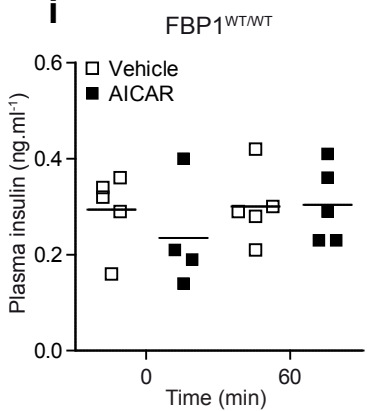
g



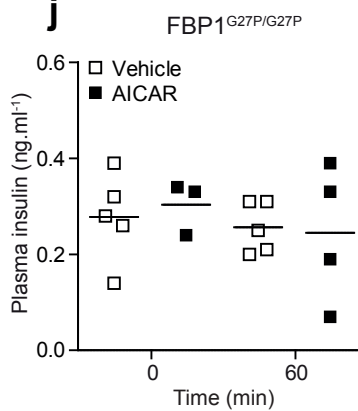
h



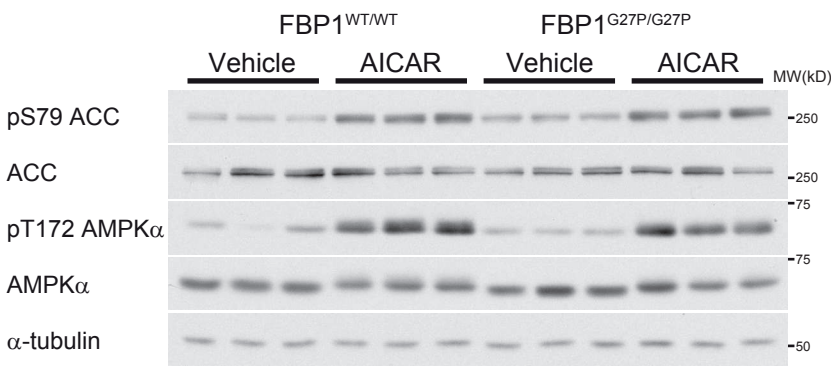
i



j



k



l

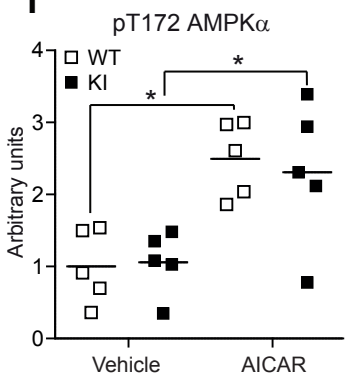


Figure 5

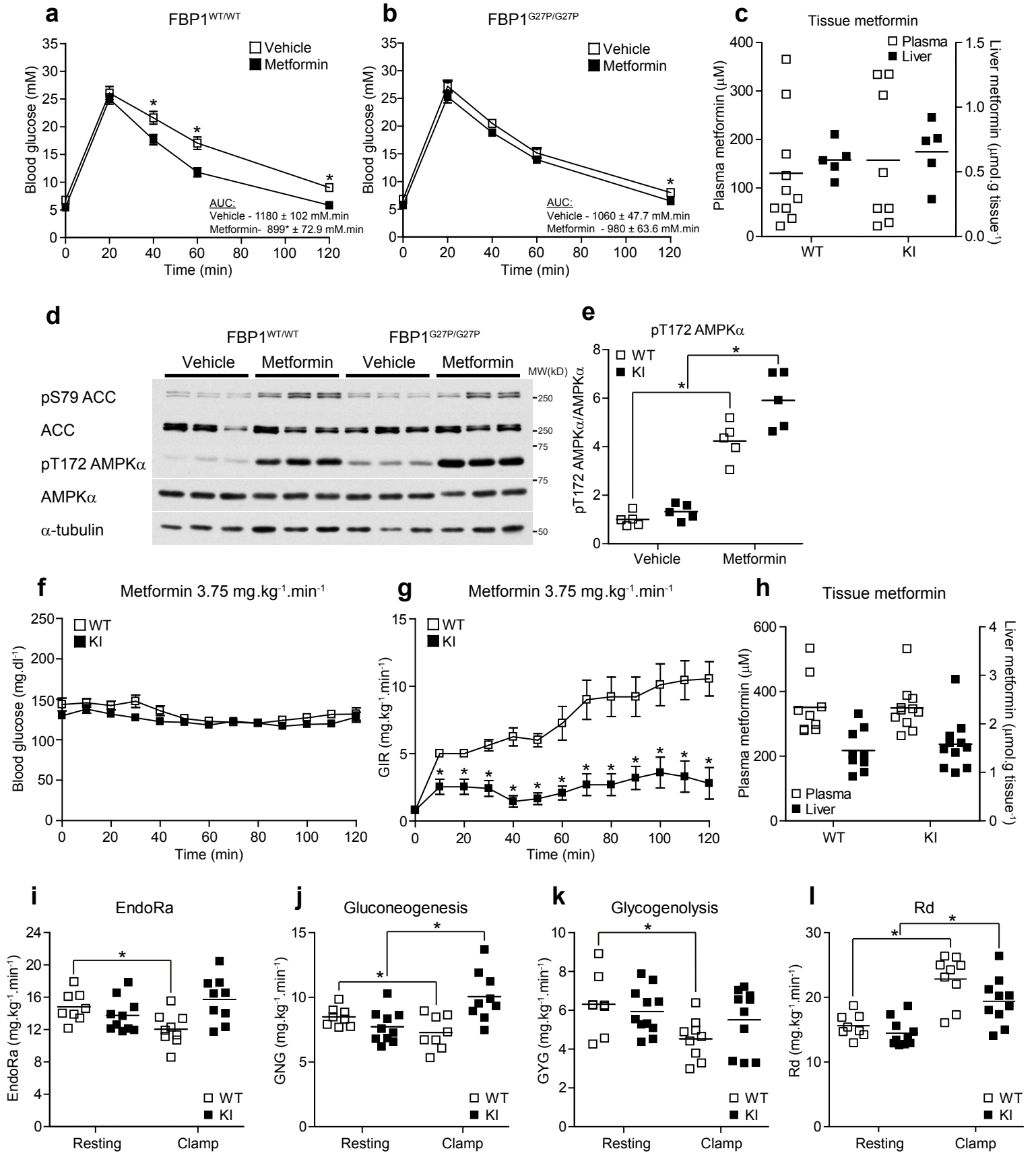
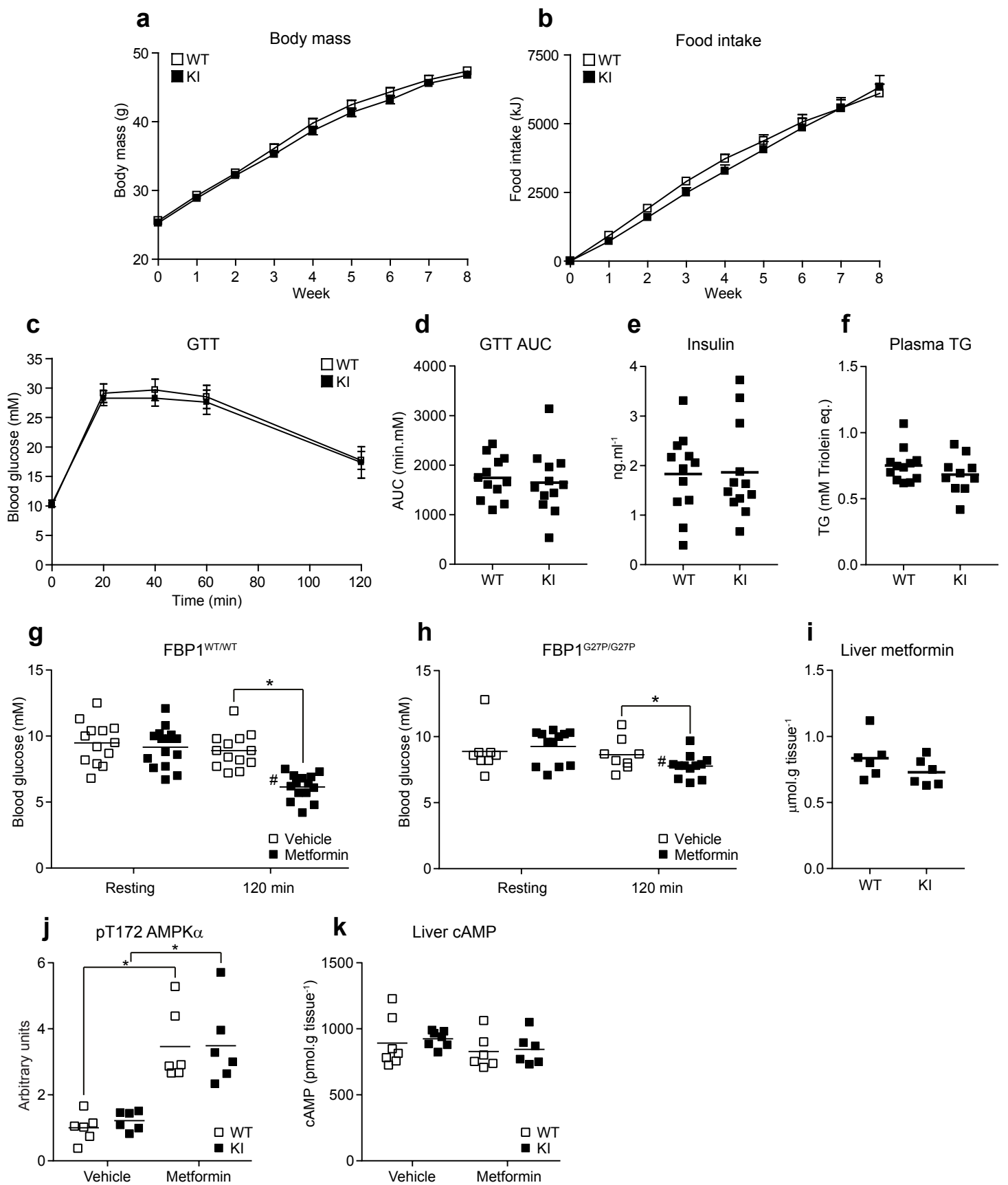


Figure 6



Supplementary Figure 1

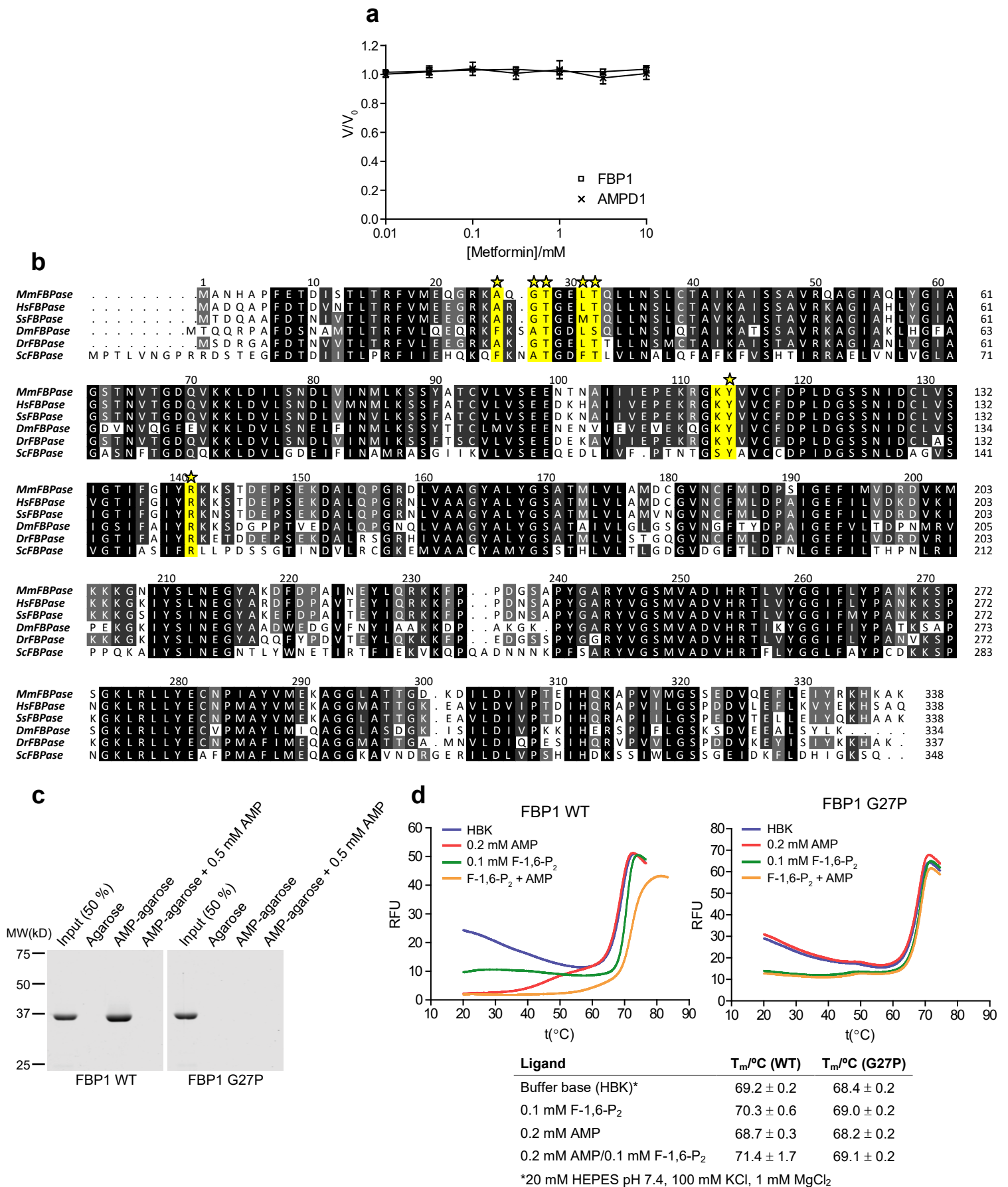


Figure S1. (a) Metformin inhibition curves of purified mouse FBP1 and rabbit muscle AMPD1 activity. Assays were performed as described in methods and results are expressed as the ratio of the maximum activity in the absence of compound (V/V_0). **(b)** Multiple sequence alignment of FBPase enzymes from different species (black = conserved, white = not conserved). Residues contributing to AMP binding are highlighted in yellow and stars represent residues mutated in this study. Numbering of mouse FBP1 is shown on the top line. Mm = *M. musculus*, Hs = *H. sapiens*, Ss = *S. scrofa*, Dm = *D. melanogaster*, Dr = *D. rerio* and Sc = *S. cerevisiae*. **(c)** Recombinant FBP1 WT or G27P were mixed with unmodified or 2′/3′-EDA-AMP-agarose (AMP-agarose) in the presence or absence of 0.5 mM free AMP. After washing, bound proteins were eluted and assessed by SDS-PAGE with Coomassie staining. Results are representative of three independent experiments. **(d)** Thermal stability curves of recombinant FBP1 WT and G27P in 20 mM HEPES pH 7.4, 100 mM KCl and 1 mM MgCl₂ (HBK) in the presence of the indicated ligands. Thermomelt curves are representative of a single experiment and T_m values represent mean ± SD of three independent experiments.

Supplementary Figure 2

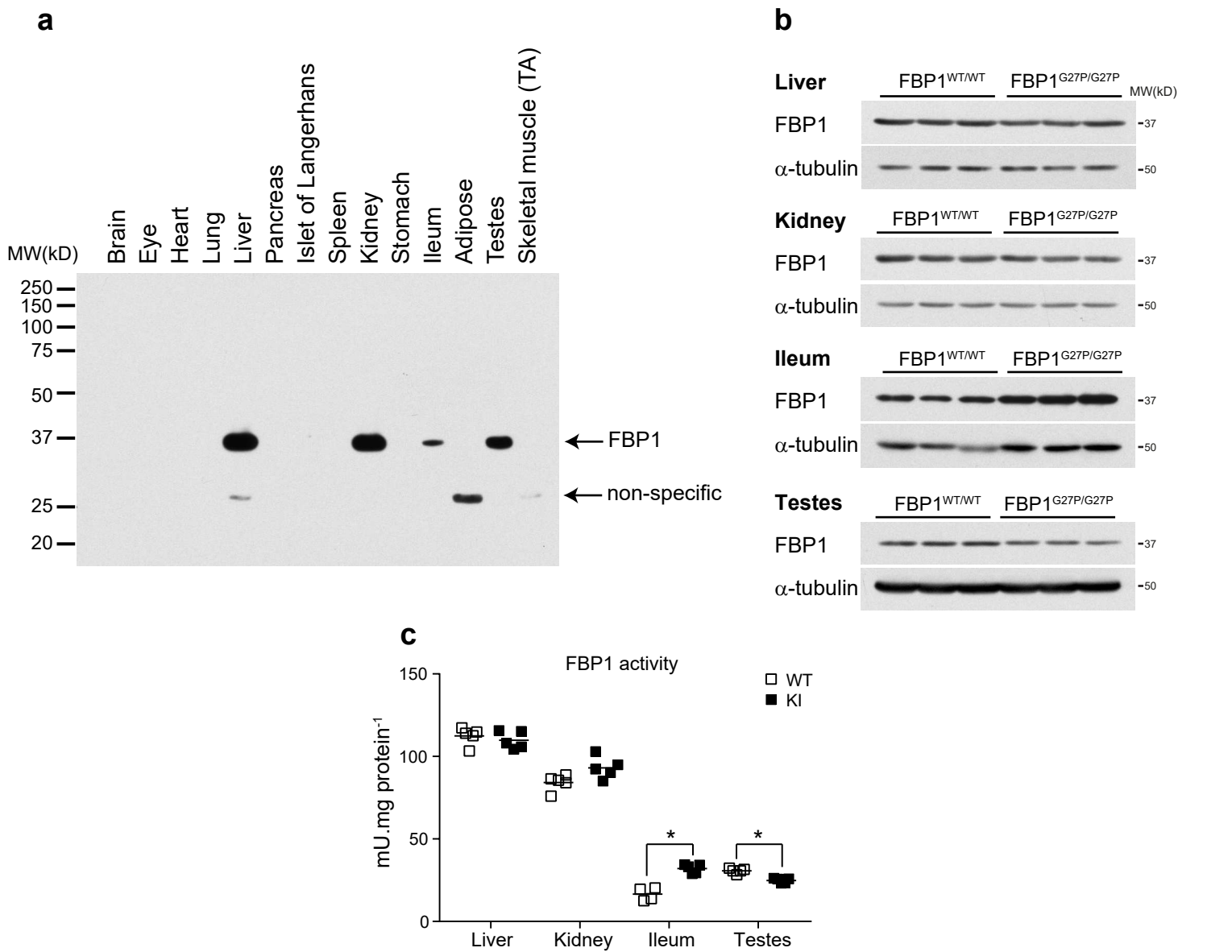


Figure S2. (a) Western blot analysis of FBP1 expression in a panel of mouse tissues (C57BL/6NTac). Equal amounts of protein (20 μ g) were loaded for each tissue. Islets of Langerhans were isolated from pancreas by intraductal collagenase digestion and hand picking under a stereomicroscope. Arrows indicate the position of FBP1 and a band of unknown identity (non-specific). TA = Tibialis anterior. (b) Western blot analysis of FBP1 expression in liver, kidney, ileum and testes from FBP1^{WT/WT} (WT) and FBP1^{G27P/G27P} (KI) mice. Representative results from three mice are shown. (c) FBPase activity in liver, kidney, ileum and testes homogenates from WT and KI mice. $n = 5$. * $P < 0.05$ (WT vs. KI). Statistical significance was determined using unpaired, two-tailed Student's t-test and an alpha level of 0.05.

Supplementary Figure 3

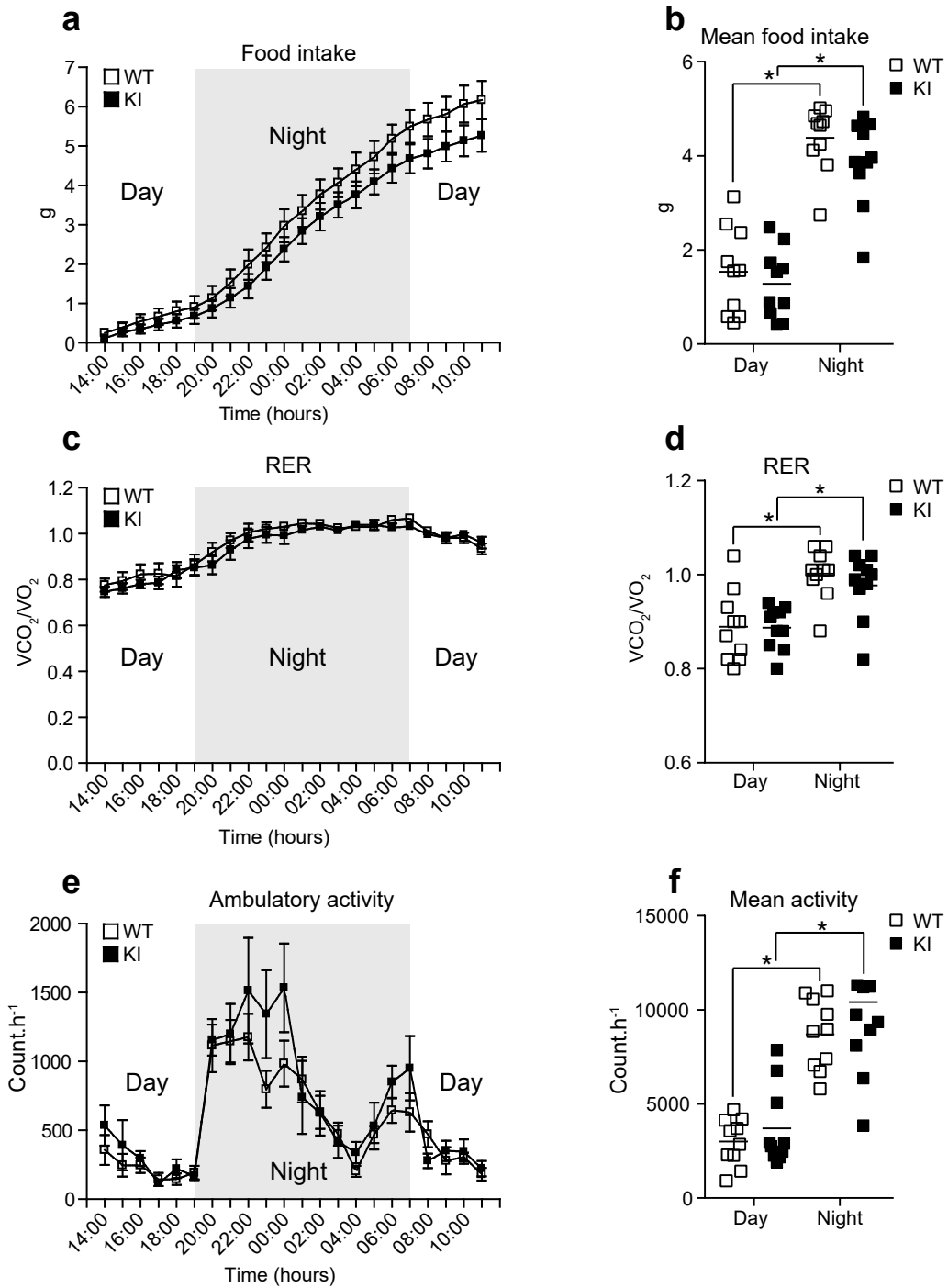


Figure S3. FBP1^{WT/WT} (WT) or FBP1^{G27P/G27P} (KI) mice were housed in metabolic phenotyping cages and after a 3 h acclimatization period, food intake (**a**, **b**) respiratory exchange ratio (RER) (**c**, **d**) and ambulatory activity (**e**, **f**) were monitored for a period of 21 h. For each parameter a line graph depicting the trend over the full 21 h period and bar graphs of the mean values observed during the day and night phase are shown. Results represent mean \pm SE, $n = 10$. * $P < 0.05$ (Day vs. night). Statistical significance was determined using unpaired, two-tailed Student's t-test and an alpha level of 0.05.

Supplementary Figure 4

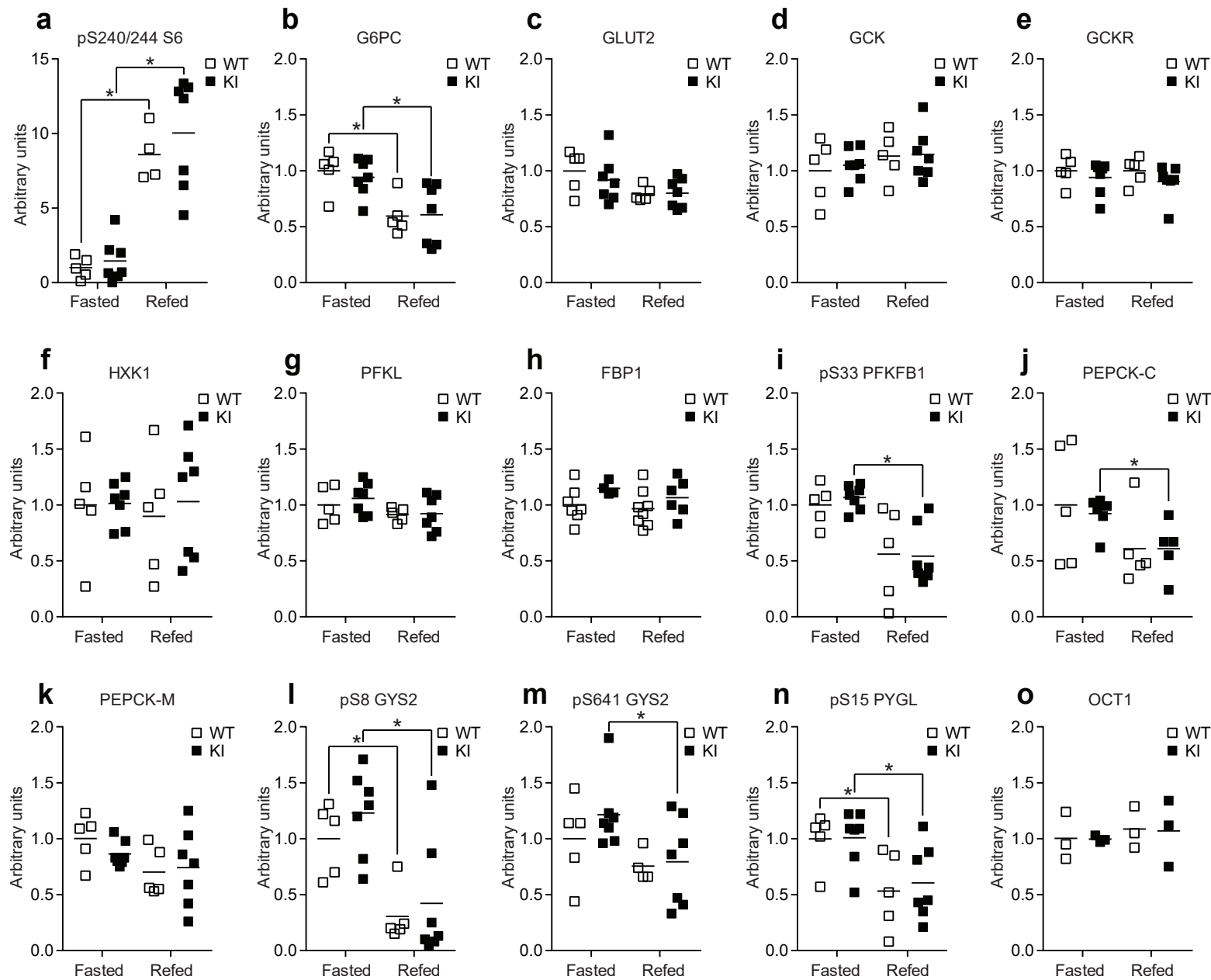


Figure S4. (a-o) Quantitative Western blot analysis of pS240/244 S6 (a), G6PC (b), GLUT2 (c), GCK (d), GCKR (e), HXK1 (f), PFKL (g), FBP1 (h), pS33 PFKFB1 (i), PEPCK-C (j), PEPCK-M (k), pS8 GYS2 (l), pS641 GYS2 (m), pS15 PYGL (n) and OCT1 (o) in liver homogenates from mice fasted overnight for 16 h (Fasted) or subsequently given free access to standard chow for 4 h (Refed). $n = 5$ FBP1^{WT/WT} (WT) and 7 FBP1^{G27P/G27P} (KI) per group with the exception of (o) where $n = 3$ for all groups. * $P < 0.05$ (Fasted vs. refed). Statistical significance was determined using unpaired, two-tailed Student's t-test and an alpha level of 0.05.

Supplementary Figure 5

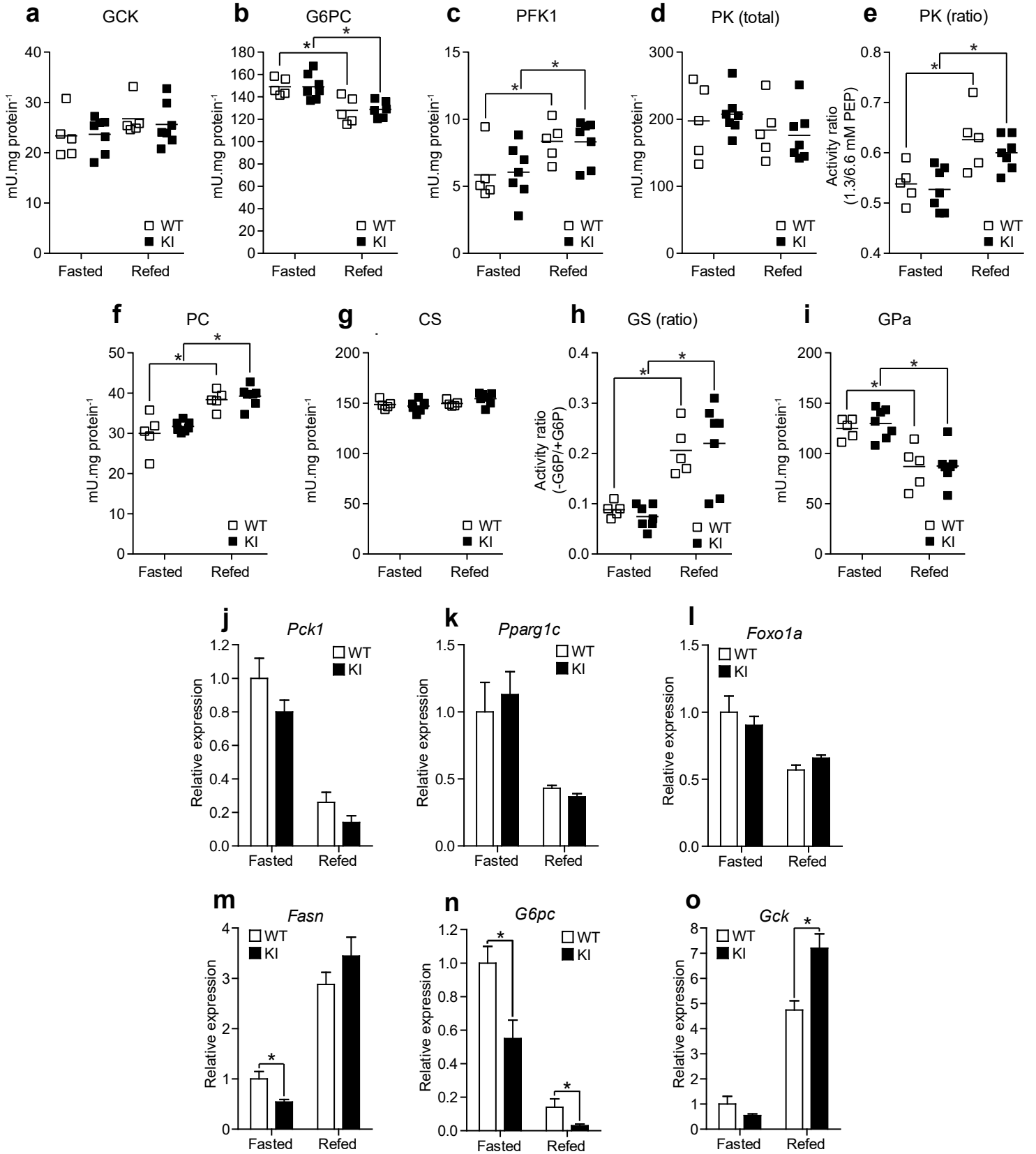


Figure S5. (a-i) Glucokinase (GCK) (a), glucose-6-phosphatase (G6PC) (b), phosphofructokinase-1 (PFK1) (c), pyruvate kinase (PK) (d), PK (1.3/6.6 mM PEP ratio) (e), pyruvate carboxylase (PC) (f), citrate synthase (CS) (g), glycogen synthase (GS ± 10 mM G6P ratio) (h) and glycogen phosphorylase (GPα) (i) activity in liver homogenates from overnight fasted (16 h) or refeed (4 h) FBP1^{WT/WT} (WT) or FBP1^{G27P/G27P} (KI) mice. (j-o) Expression of *Pck1* (j), *Pparg1c* (k), *Foxo1a* (l), *Fasn* (m), *G6pc* (n) and *Gck* (o) mRNA in liver from overnight fasted (16 h) or refeed (4 h) FBP1^{WT/WT} (WT) or FBP1^{G27P/G27P} (KI) mice determined by qPCR. Results represent mean ± SE, n = 5 (WT) and 7 (KI) per group. **P* < 0.05. Statistical significance was determined using unpaired, two-tailed Student's t-test and an alpha level of 0.05.

Supplementary Figure 6

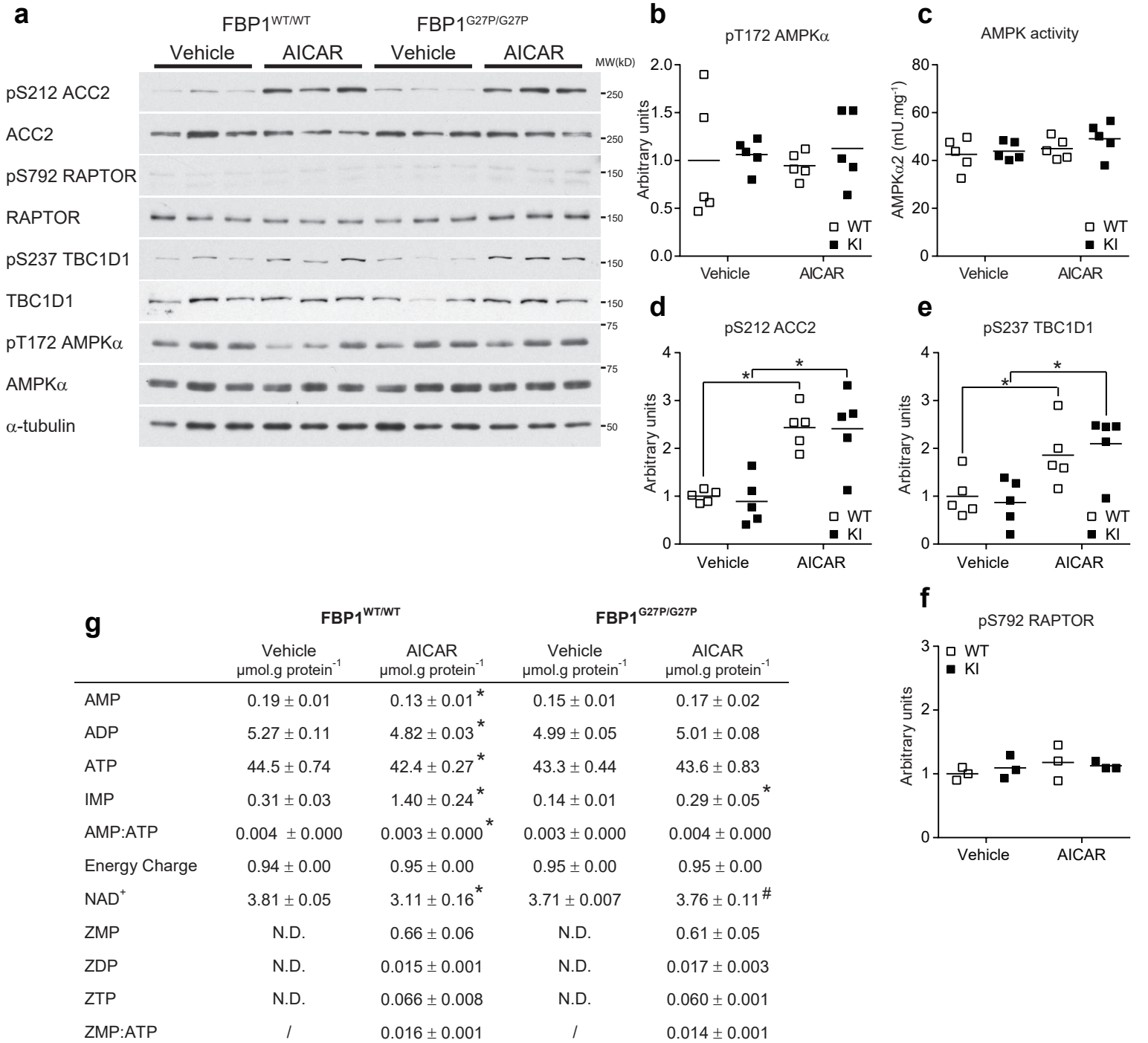


Figure S6. Effects of AICAR administration on skeletal muscle biochemistry. (a-g) Vehicle (0.9 % saline) or AICAR (250 mg.kg⁻¹ *i.p.*) was administered to fasted (16 h) mice and after 60 min exposure, gastrocnemius (GAS) muscle biopsies were taken and assayed for (a-f) AMPK activation and downstream signaling by Western blotting and (g) levels of adenine and Z-nucleotides. (a) The blot image depicts three representative mice from each treatment group. Quantitative analysis of pT172 AMPKα (b), pS212 ACC2 (d), pS237 TBC1D1 and pS792 RAPTOR (e, f) from the entire sample set was also performed. Results are expressed as phosphoprotein/total protein ratio normalized to the WT-vehicle group. (c) AMPK activation was also assessed by a radiometric immunoprecipitation kinase assay of AMPKα2 complexes. Results represent mean ± SE, n = 3-5 per treatment group. **P* < 0.05 (Vehicle vs. AICAR). #*P* < 0.05 (WT vs. KI). Statistical significance was determined using unpaired, two-tailed Student's t-test and an alpha level of 0.05.

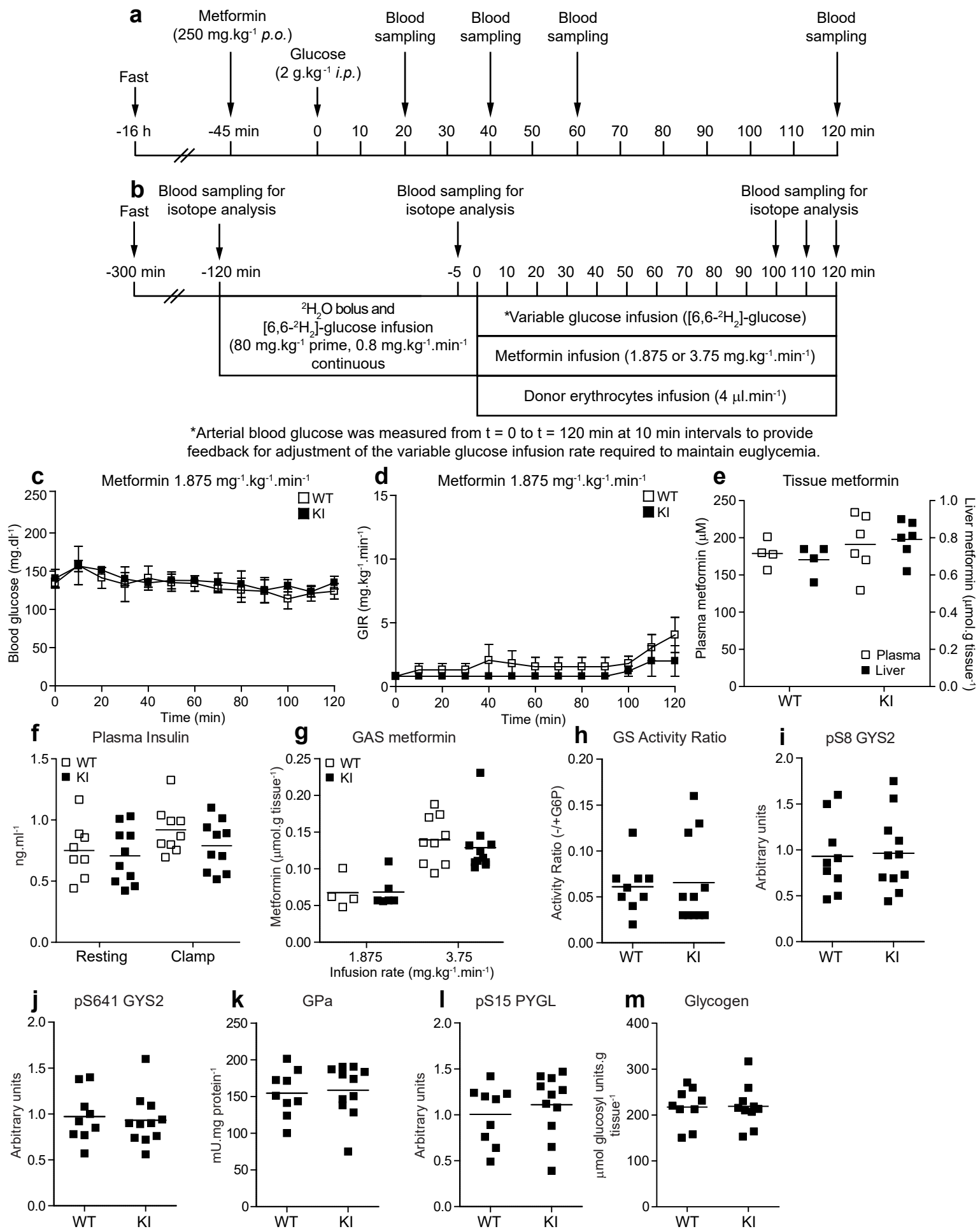


Figure S7. Schematic to illustrate the protocol followed when performing metformin tolerance tests (**a**) and metformin-euglycemic clamps (**b**). Arterial blood glucose (**c**) and glucose infusion rate (**d**) during metformin-euglycemic clamps in FBP1^{WT/WT} (WT) or FBP1^{G27P/G27P} (KI). Mice were fasted for 5 h and infused *i.v.* with metformin (1.875 mg.kg⁻¹.min⁻¹) and a variable infusion of 50 % glucose to maintain euglycemia at 120 mg.dl⁻¹ over a period of 120 min. (**e**) Plasma and liver metformin concentrations at the end of the clamp period. Results represent mean \pm SE, $n = 4$ (WT) and 6 (KI). (**f-m**) Additional analysis of tissue biopsies from WT and KI mice infused with the higher dose of metformin (3.75 mg.kg⁻¹.min⁻¹ *i.v.*) during a euglycemic clamp as described in **Fig. 5**. Plasma insulin levels at the beginning (Resting) and end of the clamp protocol (Clamp). (**g**) GAS muscle concentration of metformin at the end of the clamp protocol corrected for blood contamination. (**h**) GS activity ratio (± 10 mM G6P), (**i-j**) quantification of pS8 and pS641 GYS2 phosphorylation, (**k**) GP α activity, (**l**) quantification of pS15 PYGL phosphorylation and (**m**) glycogen content in liver biopsies. Results represent mean \pm SE, $n = 8$ (WT-resting), 9 (WT-clamp), 10 (KI-resting) and 10-11 (KI-clamp).

Supplementary Figure 8

a

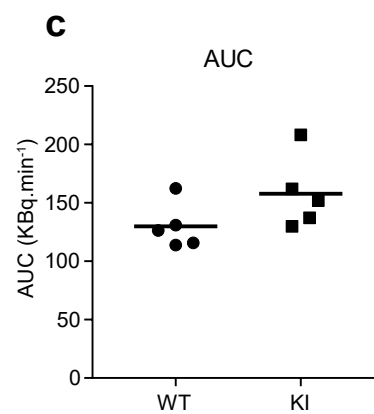
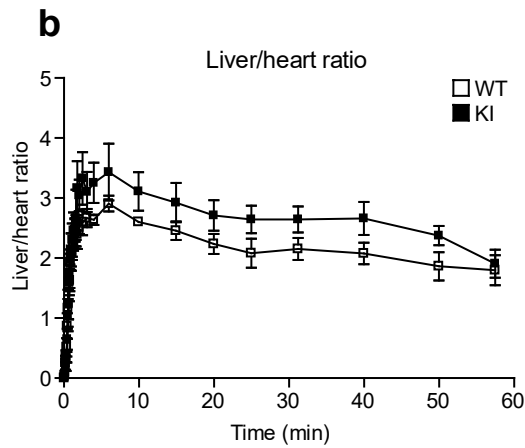
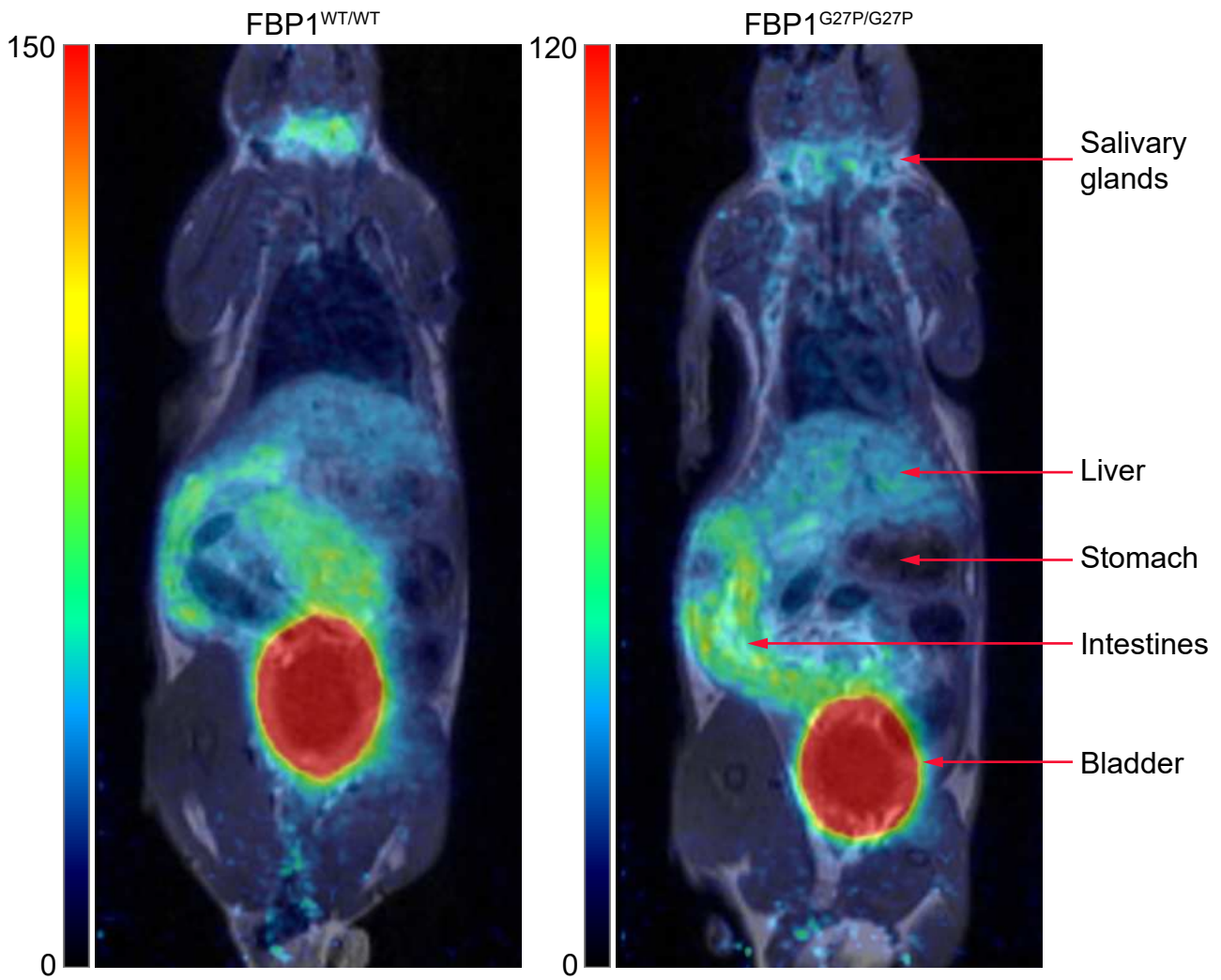


Figure S8. Metformin pharmacokinetics determined by [¹¹C]-metformin positron emission tomography (PET). Anaesthetized $FBP1^{WT/WT}$ (WT) or $FBP1^{G27P/G27P}$ (KI) were administered a single bolus injection of [¹¹C]-metformin via tail vein injection and dynamic whole-body PET acquired for a period of 60 min. **(a)** Representative coronal PET images merged with a 15 min T1-weighted Magnetic resonance imaging (MRI) scan. **(b, c)** Liver/heart activity ratios plotted against time **(b)** and the corresponding AUC **(c)** for WT and KI mice. Results represent mean \pm SE, $n = 5$.

Supplementary Figure 9

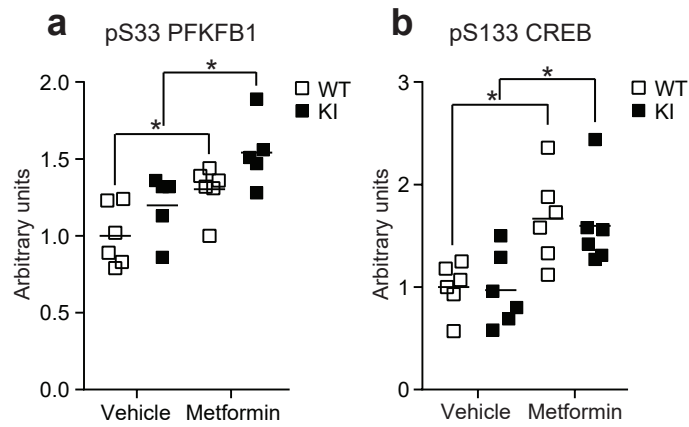


Figure S9. (a-b) Additional analysis of liver biopsies from diabetic mice (high-fat diet model) administered with vehicle (water) or metformin ($250 \text{ mg.kg}^{-1} p.o.$) for 2 h as described in **Fig. 6i-k**. Quantitative Western blotting of pS33 PFKFB1 (**a**) and pS133 CREB (**b**). Results are expressed as phosphoprotein/total protein ratio normalized to the WT-vehicle group. $n = 6$ (WT-vehicle), 6 (WT-metformin), 5-6 (KI-vehicle) and 5-6 (KI-metformin). $*P < 0.05$ (Vehicle vs. metformin). Statistical significance was determined using unpaired, two-tailed Student's t-test and an alpha level of 0.05.

Parameter	FBP1	FBP1 G27P
Specific activity (U.mg ⁻¹)	34.1 ± 2.5	32.1 ± 3.58
Ratio (pH 7.2/9.4)	2.75 ± 0.11	2.72 ± 0.15
K _m (F-1,6-P ₂) μM	2.92 ± 0.49	2.86 ± 0.16
K _a (Mg ²⁺) mM	0.36 ± 0.02	0.37 ± 0.04
<i>h</i> (Mg ²⁺)	1.86 ± 0.04	1.86 ± 0.19
IC ₅₀ (AMP) μM	13.4 ± 0.35	4520 ± 291
<i>h</i> (AMP)	1.70 ± 0.09	1.77 ± 0.15
K _d (TNP-AMP) μM	19.4 ± 1.86	>100
IC ₅₀ (F-2,6-P ₂) μM	1.69 ± 0.09	1.52 ± 0.08
<i>h</i> (F-2,6-P ₂)	1.4 ± 0.15	1.45 ± 0.14
IC ₅₀ (ZMP) μM	108 ± 13	>10,000
<i>h</i> (ZMP)	1.56 ± 0.1	ND
IC ₅₀ (IMP) μM	4530 ± 76	4620 ± 37.5
<i>h</i> (IMP)	1.71 ± 0.03	1.72 ± 0.04
IC ₅₀ (FBPase-1 inhibitor*) μM	4.58 ± 0.16	> 100
IC ₅₀ (MB05032**) μM	0.3 ± 0.03	~ 500***

* 5-chloro-2-(N-(2,5-dichlorobenzenesulfonamido))-benzoxazole (CAS 883973-99-7)

** 2-amino-5-isobutyl-4-[5-phosphono-2-furanyl]thiazole (CAS 261365-11-1)

*** Estimated value from partial curves due to limits of compound solubility

Supplementary Table 1. Table summarizing the kinetic properties of WT mouse FBP1 and the AMP-insensitive mutant G27P (6HIS tag removed by HRV-3C protease). Results represent the mean ± SD of at least three independent experiments.

	FBP1 ^{WT/WT}		FBP1 ^{G27P/G27P}	
	Fasted $\mu\text{mol.g protein}^{-1}$	Refed $\mu\text{mol.g protein}^{-1}$	Fasted $\mu\text{mol.g protein}^{-1}$	Refed $\mu\text{mol.g protein}^{-1}$
Lactate	2.68 \pm 0.12	12.0 \pm 0.6*	2.72 \pm 0.05	11.9 \pm 0.6*
Pyruvate	0.14 \pm 0.01	0.66 \pm 0.05*	0.15 \pm 0.01	0.67 \pm 0.05*
Glucose	15.5 \pm 0.4	25.4 \pm 1.6*	14.2 \pm 0.8	24.9 \pm 1.0*
G6P	0.41 \pm 0.05	0.88 \pm 0.1*	0.43 \pm 0.1	0.87 \pm 0.07*
F6P	0.11 \pm 0.01	0.24 \pm 0.03*	0.11 \pm 0.02	0.23 \pm 0.02*
F-1,6-P ₂	0.014 \pm 0.002	0.044 \pm 0.01*	0.013 \pm 0.002	0.051 \pm 0.008*
F-2,6-P ₂	0.0019 \pm 0.0003	0.0027 \pm 0.0005	0.0018 \pm 0.0002	0.0025 \pm 0.0004

Supplementary Table 2. FBP1^{WT/WT} (WT) or FBP1^{G27P/G27P} (KI) mice were fasted overnight for 16 h (Fasted) or subsequently given free access to standard chow for 4 h (Refed). Selected metabolites from fasted and refed mouse livers are summarized. Results are expressed as mean \pm SE, n = 5 (WT) and 7 (KI) per group. * $P < 0.05$ (Fasted vs. refed).

	AMP $\mu\text{mol.g protein}^{-1}$	ADP $\mu\text{mol.g protein}^{-1}$	ATP $\mu\text{mol.g protein}^{-1}$	AMP/ATP	Energy Charge
WT (Fasted)	1.36 \pm 0.04	7.58 \pm 0.24	22.93 \pm 0.33	0.060 \pm 0.002	0.838 \pm 0.003
WT (Refed)	1.58 \pm 0.07*	7.94 \pm 0.16	22.31 \pm 1.01	0.072 \pm 0.005*	0.825 \pm 0.008
KI (Fasted)	1.42 \pm 0.06	7.65 \pm 0.31	23.31 \pm 0.28	0.061 \pm 0.003	0.838 \pm 0.006
KI (Refed)	1.53 \pm 0.02	7.71 \pm 0.16	22.70 \pm 0.76	0.068 \pm 0.003	0.831 \pm 0.004

Supplementary Table 3. FBP1^{WT/WT} (WT) or FBP1^{G27P/G27P} (KI) mice were fasted overnight for 16 h (Fasted) or subsequently given free access to standard chow for 4 h (Refed). Adenine nucleotides from fasted and refed mouse livers are summarized. Results are expressed as mean \pm SE, n = 5 (WT) and 7 (KI) per group. Adenylate energy charge was calculated as defined by Atkinson (ATP + 1/2ADP)/(ATP + ADP + AMP). **P* < 0.05 (Fasted vs. refed).

	FBP1 ^{WT/WT}		FBP1 ^{G27P/G27P}	
	Vehicle μmol.g protein ⁻¹	AICAR μmol.g protein ⁻¹	Vehicle μmol.g protein ⁻¹	AICAR μmol.g protein ⁻¹
AMP	1.31 ± 0.08	1.00 ± 0.04 [*]	1.28 ± 0.10	1.68 ± 0.17 ^{*#}
ADP	7.61 ± 0.34	2.83 ± 0.04 [*]	7.64 ± 0.18	6.27 ± 0.60 ^{*#}
ATP	20.0 ± 0.46	16.5 ± 0.12 [*]	19.8 ± 0.26	18.8 ± 0.82 [#]
TAN**	28.9 ± 0.38	20.3 ± 0.13 [*]	28.7 ± 0.33	26.8 ± 1.54 [#]
AMP:ATP	0.07 ± 0.01	0.06 ± 0.00	0.07 ± 0.01	0.10 ± 0.01 ^{*#}
Energy Charge	0.82 ± 0.01	0.88 ± 0.00 [*]	0.82 ± 0.00	0.82 ± 0.00 [#]
NAD ⁺	6.24 ± 0.28	7.62 ± 0.27 [*]	6.67 ± 0.20	7.73 ± 0.34 [*]
ZMP	N.D.	40.9 ± 1.9	N.D.	34.8 ± 2.96
ZDP	Not resolved	Not resolved	Not resolved	Not resolved
ZTP	N.D.	8.57 ± 0.11	N.D.	10.6 ± 0.65 [#]
ZMP:ATP	/	2.48 ± 0.12	/	1.98 ± 0.21 [#]

**TAN = total adenine nucleotides (AMP+ADP+ATP)

Supplementary Table 4. Vehicle (0.9 % saline) or AICAR (250 mg.kg⁻¹ *i.p.*) was administered to fasted (16 h) FBP1^{WT/WT} (WT) or FBP1^{G27P/G27P} (KI) mice and after 60 min exposure, liver biopsies were taken and assayed for adenine and Z-nucleotides levels. Results represent mean ± SE, n = 5 per treatment group. **P* < 0.05 (Vehicle vs. AICAR). #*P* < 0.05 (WT vs. KI).

	AMP $\mu\text{mol.g protein}^{-1}$	ADP $\mu\text{mol.g protein}^{-1}$	ATP $\mu\text{mol.g protein}^{-1}$	AMP/ATP	Energy Charge
WT (vehicle)	1.27 \pm 0.02	6.93 \pm 0.57	23.13 \pm 1.19	0.056 \pm 0.003	0.848 \pm 0.009
WT (metformin)	2.36 \pm 0.12*	10.23 \pm 0.36*	21.52 \pm 0.55	0.109 \pm 0.003*	0.781 \pm 0.004*
KI (vehicle)	1.23 \pm 0.08	7.22 \pm 0.49	24.24 \pm 0.95	0.051 \pm 0.003	0.852 \pm 0.007
KI (metformin)	2.63 \pm 0.3*	11.54 \pm 0.64*	20.09 \pm 0.9*	0.132 \pm 0.016*	0.755 \pm 0.014*

Supplementary Table 5. FBP1^{WT/WT} (WT) and FBP1^{G27P/G27P} (KI) mice were fasted for 16 h and dosed with vehicle (water) or metformin (250 mg.kg⁻¹ *p.o.*). After 1 h exposure, blood and liver biopsies were taken and assayed for adenine nucleotides. **P* < 0.05 (Vehicle vs. metformin).

	AMP $\mu\text{mol.g protein}^{-1}$	ADP $\mu\text{mol.g protein}^{-1}$	ATP $\mu\text{mol.g protein}^{-1}$	AMP/ATP	Energy Charge
WT (vehicle)	1.23 \pm 0.14	7.00 \pm 0.29	22.64 \pm 0.73	0.055 \pm 0.007	0.847 \pm 0.07
WT (metformin)	2.29 \pm 0.36*	9.87 \pm 0.75*	19.23 \pm 0.73*	0.123 \pm 0.028*	0.763 \pm 0.017*
KI (vehicle)	1.20 \pm 0.12	6.87 \pm 0.38	22.46 \pm 1.12	0.055 \pm 0.007	0.847 \pm 0.011
KI (metformin)	2.00 \pm 0.25*	9.70 \pm 0.34*	19.87 \pm 0.47*	0.105 \pm 0.013*	0.777 \pm 0.008*

Supplementary Table 6. After 12 weeks of dietary intervention FBP1^{WT/WT} (WT) and FBP1^{G27P/G27P} (KI) mice were fasted for 16 h, administered vehicle (water) or metformin (250 mg.kg⁻¹ *p.o.*) and liver biopsies were taken after 2 h of drug treatment for adenine nucleotides. **P* < 0.05 (Vehicle vs. metformin).

	FBP1 ^{WT/WT}		FBP1 ^{G27P/G27P}	
	Vehicle μmol.g protein ⁻¹	Metformin μmol.g protein ⁻¹	Vehicle μmol.g protein ⁻¹	Metformin μmol.g protein ⁻¹
Glucose	28.7 ± 1.1	20.7 ± 1.3*	28.1 ± 1.1	24.6 ± 1.5
G6P	0.46 ± 0.02	0.40 ± 0.01	0.47 ± 0.06	0.47 ± 0.02 [#]
F6P	0.15 ± 0.01	0.11 ± 0.01	0.15 ± 0.02	0.15 ± 0.01 [#]
F-1,6-P ₂	0.013 ± 0.005	0.025 ± 0.007	0.012 ± 0.003	0.016 ± 0.004

Supplementary Table 7. After 12 weeks of dietary intervention FBP1^{WT/WT} (WT) and FBP1^{G27P/G27P} (KI) mice were fasted for 16 h, administered vehicle (water) or metformin (250 mg.kg⁻¹ *p.o.*) and liver biopsies were taken after 2 h of drug treatment for metabolites. **P* < 0.05 (Vehicle vs. metformin). #*P* < 0.05 (WT vs KI).